Università di Pisa

DIPARTIMENTO di INGEGNERIA CIVILE E INDUSTRIALE

Tesi di Laurea Magistrale in Ingegneria Nucleare

Multi-channel transient analysis of SEALER

Relatori:
Prof. Nicola Forgione
Prof. Janne Wallenius
Dott. Ing. Valerio Giusti
Dott.ssa Ing. Rosa Lo Frano

Candidato:
Francesco Pedretti

Anno Accademico 2013/2014

Abstract

The aim of this thesis work is to study the behaviour of SEALER (SwEdish Advanced LEad Reactor) under the three main unprotected accidents that could hypothetically happen for this Lead-cooled Fast Reactor (LFR): Unprotected Transient of Over Power (UTOP), Unprotected Loss Of Flow (ULOF) and Unprotected Loss Of Heat Sink (ULOHS). The work was carried out at the KTH department of Nuclear Reactor Physics, using the SAS4A/SASSYS-1 code.

The first part of the activity consisted of a model development for the reactor core, from the 1-channel one to the 4-channel one, based on the core symmetry and on the different peak factors of fuel assemblies. The main step of this part was the calculation, using the Serpent code, of the channel dependent reactivity coefficients for each channel at the three analysed conditions over the reactor lifetime: Beginning Of Cycle (BOC), Middle Of Cycle (MOC) and End Of Cycle (EOC). The second part of the work consisted of the transient simulations of the reference accidents and of some sensitivity calculations regarding the dependence of the peak fuel and cladding temperatures on the reactivity coefficients.

The obtained results show that, in the studied accident scenarios, the maximum Peak Cladding Temperature (PCT) is less than 1000 K and that the fuel temperature remains under the melting value. Moreover, for the transients UTOP, ULOF and ULOHS with the radiative heat loss through the vessel (ultimate heat sink), a new steady state condition is reached due to the reactivity feedback, while for the ULOHS accident without ultimate heat sink, the reactor is self shutdown.

Contents

List of Figures

List of Tables

List of Acronyms

ALFRED	Advanced Lead Fast Reactor European Demonstrator
BOC	Beginning of Cycle
CANDU	CANadian Deuterium Uranium
DRACS	Direct Reactor Auxiliary Cooling System
E	Equivalent Dose
ELECTRA	European Lead Cooled TRaining Reactor
ELSY	European Lead SYstem
EOC	End of Cycle
FBR	Fast Breeder Reactor
GFR	Gas-cooled Fast Reactor
GIF	Generation IV International Forum
HTGR	High Temperature Gas Reactor
IHX	Intermediate Heat eXchanger
KTH	Kungliga Tekniska Högskolan (Royal Institue of Technology)
LBE	Lead Bismuth Eutectic
LEADER	Lead-cooled European Advanced DEmonstration Reactor
LFR	Lead-cooled Water Reactor
LMFBR	Liquid Metal Fast Breeder Reactor
LWR	Light Water Reactor
MOC	Middle of Cycle

MSR	Molten Salt Reactor
MYRRHA	Multi-purpose Hybrid Research Reactor for High-tech Applications
PCT	Peak Cladding Temperature
pcm	PerCent Millirho
PF	Peak Factor
RIA	Reactivity Initiated Accident
SBO	Station Black Out
SCRAM	Safety Control Rod Axe Man
SCWR	Supercritical Water-cooled Reactor
SEALER	SwEdish Advanced LEad Reactor
SFR	Sodium-cooled Water Reactor
SG	Steam Generator
ULOF	Unprotected Loss of Flow
ULOHS	Unprotected Loss of Heat Sink
UTOP	Unprotected Transient of Over Power
VHTR	Very High Temperature Reactor

Chapter 1

Introduction

In the last decades the global warming and the air pollutants production, in particular carbon dioxide (CO_2), sulfur dioxide and trioxide (SO_x) and nitrogen oxides (NO_x), emerged as the main problems caused by human activity and more specifically by the energy production mainly due to the burning of fossil fuels. In order to overcome these concerns and to ensure a better environmental impact for the energy production in the last years the energy industry is trying to give more importance to the renewable energy (biofuels, solar power and wind power) and to improve the conditions of operation for the other sources of energy (coal, nuclear and gas) with some programs of Research & Development (R&D) for the new plants.

Regarding the improvement of the nuclear power plants, for more than a decade, the Generation IV International Forum (GIF) has led international collaborative efforts to develop next-generation nuclear energy systems that can help meet the world's future energy needs. Generation IV designs will use fuel more efficiently, reduce waste production, be economically competitive, and meet stringent standards of safety and proliferation resistance. In this framework eight technology goals have been defined for Generation IV systems in four broad areas: sustainability, economics, safety and reliability, and proliferation resistance and physical protection.

- Sustainability-1: generation IV nuclear energy systems will provide sustainable energy generation that meets clean air objectives and provides long-term availability of systems and effective fuel utilisation for worldwide energy production.

- Sustainability-2: generation IV nuclear energy systems will minimise and manage their nuclear waste and notably reduce the long-term stewardship burden, thereby improving protection for the public health and the

environment.

- Economics-1: generation IV nuclear energy systems will have a clear life-cycle cost advantage over other energy sources.
- Economics-2: generation IV nuclear energy systems will have a level of financial risk comparable to other energy projects.
- Safety and Reliability-1: generation IV nuclear energy systems operations will excel in safety and reliability.
- Safety and Reliability-2: generation IV nuclear energy systems will have a very low likelihood and degree of reactor core damage.
- Safety and Reliability-3: generation IV nuclear energy systems will eliminate the need for offsite emergency response.
- Proliferation Resistance and Physical Protection: generation IV nuclear energy systems will increase the assurance that they are very unattractive and the least desirable route for diversion or theft of weapons-usable materials, and provide increased physical protection against acts of terrorism.

With these goals in mind, GIF selected six reactor technologies for further research and development. These include: the Gas-cooled Fast Reactor (GFR), the Lead-cooled Fast Reactor (LFR), the Molten Salt Reactor (MSR), the Supercritical Water-cooled Reactor (SCWR), the Sodium-cooled Fast Reactor (SFR) and the Very High Temperature Reactor (VHTR). A brief description for each reactor is presented below:

- GFR: the gas-cooled fast reactor combines the advantages of a fast neutron core and helium coolant giving possible access to high temperatures. It requires the development of robust refractory fuel elements and appropriate safety architecture. The use of dense fuel such as carbide or nitride provides good performance regarding plutonium breeding and minor actinide burning. A technology demonstration reactor needed for qualifying key technologies could be in operation by 2020.
- LFR: the lead-cooled fast reactor system is characterised by a fast-neutron spectrum and a closed fuel cycle with full actinide recycling, possibly in central or regional fuel cycle facilities. The coolant may be either lead (preferred option), or lead/bismuth eutectic. The LFR may be operated as a breeder, a burner of actinides from spent fuel, using inert matrix fuel, or a burner/breeder using thorium matrices. Two reactor size options are considered: a small 50-150 MW_e transportable system with a very

long core life, and a medium 300-600 MW_e system. In the long term a large system of 1200 MW_e may be envisaged. The LFR system may be deployable by 2025.

- MSR: the molten-salt reactor system embodies the very special feature of a liquid fuel. MSR concepts, which may be used as efficient burners of transuranic elements from spent light-water reactor (LWR) fuel, also have a breeding capability in any kind of neutron spectrum ranging from thermal (with a thorium fuel cycle) to fast (with a uranium-plutonium fuel cycle). Whether configured for burning or breeding, MSRs have considerable promise for the minimisation of radiotoxic nuclear waste.

- SCWR: supercritical-water-cooled reactors are a class of high-temperature, high-pressure water-cooled reactors operating with a direct energy conversion cycle and above the thermodynamic critical point of water (374℃, 22.1 MPa). The higher thermodynamic efficiency and plant simplification opportunities afforded by a high-temperature, single-phase coolant translate into improved economics. A wide variety of options are currently considered: both thermal-neutron and fast-neutron spectra are envisaged; and both pressure vessel and pressure tube configurations are considered. The operation of a 30 to 150 MW_e technology demonstration reactor is targeted for 2022.

- SFR: the sodium-cooled fast reactor system uses liquid sodium as the reactor coolant, allowing high power density with low coolant volume fraction. It features a closed fuel cycle for fuel breeding and/or actinide management. The reactor may be arranged in a pool layout or a compact loop layout. The reactor-size options which are under consideration range from small (50 to 150 MW_e) modular reactors to larger reactors (300 to 1500 MW_e). The two primary fuel recycle technology options are advanced aqueous and pyrometallurgical processing. A variety of fuel options are being considered for the SFR, with mixed oxide preferred for advanced aqueous recycle and mixed metal alloy preferred for pyrometallurgical processing. Owing to the significant past experience accumulated with sodium cooled reactors in several countries, the deployment of SFR systems is targeted for 2020.

- VHTR: the very-high-temperature reactor is a further step in the evolutionary development of high-temperature reactors. The VHTR is a helium-gas-cooled, graphite-moderated, thermal neutron spectrum reactor with a core outlet temperature higher than 900℃, and a goal of 1000℃, sufficient to support high temperature processes such as production of

hydrogen by thermo-chemical processes. The reference thermal power of the reactor is set at a level that allows passive decay heat removal, currently estimated to be about 600 MW_{th}. The VHTR is useful for the cogeneration of electricity and hydrogen, as well as to other process heat applications. It is able to produce hydrogen from water by using thermo-chemical, electro-chemical or hybrid processes with reduced emission of CO_2 gases. At first, a once-through low enriched uranium ($< 20\%$ U^{235}) fuel cycle will be adopted, but a closed fuel cycle will be assessed, as well as potential symbiotic fuel cycles with other types of reactors (especially light-water reactors) for waste reduction purposes. The system is expected to be available for commercial deployment by 2020 [1].

Focusing the attention on the LFRs and their state of the art, the European Commission in its 6th and 7th Framework Program has co-founded the European Lead SYstem (ELSY [2, 3]) project and the Lead-cooled European Advanced DEmonstration Reactor (LEADER [4]) project with the purpose to obtain a preliminary design of the ELSY and ALFRED (Advanced Lead Fast Reactor European Demonstrator [5, 6]) reactors. Together with the development of these programs, in the European framework another two reactor projects have been investigated and developed: MYRRHA (Multi-purpose Hybrid Research Reactor for High-tech Applications [7, 8]) and ELECTRA (European Lead Cooled TRaining Reactor [9–11]). Since all these four reactors are prototype, demonstrator, research or training reactors their goals are to ensure that the design fully matches the requests and the objectives of the Generation IV, eventually to point out which are the areas that need an improvement (as already done for the SFR with Phénix, SuperPhénix and Monju power plants) and at the end to establish if it is possible to use them in a large scale context for the energy production, like actually performed with the Light Water Reactor (LWR). In this framework, also the reactor analysed in this thesis work the SwEdish Advanced LEad Reactor (SEALER), although some particular features (chapter 2) and its very small size that makes it a modular reactor, can be included.

During these years of R&D for all these reactors, the main concerns are related to the resistance of the materials, since they have to deal with an high corrosive and erosive environmental given by the coolant and also with an higher energy neutron flux. As a consequence of these problems, some limits on the operating temperatures, that reduce the thermal efficiency of the plants in order to ensure a proper lifetime of the materials, were adopted. As a matter of fact, the demonstration that the reactors presented before can work without any significant problems from a safety and an economic point of view together with

the development of new and improved materials or special coatings and with the progress in the design of UN, to adopt as fuel in substitution of the UO_2, could lead to establish the LFR as a reference point for the future nuclear power plant and to a more efficient and powerful reactors.

1.1 Aim of the Work

The aim of this work is to give a first assessment about the behaviour of the SEALER reactor under the three reference unprotected accidents that could hypothetically happen over its lifetime and to understand if the human intervention is necessary to stabilize the accidents development and which are the safety margin on the peak temperatures (fuel and cladding). The three accidents taken into account in this analysis are the unprotected transient of over power, the unprotected loss of flow and the unprotected loss of heat sink.

The steps conducted to achieve the final target are: SAS4A/SASSYS-1 core model extension from 1-channel to 4-channel based on peak factors and core symmetry, calculation of the channel dependent reactivity coefficients using the Serpent code, implement the results in the SAS4A/SASSYS-1 input file and then run the transients. The Doppler, the fuel and cladding axial expansion, the coolant void worth and the radial expansion are the reactivity coefficients included in the analysis. In order to evaluate them, it is necessary to give a perturbation channel by channel (like an increase in the fuel temperature or length or in the pitch between the assemblies and a reduction in the fuel or coolant density) and to assess the related variation in the core reactivity.

At the end of the work some sensitivity calculations are performed with the purpose to understand which is the dependence of the peak temperatures on each one of the reactivity coefficients.

Chapter 2

SEALER Reactor

This is an introduction chapter where a general view of the SEALER reactor is presented, pointing out the main peculiarity about its design that would help to understand the meaning of the results presented in the remainder of the work.

2.1 Philosophy and Design

SEALER is a LFR with a thermal power of 8 MW (3 MW_e), designed to produce heat and electricity for off-grid consumers. It should demonstrate the work capability of LFR which are lacking in years of reactor work with respect to the SFR, and lead the way for bigger LFR in terms of power and dimensions. In the next few years its construction should start in Canada.

The choice of the lead as a coolant over sodium and Lead Bismuth Eutectic (LBE) is due to the lower source term following a possible coolant release from the primary circuit and to the lower number of required components. As a matter of fact, lead is not activated by the neutrons contrary to what happens with the sodium and, moreover, the Intermediate Heat eXchanger (IHX) and its related systems (needed in case of SFR in order to avoid the possible exothermic reaction between the radioactive sodium and water) are not required. Regarding the LBE, the problems are related to the generation of polonium (Po^{210}) that is a highly radioactive α emitter and a chemically toxic element. The importance to have a smaller number of big components and to reduce as much as possible the source term are explained in the remainder of the chapter.

SEALER is a pool type fast reactor (figures 2.1 and 2.2) with particular features, the most relevant of which are here presented: it is very small compared to the other LFR of the same power size, it never requires the fuel reload over the entire predicted lifetime of 30 years and it has safety features that allow no public evacuation for all the accident scenarios. Since SEALER should be

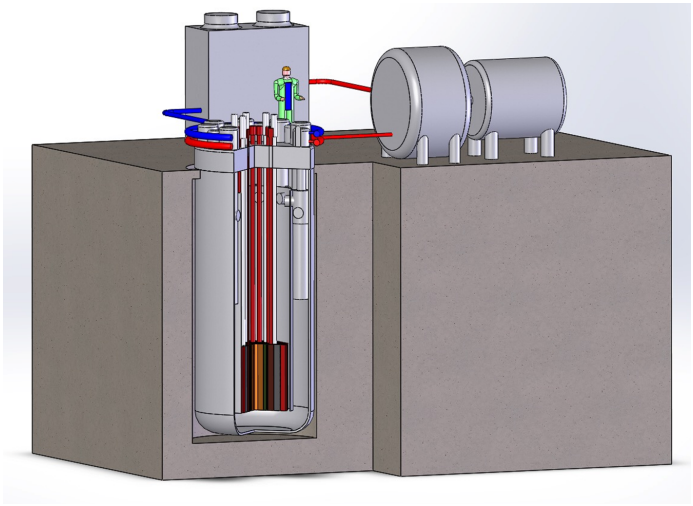

Figure 2.1: General view of the SEALER reactor.

located in off-grid sites, these could be far away from highways and the small dimensions are needed in order to have the possibility to transport all the reactor components in the easiest way in all the possible locations. The dimension of the vessel are determined upon the necessity to insert it in the cargo space of an Hercules airplane and the maximum value for the diameter is setted at 2.75 m. The height of the vessel is 6 m.

For what it concerns the no evacuation of the population, it is a consequence of the radiological impact assessment that ensures very low equivalent dose also in case of core melting ($E < 1$ mSv at 200 m from the reactor) and of the very low population density that characterizes the off-grid sites. Moreover, it could be more convenient to take shelter inside the houses than to organize an evacuation, but it depends on the site conformation and it should be determined on a case by case analysis for each site.

To prevent an accident SEALER is equipped with two independent shutdown systems based on the separate insertion of the 6 shutdown elements (figure 2.3). Since 3 out of 6 are sufficient for the SCRAM (Safety Control Rod Axe Man), the design provides two sets of 3 elements: the insertion of the first one is controlled hydraulically by the primary lead, while the second one uses a different system that implies the use of gas for the hydraulically insertion.

Another option, for a second shutdown system based on different physical phenomenon, could be the drain of the lead pool. It ensures the total amount of negative reactivity insertion required for the shutdown, but the problem is the design of an auxiliary system able to remove the decay heat in the first minutes after the drainage of the pool. From a nuclear safety point of view, the design

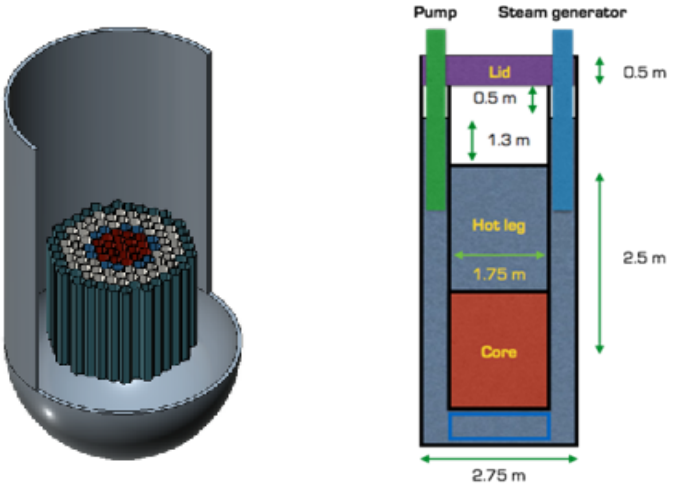

Figure 2.2: Vessel and core view (left) and a simple scheme of the reactor pool (right).

of such systems (different and independent) is necessary in order to reduce the probability of an unprotected accident (i.e. an accident where both SCRAM systems are unavailable at the same time).

As a consequence of the small size and of the absence of the fuel reloading, the main cost for the SEALER construction is strictly related the fuel production that, in its turn, is bounded to the enrichment level. The fuel is UO_2 enriched in U^{235} at 19.9%. In the future there might be the possibility to use UN as fuel and it would bring an increase in the power maintaining the same lifetime thanks to the higher density of the uranium nitrides with respect to the uranium dioxides.

The reactor core (figure 2.3) is made by 19 hexagonal wrapper tube fuel assemblies containing each one 91 fuel pins. The choice of this type of geometry is due to guide the coolant flow through the core and to limit the consequence of a cladding failure [12]. The active core diameter is 0.8 m and the height is 1.1 m, while the total length of the fuel pins is 1.55 m (2 insulation pellets made by ZrO_2 of 0.5 cm at the bottom and at the top and 35 cm of gas plenum). The gas plenum is above the fuel pellets and the gap between the fuel pellets and the cladding is filled with Krypton. A particular feature of the core design is the position of the burn-up control elements, which are located outside the fuel region. They form a ring made of 12 elements for the burn-up control and 6 elements for the reactor shutdown. These kind of elements are made by B_4C but with different enrichment: natural for the first, while 90% in B^{10} for the second. The reason for which no burn-up control elements are placed between the hexagonal fuel assemblies, like in any other reactor, is the need to have a

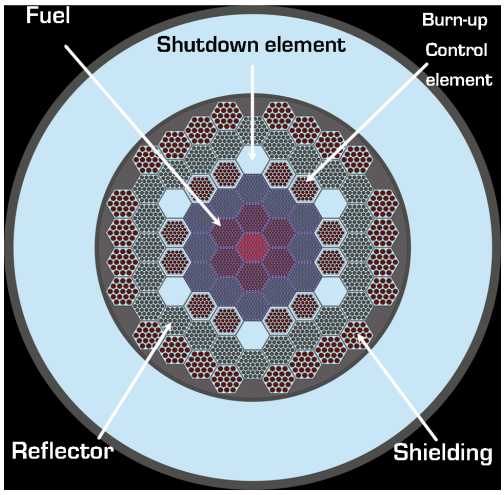

Figure 2.3: Core radial cross section.

reactor vessel diameter as small as possible (maximum diameter value of 2.75 m). This tight request brings to have some disadvantages, the most important of which is the relatively high difference in the peak factors between the core zones at the Beginning Of Cycle (BOC). The reactivity worth related to each one of the burn-up control element is 0.5 \$. The core periphery is filled with 2 rings of 24 elements each one: the first constitutes the reflector (Yytra stabilised zirconia) while the second the shielding (B_4C enriched at 90% in B^{10}).

Another important aspect related to the absence of the fuel reloading, is that the fuel cladding must be designed to withstand against the high corrosion generated by the cooling lead. With the purpose to satisfy this requirement, two main actions are planned: the first is to reduce the operating temperature in the core in such a way that during normal operation the maximum cladding temperature should not exceed 450℃, a condition that can be achieved with a coolant forced flow of 1311 kg/s; the second is to adopt a special coating of FeCrAlY in order to reduce the fretting corrosion that under oscillating loads produces unacceptable results for the cladding material Sandvik's 12R72, a 15-15 Ti steel with 0.4% Si [13–19]. The special coating is necessary for all the length of the cladding except for the lower end cap that is expected to work at a temperature lower than 400℃, since the core inlet temperature during normal operation is 390˚C with the aim to provide a minimum margin for freezing of the lead [20].

The forced flow through the primary system is secured by 8 pumps. This relatively high number of pumps is due to the fact that in this way the availability of the system increases as the forced flow can be satisfied by only 6 pumps. Moreover, it permits to use the pumps in a working range that is very similar to

that of the normal industry pumps. The peculiar aspect related to the pumps is the position. Indeed, they are located in the hottest part of the primary circuit, between the outlet plenum of the core and the entrance of the Steam Generators (SGs). This is due to the need to reduce the shaft height and to the fact that this change in the configuration of the primary circuit does not affect the performance of the reactor. In addition, the rather small difference in the coolant temperature between the hottest and the coldest part of the primary circuit of about 40°C makes this solution feasible.

The same problem, previously described for the fuel cladding, is present also for the components of the 8 SGs which have to resist to the lead corrosion at 430-450℃, although with lower pressure and induced stress comparing with the fuel cladding, for the whole reactor lifetime of 30 years without any significant problem that could bring to a reactor shutdown. To match this request the material chosen for the SGs is an aluminium bearing ferritic steel like Fe-10Cr-4Al-RE [21]. A very important characteristic of the SGs is the relative height with respect to the core in order to ensure a proper natural circulation flow during the accident scenario of unprotected loss of flow. In SEALER this height is 2.5 m. The geometry of the SGs tubes is spiral like for the reactor Elsy [22, 23].

Chapter 3

Background

In this chapter, the two codes used for this project, namely SAS4A/SASSYS-1 and Serpent, and the corresponding reactor models are described. Moreover, a discussion regarding the reactivity coefficients, their definition and the physics behind the different phenomena is also presented.

3.1 SAS4A/SASSYS-1 Code

3.1.1 General Overview

The SAS4A/SASSYS-1 code is a combination of two deterministic codes that provide safety analysis for design basis and beyond design basis accident in Liquid Metal Fast Breeder Reactor (LMFBR).

Within the SAS4A and SASSYS-1 codes detailed, mechanistic models of steady-state and transient thermal, hydraulic, neutronic, and mechanical phenomena are employed to describe the response of the reactor core and its coolant, the fuel elements and structural members as well as the reactor primary and secondary coolant loops, the reactor control and protection systems, and the balance-of-plant to accident conditions caused by loss of coolant flow, loss of heat rejection, or reactivity insertion. The SAS4A analysis is terminated upon loss of subassembly hexcan integrity while the SASSYS-1 analyses is terminated upon demonstration of reactor and plant shutdown to permanently coolable conditions, or upon violation of design basis margins. The objective of SAS4A and SASSYS-1 analysis is to quantify severe accident consequences as measured, for the first, by the generation of energetics sufficient to challenge reactor vessel integrity, leading possibly to public health and safety risk, while, for the second, by the transient behaviour of system performance parameters, such as fuel and cladding temperatures, reactivity, and cladding strain [24].

In this work only the neutronic and thermo hydraulic parts of the codes are taken into account neglecting the mechanical analysis related to pre-failure and failure phases of the cladding and also the fuel and clad relocation mechanisms following a severe accident.

For what it concerns the neutronic part, these codes utilize the point kinetic scheme, in which the spatial flux shapes $\phi(\vec{r})$ in both directions, radial and axial, are given as fixed parameters in the input file, while the flux development during a transient is calculated using the following set of equations:

$$\begin{cases} \dfrac{d\phi(t)}{dt} = \phi(t)\dfrac{\rho(t)-\beta}{\Lambda} + \displaystyle\sum_{i=1}^{6} \lambda_i C_i(t) \\ \dfrac{dC_i(t)}{dt} = \dfrac{\beta_i \phi(t)}{\Lambda} - \lambda_i C_i(t) \\ \phi(0) = 0 \\ C_i(0) = \dfrac{\beta_i}{\lambda_i \Lambda} \end{cases} \tag{3.1}$$

where $\phi(t)$ is the neutron flux, $\rho(t)$ the net reactivity, β the total effective delayed neutron fraction, Λ the effective prompt neutron generation time and λ_i is the decay constant for the *i-th* group of delayed neutron precursors whose population is $C_i(t)$. The net reactivity is assessed with the following general formula:

$$\rho(t) = \rho_p(t) + \rho_{CS}(t) + \rho_D(t) + \rho_d(t) + \rho_{Pb}(t) + \rho_{re}(t) + \rho_{cr}(t) + \rho_{fu}(t) + \rho_{cl}(t)$$

where

- ρ_p(t)=user programmed reactivity,
- ρ_{CS}(t)=control system reactivity,
- ρ_D(t)=fuel Doppler feedback reactivity,
- ρ_d(t)=fuel and cladding axial expansion feedback reactivity,
- ρ_{Pb}(t)=coolant density or voiding feedback reactivity,
- ρ_{re}(t)=core radial expansion feedback reactivity,
- ρ_{cr}(t)=control rod drive expansion feedback reactivity,
- ρ_{fu}(t)=fuel relocation reactivity feedback,
- ρ_{cl}(t)=cladding relocation reactivity feedback.

Regarding the thermal hydraulic part, as in any other deterministic code, SAS4A/SASSYS-1 uses a numerical discretization method to solve the mass, momentum and energy partial differential equations:

$$\begin{cases} \dfrac{\partial \rho}{\partial t} + \dfrac{1}{A}\dfrac{\partial (GA)}{\partial z} = 0 \\ \dfrac{\partial G}{\partial t} + \dfrac{1}{A}\left(\dfrac{G^2 A}{\rho}\right) = -\dfrac{\partial p}{\partial z} - \rho g sin(\theta) - \tau_w \dfrac{P_f}{A} \\ \dfrac{\partial \rho e}{\partial t} + \dfrac{1}{A}\dfrac{\partial [GA(e+pv)]}{\partial z} = q^{''}\dfrac{P_h}{A} + q^{'''} \end{cases} \tag{3.2}$$

in the equations (3.2) ρ is the density, G the mass velocity, A the cross section area, p the pressure, τ_w the wall friction factor, P_f the heated perimeter, e is the specific energy per unit of volume, pv is the flow work, $q^{''}$ the heat flux, P_h the wetted perimeter and $q^{'''}$ the heat power source.

The equations presented are for general geometry and component. For the specific treatment of different elements (core structures, SG, fuel, coolant, etc.), starting from these equations, the terms that are not needed can be cancelled, while correlations or special models can be added in order to close the set of equations for a specific phenomenon in a specific element.

The discretization method implemented in SAS4A/SASSYS-1 is the finite difference method. It consists in the substitution of the partial derivatives, in the equations (3.2), for finite differences of the independent variable with finite increments in space and time. For example the mass balance equation becomes:

$$\frac{\partial \rho}{\partial t} + \frac{1}{A}\frac{\partial (GA)}{\partial z} = 0 \Rightarrow \frac{\rho_i^{n+1} - \rho_i^n}{\Delta t} + \frac{1}{A}\frac{G_{i+1}^n A - 2G_i^n A + G_{i-1}^n A}{\Delta z} = 0$$

where i corresponds to the spatial location in the mesh and n to the time step. For a better understanding of these concepts the reader has to refer to the appendix.

In SAS4A/SASSYS-1 the spatial discretization of the primary circuit consists in the definition of compressible volumes, filled with liquid, gas or both, connected between them by liquid or gas segments divided, in their turn, into elements and into temperature groups. A compressible volume can represent many parts of the primary circuit like inlet plenum, outlet plenum with or without cover gas (depending on the coolant choice lead or sodium), pool, expansion tank, pipe rupture source and pipe rupture sink; on the other hand a liquid or gas element can represent core assemblies, pipes, valves, SG shell or tube side, pump impeller, steam generators and DRACS (Direct Reactor Auxiliary Cooling System) heat exchangers. The segments are mono-dimensional and characterized by an incompressible single phase flow, with the exception of the core region,

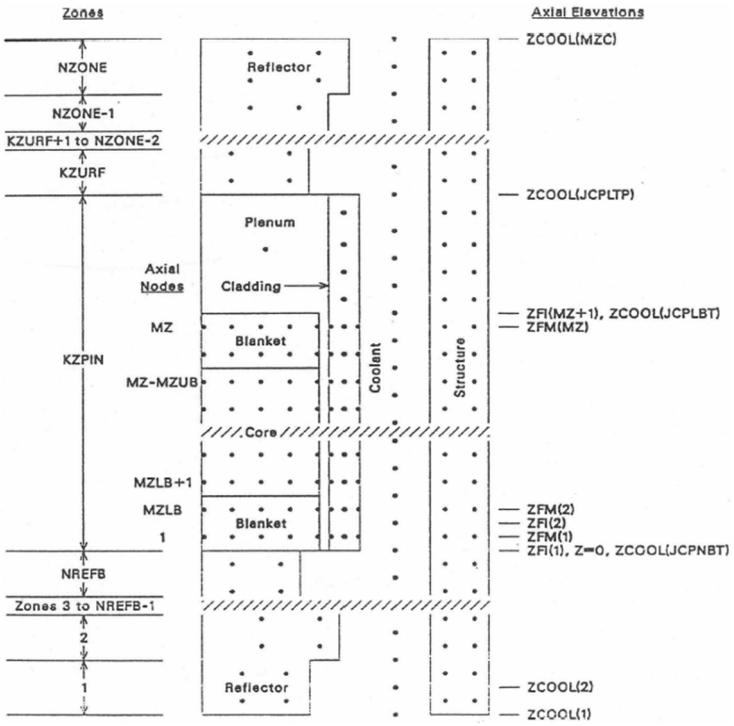

Figure 3.1: Example of channel discretization in SAS4A/SASSYS-1.

and they can be made by different elements. The temperature groups can be defined inside the segments or the elements, except for the core, and they adopt the same heat transfer routine for the calculation, thus for this reason to use the same temperature groups for different segments is not advised.

The core region is discretised axially and radially through a suitable mesh structure and the number of points used in the discretization vary depending on the structure analysed. In the figure 3.1 a general example of the core discretization scheme is presented. Along the axial direction the core region can be divided at maximum into 7 different regions (lower and upper reflector and blanket, core, gas plenum above or below the core) and the sum of the axial nodes must be equal or lower than 48. Moreover the sum of the reflector nodes must be lower than 7. Regarding the radial direction, the fuel (included the blanket) has a minimum of 4 nodes and a maximum of 11, the cladding has 3 nodes, the coolant 1, the structure and the reflector 2, the gas plenum and the cladding in the gas plenum region have 1 radial node.

It is important to keep in mind that the temperature and pressure values, for the coolant along the axial direction, are assessed in the junction between two mesh elements while the temperatures for the fuel, the cladding and the structures are evaluated in the middle of a mesh element (in the node).

The thermal hydraulics calculations are carried out in a number of separate modules. A steady-state thermal hydraulics module provides the initial conditions for the transient. The transient temperatures are calculated in a pre-voiding module until the onset of boiling. After the onset of boiling, the fuel pin temperatures are calculated in a separate module coupled with the boiling module. The core thermal hydraulic routines interact with a number of other modules, before the onset of voiding, a routine calculates the coolant temperatures used in the hydraulic calculations and the initial coolant flow rate and pressure distribution are supplied by the pre-voiding hydraulics routines. The point kinetics module supplies the power level (including the decay power) used in the heat transfer routines, and the heat transfer routines supply the temperature dependent reactivity feedback. This module is based on the approximation that the neutron flux spatial shape is invariant during a transient and the effects of the changes in geometry can be neglected.

The transient calculations uses a multi level time step approach, with separate time steps for each module. For the heat transfer routines, all temperatures are known at the beginning of a heat transfer step, and the routines calculate the new temperatures at the end of the step. The heat transfer time step can be longer than the coolant time step, but the heat transfer time step can be no longer than the main time step that is used for reactivity feedback and main printouts. All the calculations are performed with semi-implicit or fully implicit methods. The degree of implicitness is automatically calculated by the code with empirical relations based on the time step and other heat transfer time constants given by the user and dependent on the type of routine. The user must specify also the minimum grade of implicitness achievable during the calculations [25].

3.1.2 Input File

The SAS4A/SASSYS-1 input file is organized by functional purpose and it is not strictly related to the input blocks of the code structure. This is done with the purpose to make modifications and revisions in the easiest way and to help the comprehension of the file also for new users. It is divided into many parts or sections: coolant property, core and decay power, point kinetics parameters, fuel and cladding properties, average channel geometry and discretization, feedback models, different channels feedback and properties, primary circuit definition, running parameters and accident simulation.

Regarding the coolant properties, once chosen the type of coolant, the related properties are taken from a data library implemented in the codes. For the fuel and cladding properties, it is necessary to create some tables specifying the temperatures and the values of some specific parameter. For the cladding, the

thermal conductivity, the specific heat and the specific heat multiply by the cladding density have to be specified; for the fuel, in addition to these properties, the theoretical density and the porosity grade have to be defined.

The point kinetics part defines the parameters described in the set of equations (3.1). The core and decay heat power section requires the total reactor power, the fraction of the total power produced in the fuel and the number of decay groups to take into account in the decay heat calculations.

The field related to the average channel geometry and discretization defines the geometry of the fuel pin, the cladding and the structures in the core region. Since all the fuel pins and the assemblies have the same dimensions (height, radius, thickness, coolant flow area, hydraulic perimeter and gas plenum position) and the same power profile (radial and axial) this section refers to all the 19 assemblies while the channel depending properties (peak factors and reactivity feedback) are defined in a different section of the input file. The coolant mass flow and the coefficients to be used in the different correlations, together with the information on when it occurs the transition from the laminar to the turbulent flow, are also included in this section. Since SAS4A/SASSYS-1 uses a per pin concept, some of these values must be inserted per number of total pins ($19 \cdot 91 = 1729$). Here the same table for the properties listed before for the cladding and the fuel are described for the reactor structures. Finally, into this section are also defined the discretization parameters (e.g. the number and length of the axial and radial nodes of each structure) and the degree of implicitness to be used in the calculation (0.5, i.e. semi-implicit method).

The feedback models section specifies the type of feedback taken into account during the transient: for the control rod driveline no expansion and for the core structures free axial expansion and radial expansion proportional to the core inlet coolant temperature. For the latter case, the core flower effect is neglected. In this section the radial expansion coefficient is also defined.

For what it concerns the different channel feedback and properties, this part contains the information needed to complement the previous ones about the geometry and the dimensions of each one of the channels: i.e. the number of assemblies in each channel, the peak factors, the Doppler coefficient, the coolant void worth and the fuel and cladding reactivity worth. The reactivity coefficients must be implemented per unit of mass (of coolant, fuel or cladding) except for the Doppler one that requires the definition of two core state: the normal one, with the coolant, and the voided one without the coolant. In addition, the fuel thermal expansion coefficient and the Young elasticity module for the free axial expansion model chosen in the previous section are here also defined.

The primary circuit (figure 3.2) is modeled with 3 compressible volumes: inlet plenum, outlet plenum and cold leg. These volumes are connected by 3 segments:

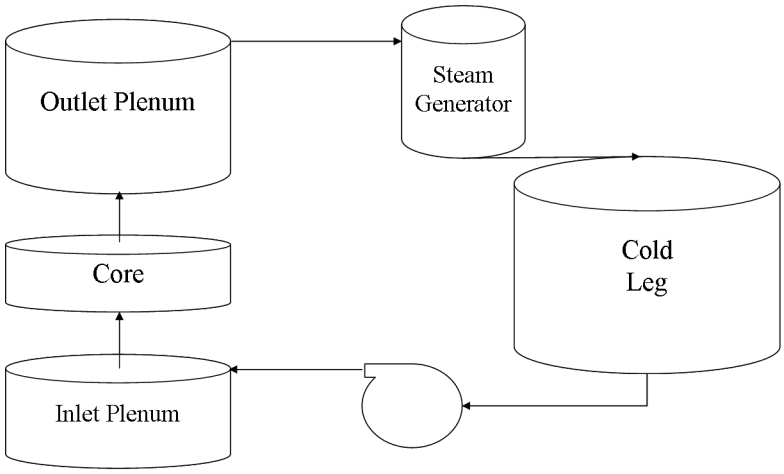

Figure 3.2: Simple scheme of the primary circuit model implemented in SAS4A/SASSYS-1.

core, SG and pump. The 3 segments are divided in 7 elements. The core segment is equal to the core element, while the other two segments (SG and pump) are made by 3 elements each one. The elements pipe, SG and pipe form the SG segment and the elements pipe, pump and pipe constitute the pump segment. Moreover, 4 temperature groups are defined: 3 for the segment SG and 1 for the segment pump. For the first a temperature group for each one of the elements (pipe, SG and pipe) is specified, while for the second an unique temperature group that includes all the elements (pipe, pump and pipe) is setted. The core is modeled as a 4-channel segment that contains only the fuel, neglecting the presence in the external region of the reflector and the shielding. In the figure 3.2 the two arrows, that connect the inlet and outlet plenum with the core, represent only the coolant flow direction, while the other four arrows symbolize the pipe segments. For each one of the volumes and of the segments are defined the volume, the elevation, the length, the flow area and the hydraulics diameter. In addition, the relative elevation between the core and the SG, the conductance coefficients of pipes and SG are specified. In this primary circuit model the eight pumps and the eight steam generators are simulated by only one pump and one SG. The minimum degree of implicitness is here setted to 0.8, thus an almost fully implicit calculations.

Here a specification is in order. Indeed, in the figure 3.2 the pump is located in the coldest part of the primary circuit, after the SG and the cold leg, while in the actual design of the SEALER reactor the pumps are located before the SG in the hottest part of the primary circuit. This inconsistency in the model is due to the fact that the design of the reactor has changed and with it also

the pumps position. However, the influence during an accident scenario of this different positioning of the pumps is expected to be negligible.

Continuing the description of the input file, the running parameters are: the total transient time, the maximum number of time step, the initial and maximum time step for the main time step and for the primary circuit time step, the maximum change in the temperature for each heat transfer time step, the flux and temperature convergence value and, finally, the time step intervals between two printed outputs regarding the main parameters (temperatures, pressure, coolant flow, etc.).

The last section is dedicated to the accident simulation that, in the case of UTOP, is represented by an external linear reactivity insertion in 1 second, for the ULOF scenario it is a linear coast down of the pump in 10 seconds and, finally, for the ULOHS it is a complete loss of the power removal capabilities of the SGs. A more detailed description of the accidents is done in chapter 5.

3.2 Serpent Code

3.2.1 General Overview

Serpent is a three-dimensional continuous-energy Monte Carlo reactor physics burnup calculation code and like any other Monte Carlo (probabilistic) code in the nuclear field it solves the problem of radiation transport simulating the particles behaviour, from the birth up to their death, by sampling all the events that they can undergo, according to defined occurrence probabilities. For example if σ_c, σ_f, $\sigma_{s,i}$, $\sigma_{s,e}$ and σ_T are respectively the capture, fission, inelastic scattering, elastic scattering and total cross sections of a given material the probabilities of occurrence for each possible kind of collision are:

$$
\begin{aligned}
P_c &= \frac{\sigma_c}{\sigma_T}, \\
P_f &= \frac{\sigma_f}{\sigma_T}, \\
P_{s,i} &= \frac{\sigma_{s,i}}{\sigma_T}, \\
P_{s,e} &= \frac{\sigma_{s,e}}{\sigma_T}, \\
P_c + P_f + P_{s,i} + P_{s,e} &= 1
\end{aligned}
$$

Using these definitions and introducing the cumulative probabilities as follow:

- $P_1 = P_c$;

- $P_2 = P_c + P_f$;
- $P_3 = P_c + P_f + P_{s,e}$;
- $P_4 = P_c + P_f + P_{s,i} + P_{s,e} = 1$;

thus generating a random number M, between 0 and 1, it is possible to determine which type of event takes place in this way:

- if $M \leq P1$ the simulated neutron is captured by the material nuclei;
- if $P1 \leq M \leq P2$ the simulated neutron generates a fission;
- if $P2 \leq M \leq P3$ an elastic scattering process takes place between neutron and the nuclei,
- if $P3 \leq M \leq P4$ an inelastic scattering process takes place.

This process used to determine the type of interaction can be extended also to all particles properties (energy, angle of motion etc.).

The random numbers in a Monte Carlo code are actually pseudo-random numbers because they are determined by generated through a suitable algorithm. As a consequence, running twice the same simulation, despite the stochastic character of the code, exactly the same results will be obtained.

The advantages of a Monte Carlo code with respect to a deterministic code that uses real discretised equations are the absence of any type of spatial meshes and energy discretization (figure 3.3). It with a probabilistic code the required computational time for a calculation is much longer, there is a difficulty to sample events with a very low probability of occurrence and it is possible to evaluate only the required tallies.

In a probabilistic code it is very important to achieve results with very low statistical errors, that means to have an high grade of precision. The parameters on which the precision depends are:

- tally type;
- variance reduction techniques;
- number of history to run.

For this kind of error the most significant element is the number of history to run (N), since the precision is proportional to $\frac{1}{\sqrt{N}}$: more histories (neutrons) are ran more precise will be the result. The obvious inconvenience is the great increase of the calculation time. The tally error might become relevant when there is a very small tally region or a very low occurrence probability of the

tallied event. Since in both these cases it is more difficult to get contributions to the tally estimate. The variance reduction techniques can help to increase the sampling efficiency in the previous cases.

In a probabilistic code the statistical errors are added to the systematic ones that are due to these three main factors:

- the code;
- the model that simulates the physics of the problem;
- the user.

The code contribution to the systematic error might come from the uncertainties in the data (such as the transport and reaction cross sections, Avogadro's number, atomic weights, etc.) or from the approximation of the mathematical models used to solve the equations (only for deterministic code). Instead the errors in the model are based on which kind of approximation are done for example in the geometry description or in the number of energy groups into which the neutron spectrum is divided. Finally, the user can be a very important source of errors due to his inexperience or his disattention during the preparation of the input file.

In order to obtain a good result it is necessary to reach both low statistical and systematic errors, that means precision and accuracy. Because it is useless to obtain a very precise result that does not represent the real behaviour of the physical process and the same is true for a very accurate result with a not properly precision. A deterministic code has only the systematic error.

Another important aspects that characterize Serpent are the geometry definition, the cross sections use and the Doppler routine. The geometry consists of material cells, defined by elementary quadratic and derived macrobody surface types. The code also provides some additional geometry features specifically for fuel design. These features include simplified definition of cylindrical fuel pins and spherical fuel particles, square and hexagonal lattices for LWR and fast reactor geometries, and circular cluster arrays for CANDU fuels. The random dispersion of microscopic fuel particles in high-temperature gas-cooled reactor fuels and pebble distributions in pebble-bed type HTGR cores can be modeled using geometry types specifically designed for the task.

Continuous-energy cross sections in the library files are reconstructed on a unionized energy grid, used for all reaction modes. Macroscopic cross sections for each material are pre-generated before the transport simulation. Instead of calculating the cross sections by summing over the constituent nuclides during tracking, the values are read from pre-generated tables, which is another effective way of improving the performance.

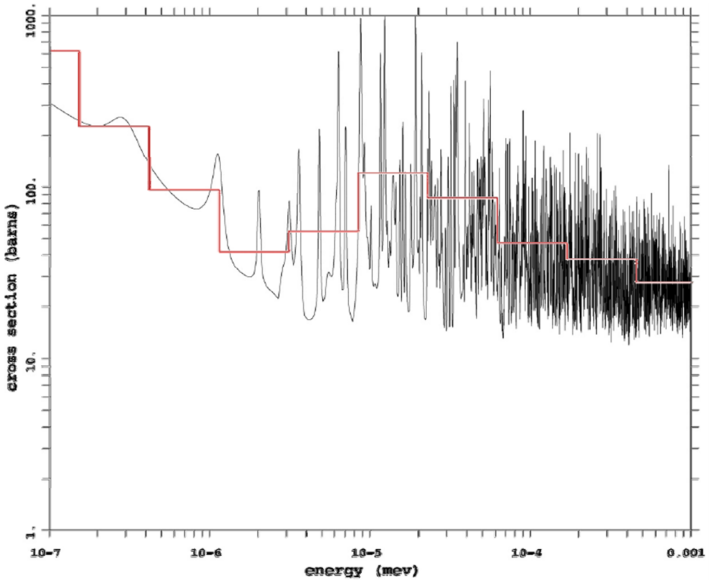

Figure 3.3: Comparison between a multigroup (red line) and a Monte Carlo point-wise (black line) cross section for the U^{235}.

A built-in Doppler-broadening preprocessor routine allows the conversion of ACE format cross sections into a higher temperature. This capability results in a more accurate description of the interaction physics in temperature-sensitive applications, as the data in the cross section libraries is available only in 300 K intervals [26].

3.2.2 Input File

The Serpent input file provides a very detailed 3 Dimensional description of the SEALER core. It starts with the definition of the pins and of their geometry and physical properties. They represent the elements to use to fill the other components of the Serpent universe-based geometry model: the lattices, the cells and the universe cells. Each pin is circular and it is made by different elements in the radial direction. For example, a fuel pin is made of fuel (UO_2), Krypton in the gap, cladding and coolant. In addition, there is a further division in axial levels due to the fact that the physical properties changes along the axial development of the core. After this step, the assembly lattices are defined. They are hexagonal and they contain the pins defined before in order to create axial slices of assemblies for each regions in the core (fuel, reflector, shielding and burn-up control elements). In the final step these slices are putted together to create the entire core, but before it is needed to define the cells and the universe cells with the purpose to reach the right radial geometry.

The cells define, in the radial direction, the geometry of the hexcan duct that has within it the assembly lattices defined before and outside it the coolant. Then these cells are used to fill the universe cells, that correspond to the whole core frame in the radial direction, but divided in axial levels. Thus these universe cells are putted together to obtain the whole core model, to do that, before, it is necessary to define the axial and radial dimensions of the whole core and also the length of all the single axial level for each region (fuel, reflector, shielding, and burn-up control elements).

The core is modeled as follow: the active zone is divided in 4 batches, that represent the 4 channels subdivision required by the SAS4A/SASSYS-1 model, and in 5 axial levels (figure 3.4).

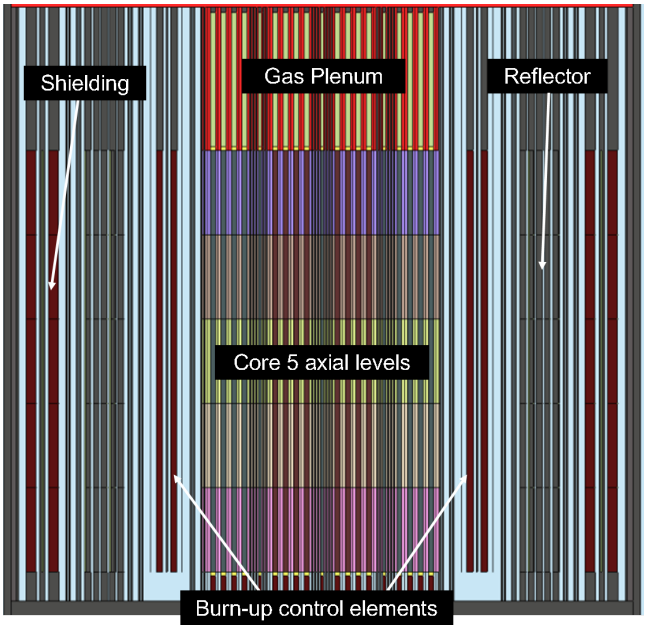

Figure 3.4: Core axial cross section.

The fuel region is completed by the definition of the gas plenum, the upper and lower insulator pellets and the lower shield inside the fuel pins (B_4C). The reflector and the shielding regions are divided in only 5 axial levels, instead for the burn-up control elements, there is any type of division. Moreover for all these three regions, the lower and the upper end caps are defined. In the 6 channels left empty by the withdrawn shutdown elements, there is lead with the same properties of that one in the lower plenum. This is an approximation that affects the K_{eff} but not the reactivity coefficients that depend on the difference between two K_{eff}. As explained in the section 4.2.4, this is true for all the reactivity coefficients with the exception of the coolant void worth that deserves

a specific treatment with some differences. The most important of which is the division in 5 axial levels also for the burn-up control elements in order to give a trend at the coolant temperature in that region.

3.3 Reactivity Coefficients

A reactivity coefficient expresses the change in the core reactivity value caused by a change in a given parameter and thus it is defined as the derivative of reactivity with respect to that parameter:

$$\alpha_i = \frac{\partial \rho}{\partial i} \tag{3.3}$$

where i is the parameter (fuel or coolant temperature, power, pressure etc.) that affects the reactivity ρ.

The reactivity coefficients are used to assess the influence of the different parameters on the core reactivity and its total amount determines the time change of the neutron population, thus the reactor power (figure 3.5). A general reactivity coefficient α_i produces a negative feedback when the variation of the parameter i gives an opposite response on the total reactivity. Therefore $\frac{\partial \rho}{\partial i} < 0$ means negative feedback and $\frac{\partial \rho}{\partial i} > 0$ means positive feedback.

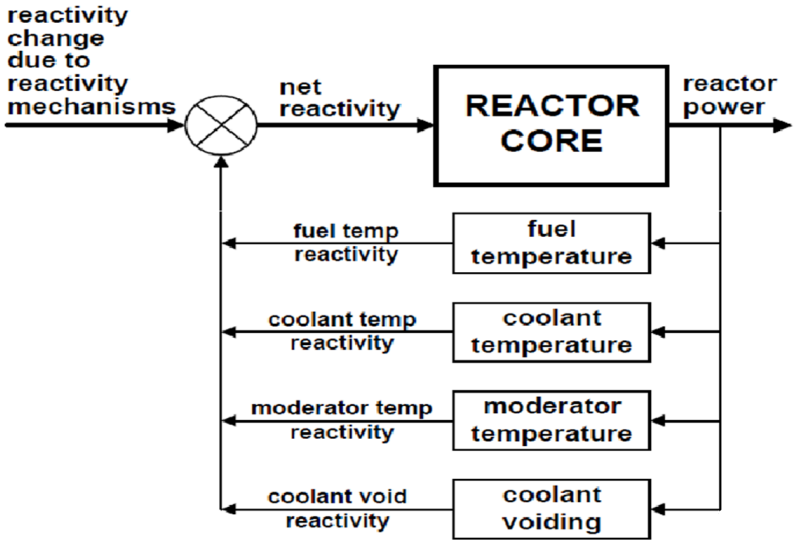

Figure 3.5: General scheme that represents the variation mechanism of the reactor power as a result of a perturbation.

The core reactivity is defined as follow:

$$\rho = \frac{K_{eff} - 1}{K_{eff}} \tag{3.4}$$

when the reactivity is greater than zero ($K_{eff} > 1$) the reactor is supercritical, when it is equal to zero ($K_{eff} = 1$) the reactor is critical and when it is lower than zero ($K_{eff} < 1$) the reactor is sub-critical. Generally, the reactor condition during normal operation indicates a steady state very close to the criticality (power constant), thus the equation (3.4) can be simplified:

$$\rho \simeq K_{eff} - 1$$

K_{eff} is the effective multiplication factor and it is defined as the ratio between number of neutrons generated in one generation divided by the sum of the number of neutrons absorbed and leaked in the previous one. For a thermal reactor the K_{eff} can be expressed with the 6 factors formula:

$$K_{eff} = \varepsilon p f \eta P_1 P_2 \tag{3.5}$$

where:

- $\varepsilon = \frac{number\ of\ neutrons\ generated\ by\ fast\ and\ thermal\ fissions}{number\ of\ neutrons\ generated\ by\ thermal\ fissions}$ is the fast fission factor;
- $p = \frac{number\ of\ neutrons\ that\ reach\ thermal\ energy}{number\ of\ fast\ neutrons\ that\ start\ to\ slow\ down}$ is the resonance escape probability;
- $f = \frac{number\ of\ thermal\ neutrons\ absorbed\ by\ the\ fuel}{total\ number\ of\ thermal\ neutrons\ absorbed\ in\ any\ reactor\ material}$ is the thermal utilization factor;
- $\eta = \frac{number\ of\ fast\ neutrons\ produced\ by\ thermal\ fission}{total\ number\ of\ thermal\ neutrons\ absorbed\ in\ the\ fuel}$ is the thermal fission factor;
- $P_1 = \frac{number\ of\ fast\ neutrons\ that\ do\ not\ leak\ from\ reactor}{number\ of\ fast\ neutrons\ produced\ by\ all\ fissions}$ is the fast neutrons non leakage probability;
- $P_2 = \frac{number\ of\ thermal\ neutrons\ that\ do\ not\ leak\ from\ reactor}{number\ of\ neutrons\ that\ reach\ thermal\ energies}$ is the thermal neutrons non leakage probability.

For a fast reactor the meaning of some factors are slightly different while some others are meaningless (p and P_2) and the 6 factors formula becomes a 4 factors one:

$$K_{eff} = \varepsilon P_1 f \eta \approx \varepsilon P_1 \sum_{i=1}^{N} \nu \frac{\sigma_{f,i}}{\sigma_{f,i} + \sigma_{c,i}} \tag{3.6}$$

where:

- $\varepsilon = \frac{number\ of\ neutrons\ generated\ by\ all\ fast\ fissions}{number\ of\ neutrons\ generated\ by\ fast\ fissions\ in\ fissile\ material}$ is the fast fission factor;
- $f = \frac{number\ of\ fast\ neutrons\ absorbed\ by\ the\ fuel}{total\ number\ of\ fast\ neutrons\ absorbed\ in\ any\ reactor\ material}$ is the fast utilization factor;
- $\eta = \frac{number\ of\ fast\ neutrons\ produced\ by\ fast\ fission}{total\ number\ of\ fast\ neutrons\ absorbed\ in\ the\ fuel}$ is the fast fission factor;
- $P_1 = \frac{number\ of\ fast\ neutrons\ that\ do\ not\ leak\ from\ reactor}{number\ of\ fast\ neutrons\ produced\ by\ all\ fissions}$ is the fast neutrons non leakage probability.

Without focusing on what type of reactor is studied, what is important to know in order to understand how a parameter like the fuel or coolant temperature affects the change in reactivity of any reactor, is how this parameter influence each one of the factor of the equations (3.5 or 3.6) and which is their relative magnitude. With the purpose to better understand this concept, a general reactivity coefficient, combining the equations (3.3), (3.4) and 3.5 and taking advantage of the reactor criticality condition during normal operation, can be expressed in this form:

$$\begin{cases} \alpha_i = \dfrac{\partial}{\partial i}\left(\dfrac{K_{eff}-1}{K_{eff}}\right) = \dfrac{1}{K_{eff}^2}\dfrac{\partial K_{eff}}{\partial i} \simeq \dfrac{1}{K_{eff}}\dfrac{\partial K_{eff}}{\partial i} \\ \alpha_i \simeq \dfrac{1}{K_{eff}}\dfrac{\partial K_{eff}}{\partial i} = \dfrac{1}{\varepsilon}\dfrac{\partial \varepsilon}{\partial i} + \dfrac{1}{p}\dfrac{\partial p}{\partial i} + \dfrac{1}{f}\dfrac{\partial f}{\partial i} + \dfrac{1}{\eta}\dfrac{\partial \eta}{\partial i} + \dfrac{1}{P_1}\dfrac{\partial P_1}{\partial i} + \dfrac{1}{P_2}\dfrac{\partial P_2}{\partial i} \end{cases} \tag{3.7}$$

The choice of using the 6 factors formula is just for a more general treatment of the topic, since the 4 factors one is simply derived from it as described above.

For a typical LWR the reactivity coefficients of interest are: Doppler (fuel temperature), moderator (moderator to fuel ratio), coolant void worth (coolant density or temperature), pressure and power. Instead for a LFR, since there is any type of moderator and the pressurization of the primary system is not needed (pressure serves only to overcome the pressure drop along the primary circuit) only Doppler and coolant void worth coefficients are of practical interest. Besides these two, there are also other coefficients own by fast reactors, on which it is useful to put the attention: fuel and cladding axial expansion, core radial expansion, and control elements driveline expansion. The addition of these parameters is essentially due to the configuration of the LFR cores: more flat and small, with a bigger surface to volume ratio and with greater neutron mean free path. All these things contributes to make the fast reactors more sensitive

to geometry variations than thermal one. A further and less important addition is the greater change in the temperatures of the core material due to the higher heat transfer property of the lead or sodium with respect to the water.

In this work the control elements driveline expansion is not taken into account because of their peripheral position in the core region that allows a negligible thermal expansion effect.

The reactivity coefficients described below are presented according to their response time, indeed the ones related to the fuel temperature are said prompt reactivity coefficients because they have a prompt feedback (in the order of microseconds), while the ones related to the coolant temperature are said delayed reactivity coefficients because they have a delayed feedback (in the order of seconds). The time on which the feedback acts is very important for safety reason and to have more negative feedback from the prompt ones, in order to have an immediate safety reaction in case of nuclear incident or accident, is preferred.

3.3.1 Doppler Coefficient

The Doppler coefficient is defined as follow:

$$\alpha_D = \frac{\partial \rho}{\partial T_{fuel}}$$

often the value of α_D is substituted by a more practical parameter:

$$K_D = \frac{\partial \rho}{\partial T_{fuel}} T_{fuel} = \alpha_D T_{fuel} \tag{3.8}$$

The Doppler coefficient is strictly related to the Doppler effect according to which there is a wide spectrum of relative energy between monoenergetic neutrons and the target nuclei, as a result of the vibration energy spectrum related to the material temperature (Maxwell-Boltzmann law). The nuclei vibration energies increase with the temperature and the cross sections broaden, and as a consequence there is a reduction in the height of the cross sections and an enlargement in their width (figure 3.6). This change in the cross sections shape is due to the fact that their area must be constant because it represents the interaction probability between the incident neutrons and the target nuclei. Like for any other cross section, the resonance peaks in the capture cross section undergo at this broadening effect. The change of the resonance peaks shape causes the increment of the neutron flux and thus of the capture reaction rate, because it enlarges the neutron spectrum that has to considered in the flux evaluation related to that peak. It means that a fuel temperature increase in a

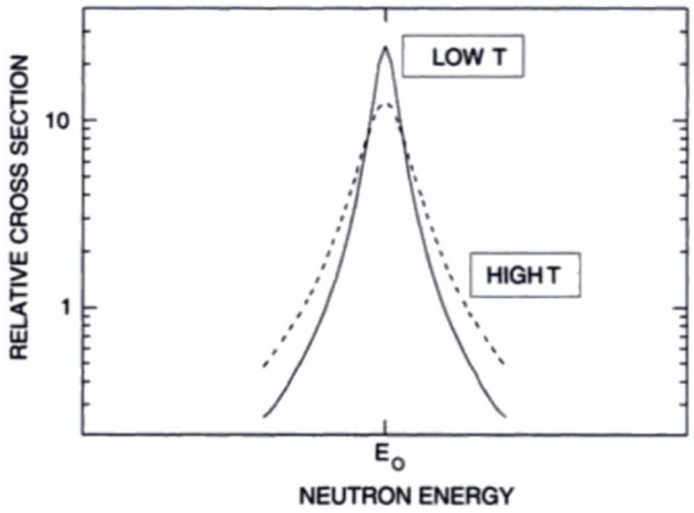

Figure 3.6: Example of cross section broadening following an increase in the temperature of the target nuclei.

material has the effect to reduce the neutron population (reactivity), since the capture reaction rate grows and less neutrons are able to reach the thermal energy (thermal reactor) or less neutrons are available to sustain the chain reaction (fast reactor). Thus, as a consequence, the Doppler coefficient is negative and it provides negative feedback. For a nuclear safety point of view this coefficient is very important both for its intrinsically and fast response to an accident scenario.

For fast reactor, the absolute value of the cross sections are lower, with the exception of σ_f for the U^{238}, if compared with the ones of a thermal reactor, but what is important is the relative magnitude of the capture cross section with respect to the fission one and it is almost the same. Moreover, the Doppler coefficient in a fast reactor has a lower value, since the neutron spectrum is harder than the energy region for the capture resonances.

It is not already mentioned but this phenomenon induces also a rise in the fission reaction rate and thus an increase in the core reactivity. This effect starts to be significant only with greater enrichment in fissile material with respect to the actual law limitation of 5% and 20%, respectively for thermal and fast reactors. Anyway this contribution gives a very little reduction in its magnitude.

The Doppler coefficient is related to the neutron spectrum hardness so that a harder spectrum gives lower (more positive) Doppler coefficient. For this reason putting uranium dioxide with lower enrichment as a fuel or more quantity (less porosity) of B_4C in the burn-up control elements or simply the build up of fission products in the fuel are all factors that bring an higher (more negative) Doppler coefficient. The minor actinides generated during the reactor life, especially the

americium, make it less negative due to their greater capture cross section for the neutron with respect to the uranium.

3.3.2 Fuel Axial Expansion Coefficient

This reactivity coefficient depends on two parameters: the fuel length and the fuel density. Indeed, a fuel temperature growth leads to an increase in the total core height (approximation of only axial expansion) and to a consequent reduction in the fuel density. In addition, these two contributions provide an opposite feedback: the first gives a positive reactivity insertion and the second a negative one as a result of the same fuel temperature increment. Their opposite feedback is valid also for the case of fall in the fuel temperature.

Studying the two effects separately, it is observed that the gain in the fuel length creates a new zone in which the fuel is present, while the lower density value decreases the total mass of the fuel reducing the number of fissions.

For a good core design the second effect must be greater than the first one in order to have an intrinsic negative feedback in case of fuel temperature rise and it is nearly always verified without any type of particular expedient. As a matter of fact, the reduction in the fuel density for a 1 m of active length has a greater effect than the increase of the fuel length of about few centimetres.

3.3.3 Cladding Axial Expansion Coefficient

The cladding material (Sandvik's 12R72 with FeCrAlY coatings) is composed mainly by non heavy atoms and, from a neutronic point of view, they act like a moderator. Thus, the cladding response, following a fuel or coolant temperature increase, supplies a reduction in the involuntary moderation and an hardening in the neutron spectrum. Like the fuel axial expansion coefficient, also this one for the cladding is made by the contributions of the change in the material density and length as a result of a temperature perturbation. However, the length effect variation can be neglected with respect to the one of the density, since the change of the moderation given by the cladding expansion or contraction is negligible if compared with the one given by the density reduction or increase in all the claddings.

An hypothetically diminution in the cladding density generates a decrease in the capture cross sections (σ_c) and an increase in the leakages with more effort in the periphery in both the direction radial and axial. Regarding the fission cross sections (σ_f), taking into account the fuel composition with an enrichment of 19.9%, its trend as a function of the energy and the energy of the neutron spectrum, both an increase and a reduction are expected. As shown in the figure 3.7, the reference energy for the neutron is a little bit lower than 1 MeV and as

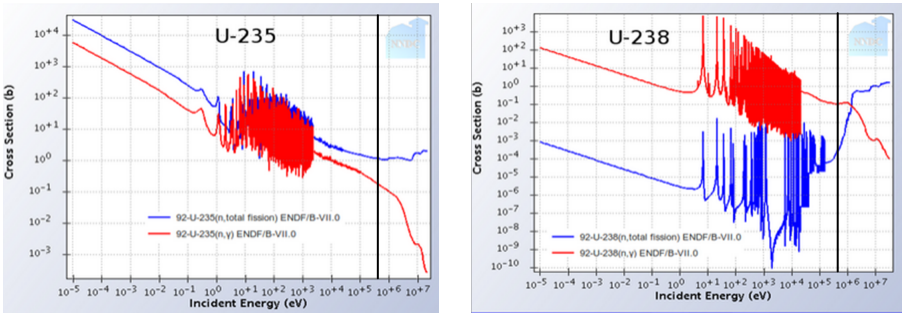

Figure 3.7: Capture and fission cross sections for the U^{235} and U^{238} with the marker for the mean neutron spectrum energy assessed at BOC.

a consequence of a reduction in the cladding density the σ_c^{238} is decreased and the σ_f^{238} is incremented, while the σ_c^{235} and the σ_f^{235} are both reduced.

Remembering the equation (3.6), the K_{eff} is proportional to the ratio $\sum_{i=1}^{N} \frac{\sigma_{f,i}}{\sigma_{f,i}+\sigma_{c,i}}$ and it is possible that a greater decrease in the $\sigma_{c,i}$ can have the effect to increase that ratio also with a reduction of $\sigma_{f,i}$. Thus, the feedback in each channel is a combination of all these effects and their relative magnitude decides if it is a positive or a negative one.

As a matter of fact, considering the effect of the new nuclides generation in the fuel (fission and activation products), it leads to a more positive value for the cladding axial expansion coefficient. This because the activation products give a great contribution to the total capture cross section of the fuel, thus when the spectrum becomes harder, as a result of reduction in the cladding density, there are more neutrons that escape from these captures and therefore the neutron population rise increasing the total reactivity. This effect is more important in the central part of the core where the production of these isotopes is higher. The softening in the neutron spectrum leads to have a reference starting energy at MOC and EOC a little bit moved on the left with respect to the lines in the figure 3.7.

3.3.4 Coolant Void Worth

The coolant void worth is defined as:

$$\alpha_C = \frac{\partial \rho}{\partial \alpha} \tag{3.9}$$

where α at the denominator is the coolant void fraction.

The coolant in a FBR deteriorates the neutron spectrum, thus a reduction in the coolant density, caused by an increment in the temperature or by a void formation for boiling (this latter case in LFR could happen rarely due to the

high boiling temperature of lead but for SFR it is a real possibility), determines an hardening in the spectrum, but with a less effort with respect to the cladding due to the greater atomic number of the lead. This fact reduces the magnitude in the variation of the parameters and it could promote the effect of the leakages over the others as a result of the small core dimension.

The impact on the total reactivity is the same of that described for the cladding axial expansion, thus this perturbation modifies the same parameters: the ratio $\sum_{i=1}^{N} \frac{\sigma_{f,i}}{\sigma_{f,i}+\sigma_{c,i}}$ and the leakages. Once again what decides the sign of total feedback is the relative magnitude between them.

The formation of new nuclides in the fuel due to the burn-up increase, leads to a degradation of the negative feedback especially given by the generation of americium and of the even isotopes of the plutonium. The reasons that explain this fact are the same of those described for the cladding axial expansion coefficient.

3.3.5 Radial Expansion Coefficient

The radial expansion coefficient is associated to the contraction and the expansion of the core structures as a consequence of the variation in the coolant temperature. The reasons for which a fast reactor is so sensitive to a geometry change are the small dimension, the greater value surface to volume ratio and the high neutrons mean free path. Moreover, since the coolant is lead and it has, like the other heavy metal, very good heat transfer property also in case of non fluid motion, the induced temperature variation in the structural materials can be quite high as well as the radial expansion. Along the axial direction the coolant temperature increases, therefore also the radial expansion of core does the same generating the so-called flower effect, that in the framework of this project is neglected.

As seen for the other coefficients, the reactivity tends to be greater in the central part of the core and lower in the periphery where there are more neutrons leakages. For this reason a radial expansion of the core moves the fuel assemblies from a region at high reactivity to another one with lower reactivity introducing a negative feedback. The opposite case of radial contraction instead produces a positive reactivity insertion.

This coefficient should be independent from the type of nuclides generated during the reactor life and also on the type of fuel enrichment and a constant value over the reactor life in criticality conditions is expected.

Chapter 4

SAS4A/SASSYS-1 Core Model Extension

This chapter deals with core model extension done in the SAS4A/SASSYS-1 input file. The reactivity coefficients are assessed at three different burn-up values for the fuel that correspond to Beginning Of Cycle (BOC) 0 days and 0 $\frac{MWday}{kg}$, Middle Of Cycle (MOC) 5913 days and 19.31 $\frac{MWday}{kg}$ and End Of Cycle (EOC) 9855 days and 32.19 $\frac{MWday}{kg}$. The fuel composition at EOC is evaluated with the hypothesis that the reactor works for 27 years at full power or for 30 years with 90% of availability. In addition, the presented data are evaluated according to the SAS4A/SASSYS-1 input file specifics and not properly to the rigorous definitions described in the previous chapter. For the latter case, in the last section of the chapter there is a table that summarizes the time evolution of the reactivity coefficients (table 4.18).

4.1 From 1-channel to 4-channel Model

This is the preliminary part of the work and it consists in the extension of the core model from a 1-channel one to a 4-channel one. The choice of a 4-channel model is based on core geometry and assemblies Peak Factors (PFs). As it is possible to see in the figure 4.1, the 19 core assemblies can be subdivided in 4 channels each one with a different peak factor:

- Channel 1 = central assembly (PF=1.52)
- Channel 2 = first ring of 6 assemblies (PF=1.30)
- Channel 3 = 6 assemblies of the second ring not in touch with shutdown elements (PF=0.88)

- Channel 4 = 6 assemblies of the second ring in touch with shutdown elements (PF=0.73)

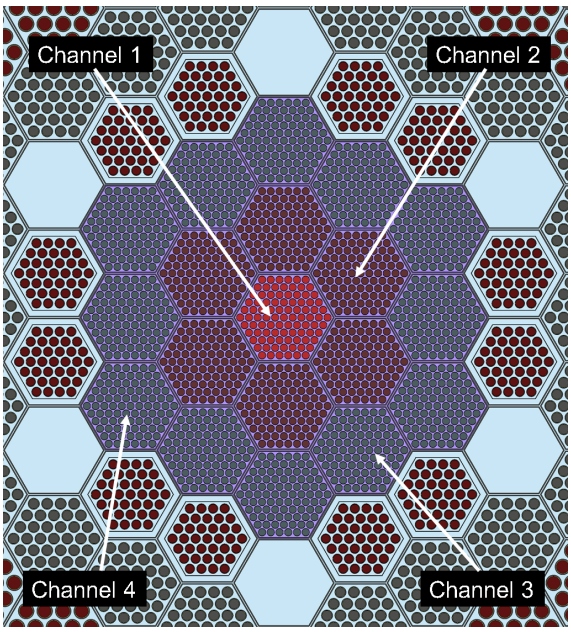

Figure 4.1: Zoomed view on the 19 fuel assemblies and on the ring of 12 burn-up control elements.

The second ring of assemblies can be divided in two different channels because the 6 shutdown elements, the azure hexagons without pins inside in figure 4.1, during reactor normal operation are withdrawn. The space left free by them is occupied by the lead, thus in the 6 fuel assemblies of the second ring that are in touch also with these elements, the PF is lower due to the more leakages with respect to the other 6 fuel assemblies that are in touch only with the burn-up control elements. The PFs presented above are assessed for the BOC core configuration and the approximation, that they are the same over the reactor lifetime, is made. This is a conservative assumption, indeed as a result of the different fuel consumption and of the withdrawal of the burn-up control elements, the PFs tend to be more uniform along the radial direction as the reactor life increase. Their quite high difference at BOC is a consequence of the burn-up control elements periphery position.

4.2 Channel Dependent Reactivity Coefficients

The second and more important step consists of to calculate, with the Serpent code, the channel dependent reactivity coefficients for the 4 channels, to

implement these data in the SAS4A/SASSYS-1 input file and to perform the multi-channel transient analysis of SEALER in a much more completed and detailed way.

The importance of the reactivity coefficients during an unprotected accident is basic because there is no activation of both the reactor shutdown systems and they are the only inherent feature that can prevent a serious accident development with possible fuel and cladding damage. Thus, it is necessary to evaluate their behaviour over the reactor life and to make sure that the core design is such as to ensure intrinsic negative feedback following an accident initiating event. Moreover for the ULOF scenario, it is important to establish if the natural circulation takes place in order to cool the reactor in middle and long term.

In the following part of this chapter all the results presented for the K_{eff} are obtained with a statistical error of 4 pcm ($\sigma = \pm 0.00004$). To find this very low value of uncertainty all the calculations are performed with this configuration: 1000000 neutrons 330 active cycles and 30 inactive cycles.

Three values of K_{eff} with reference geometry, all the cross sections data library for the fuel assessed at 600 K and with fuel, cladding and coolant density at nominal values as well as fuel length and pitch between the assemblies, are taken as reference for the three burn-up cases:

$$\begin{cases} K_{eff600\_BOC} = 1.00108 \\ K_{eff600\_MOC} = 0.99485 \\ K_{eff600\_EOC} = 1.00596 \end{cases} \tag{4.1}$$

Analysing these three data, it is possible to see that they are quite far from the criticality condition ($K_{eff} = 1$), in which the reactor is supposed to work during its entire life. The reasons of this fact are multiple. The first is that the criticality configuration for the fuel cross sections data library over the entire life is 600 K for the lower axial level and 900 K for the remaining four, with this configuration a lower value of K_{eff} is obtained. The second and more effective is the burn-up control elements position. The core model in Serpent allows to move them only by discretised positions of 22 cm and thus it is almost impossible to match the criticality condition. At MOC, when they are all withdrawn of 3 axial levels, there is a sub-criticality condition of about 500 pcm, if another level of extraction is applied the results is $K_{eff600\_MOC} = 1.01467$. It is clear that the correct position of the burn-up control elements, to reach the criticality, should be in the lower part of third axial level. Regarding the K_{eff600_EOC}, when all the burn-up control elements are withdrawn, the almost 600 pcm of excess in reactivity mean that there is some margin with the purpose to extend the reactor life without any fuel reload for brief time (3 years). Since the EOC

fuel is assessed for 30 years at 90% of availability, this fact can be also seen as a possibility to have a reactor that works 30 years with an availability of 100%. The last factor that increases the values of the K_{eff} in the equation (4.1) is the approximation of constant coolant temperature in the channels left free by the withdrawn shutdown elements and occupied by the burn-up control elements. As a matter of fact, with a coolant temperature that increases along the axial direction, the leakages grows and lower K_{eff} values are obtained.

Regarding the latter assumption, as explained in the coolant void worth section (4.2.4), it is not still valid for this coefficient and thus it is necessary to take other three reference values for the K_{eff} with a variation of the lead temperature and of the density along the axial direction also in this core region. The results are:

$$\begin{cases} K_{eff600\_BOC} = 1.00037 \\ K_{eff600\_MOC} = 0.99443 \\ K_{eff600\_EOC} = 1.00578 \end{cases} \tag{4.2}$$

Making a comparison between the values given in the equations (4.1) and (4.2), it can be noted a K_{eff} reduction with the second configuration and that this drop is decreasing over the reactor lifetime. The latter consideration is a consequence of the neutron spectrum softening (less leakages) due to the generation of fission products in the fuel and of the withdrawal of the burn-up control elements that promote the moderation provided by the reflector elements.

4.2.1 Doppler Coefficient

For what it concerns this reactivity coefficient in the SAS4A/SASSYS-1 input file one has to insert two different values for each channel, one for normal state and one for voided state of the core. The first value is simply calculated by changing channel by channel the fuel temperature from the reference value of 600 K to 1800 K and putting the corresponding value of $K_{eff1800\_i,j}$ in the equation:

$$K_{Di,j} = \left(\frac{K_{eff1800\_i,j} - 1}{K_{eff1800\_i,j}} - \frac{K_{eff600\_j} - 1}{K_{eff600\_j}} \right) \Big/ log(1800/600) \tag{4.3}$$

where i is the fuel channel that is at 1800 K (i=1, 2, 3, 4 or Tot), j the core burn-up (j=BOC, MOC or EOC) and $K_{Di,j} = [pcm]$.

The second value is determined setting equal to zero the lead density (voided state of the core) and evaluating the Doppler coefficient using the equation (4.3) between the configurations in which all the fuel is respectively at 600 K and 1800 K. Then, in order to give a different value to each channel, it is multiplied

by the ratios: Doppler coefficient of one channel divided by the total Doppler coefficient, both assessed for the normal state of the core.

4.2.1.1 BOC

The results for $K_{eff1800\_i,BOC}$ of each channel for normal and voided state conditions are:

$$K_{eff1800\_1,BOC} = 1.00081 \tag{4.4}$$

$$K_{eff1800\_2,BOC} = 0.99958 \tag{4.5}$$

$$K_{eff1800\_3,BOC} = 1.00046 \tag{4.6}$$

$$K_{eff1800\_4,BOC} = 1.00062 \tag{4.7}$$

$$K_{eff1800\_Tot,BOC} = 0.99817 \tag{4.8}$$

$$K_{eff600\_Tot\_VOID,BOC} = 0.97095 \tag{4.9}$$

$$K_{eff1800\_Tot\_VOID,BOC} = 0.96824 \tag{4.10}$$

Putting the previous values (4.4), (4.5), (4.6), (4.7) and (4.8) in the equation (4.3) with also the reference value (4.1), one obtains the data presented in the table 4.1. The last line of this table contains the data calculated for all the fuel with a temperature of 1800 K and it has to be compared with the data of the penultimate line, obtained summing up the values for each channel.

$[pcm]$	**Per Channel**	**Per Assemblies (-)**
K_{D1}	-24.5	-24.5 (1)
K_{D2}	-136.4	-22.7 (6)
K_{D3}	-56.3	-9.4 (6)
K_{D4}	-41.8	-6.9 (6)
K_{D_TOTAL}	-259.1	-13.7 (19)
K_{D_TOTAL}	-265.1	-13.9 (19)

Table 4.1: Doppler coefficient evaluated in core normal state at BOC.

Making use of the data in the equations (4.9) and (4.10), placing them in the equation (4.3) and remembering how to calculate the Doppler coefficient for the voided state core condition presented above, the data of the table 4.2 are achieved.

$[pcm]$	**Per Channel**	**Per Assemblies (-)**
K_{D1}	-24.3	-24.3 (1)
K_{D2}	-135.1	-22.5 (6)
K_{D3}	-55.8	-9.3 (6)
K_{D4}	-41.4	-6.9 (6)
K_{D_TOTAL}	-262.4	-13.8 (19)

Table 4.2: Doppler coefficient evaluated in core voided state at BOC.

4.2.1.2 MOC

The results for $K_{eff1800\_i,MOC}$ of each channel for normal and voided state conditions are:

$$K_{eff1800\_1,MOC} = 0.99456 \tag{4.11}$$

$$K_{eff1800\_2,MOC} = 0.99344 \tag{4.12}$$

$$K_{eff1800\_3,MOC} = 0.99405 \tag{4.13}$$

$$K_{eff1800\_4,MOC} = 0.99419 \tag{4.14}$$

$$K_{eff1800\_Tot,MOC} = 0.99158 \tag{4.15}$$

$$K_{eff600\_Tot\_VOID,MOC} = 0.97033 \tag{4.16}$$

$$K_{eff1800\_Tot\_VOID,MOC} = 0.96738 \tag{4.17}$$

Putting the previous values (4.11), (4.12), (4.13), (4.14) and (4.15) in the equation (4.3) with also the reference value (4.1), one obtains the data presented in the table 4.3. The last line of this table contains the data calculated for all the fuel with a temperature of 1800 K and it has to be compared with the data of the

penultimate line, obtained summing up the values for each channel.

$[pcm]$	Per Channel	Per Assemblies (-)
K_{D1}	-26.7	-26.7 (1)
K_{D2}	-129.9	-21.6 (6)
K_{D3}	-73.6	-12.3 (6)
K_{D4}	-60.7	-10.1 (6)
K_{D_TOTAL}	-290.9	-15.3 (19)
K_{D_TOTAL}	-301.7	-15.9 (19)

Table 4.3: Doppler coefficients assessed in core normal state at MOC.

Making use of the data in the equations (4.16) and (4.17), placing them in the equation (4.3) and remembering how to calculate the Doppler coefficient for the voided state core condition presented above, the data of the table 4.4 are achieved.

$[pcm]$	Per Channel	Per Assemblies (-)
K_{D1}	-25.3	-25.3 (1)
K_{D2}	-123.1	-20.5 (6)
K_{D3}	-69.8	-11.6 (6)
K_{D4}	-57.6	-9.6 (6)
K_{D_TOTAL}	-286.1	-15.1 (19)

Table 4.4: Doppler coefficients assessed in core voided state at MOC.

4.2.1.3 EOC

The results for $K_{eff1800\_i,EOC}$ of each channel for normal and voided state conditions are:

$$K_{eff1800\_1,EOC} = 1.00564 \tag{4.18}$$

$$K_{eff1800\_2,EOC} = 1.00437 \tag{4.19}$$

$$K_{eff1800\_3,EOC} = 1.00477 \tag{4.20}$$

$$K_{eff1800\_4,EOC} = 1.00499 \tag{4.21}$$

$$K_{eff1800\_Tot,EOC} = 1.00208 \tag{4.22}$$

$$K_{eff600\_Tot\_VOID,EOC} = 0.98933 \tag{4.23}$$

$$K_{eff1800\_Tot\_VOID,EOC} = 0.98566 \tag{4.24}$$

Putting the previous values (4.18), (4.19), (4.20), (4.21) and (4.22) in the equation (4.3) with also the reference value (4.1), one obtains the data presented in the table 4.5. The last line of this table contains the data calculated for all the fuel with a temperature of 1800 K and it has to be compared with the data of the penultimate line, obtained summing up the values for each channel.

$[pcm]$	**Per Channel**	**Per Assemblies (-)**
$\boldsymbol{K_{D1}}$	-28.8	-28.8 (1)
$\boldsymbol{K_{D2}}$	-143.2	-23.9 (6)
$\boldsymbol{K_{D3}}$	-107.2	-17.9 (6)
$\boldsymbol{K_{D4}}$	-87.3	-14.6 (6)
$\boldsymbol{K_{D\_TOTAL}}$	-366.5	-19.3 (19)
$\boldsymbol{K_{D\_TOTAL}}$	-350.3	-18.4 (19)

Table 4.5: Doppler coefficients calculated in core normal state at EOC.

Making use of the data in the equations (4.23) and (4.24), placing them in the equation (4.3) and remembering how to calculate the Doppler coefficient for the voided state core condition presented above, the data of the table 4.6 are achieved.

$[pcm]$	**Per Channel**	**Per Assemblies (-)**
$\boldsymbol{K_{D1}}$	-28.1	-28.1 (1)
$\boldsymbol{K_{D2}}$	-140.1	-23.3 (6)
$\boldsymbol{K_{D3}}$	-104.8	-17.5 (6)
$\boldsymbol{K_{D4}}$	-85.4	-14.2 (6)
$\boldsymbol{K_{D\_TOTAL}}$	-342.6	-18.0 (19)

Table 4.6: Doppler coefficients calculated in core voided state at EOC.

4.2.1.4 Results Discussion

Comparing the data presented in the tables 4.1, 4.2, 4.3, 4.4, 4.5 and 4.6, it is possible to note the increase in the negative value of the Doppler coefficient. This trend has more effort passing from MOC to EOC and in the peripheral channels (3 and 4). This is due to softening of the neutron spectrum over the reactor lifetime, as a consequence of the fission products generation and also of the greater moderation given by the reflector elements when the burn-up control ones are withdrawn. As a matter of fact, when there is a fuel temperature growth and a broadening of the cross sections, with a softer neutron spectrum, the number of neutrons affected by the capture phenomenon rises and also the negative reactivity insertion has the same behaviour.

The values for the total core Doppler coefficient presented in the table 4.1 are lower if compared with the ones for LWR and also with the others LFR [5, 27–29]. For the first case, one can think that it is an obvious thing for the harder neutron spectrum of a LFR with respect to a LWR, while for the second one, the reason of that must be searched in the small dimension of the SEALER reactor. Indeed it leads to have a smaller quantity of coolant in the core region, thus to a smaller moderation by the lead and at the end to an harder neutron spectrum with respect to the other LFR.

As can be seen from the results presented above, the Doppler coefficient in the voided state is the $95-99\%$ of the one in the normal state. This is due to the absence of the lead and of its involuntary moderation that makes the neutron spectrum harder. Moreover, comparing the data presented in the equations (4.1), (4.9), (4.16) and (4.23), it is possible to understand why the drain of the pool could be taken as an alternative second SCRAM system: negative insertion of about 3100 pcm at BOC, 2500 pcm at MOC and 1700 pcm at EOC. The decrease in the reactivity insertion is due to the softening of the neutron spectrum that generates less leakages as the burn-up increase.

4.2.2 Fuel Axial Expansion Coefficient

As discussed in the section 3.3.2, the fuel axial expansion coefficient depends on the change in fuel density and fuel length. The general formula to assess these two contributions are presented below (equations (4.25) and (4.26)). Both are divided by the fuel mass fraction that generates the variation in the reactivity with the purpose to satisfy the SAS4A/SASSYS-1 input file requests, that include also to give a value for this coefficient at each one of the 23 axial nodes in which the core is divided. The assumption that this coefficient does not change along the axial direction is made. Regarding the raise of the fuel axial length another approximation is done: the uniform axial expansion of the core, as a matter of

fact in the real case there is a different expansion based on the different fuel temperatures in the 4 channels (different PFs). As a consequence, the equation (4.26) refers to the whole core expansion and to evaluate the contribution of each channel, it is necessary to divide its value by the total number of assemblies (19) and then to multiply for the number of assemblies of the related channel (1-6-6-6).

The values for $K_{eff\_i,j}$ in the equation (4.25) are achieved reducing the fuel density of 5% in one channel at a time keeping constant the fuel length, while for the values of $K_{eff\_length,j}$ in the equation (4.26), the total active length of the fuel is increased by 5% keeping constant the fuel density.

$$R_{fd\_i,j} = \left(\frac{K_{eff\_i,j} - 1}{K_{eff\_i,j}} - \frac{K_{eff600\_j} - 1}{K_{eff600\_j}} \right) \Big/ (\alpha_1 \cdot M_{Fuel\_i}) \tag{4.25}$$

$$R_{fh\_j} = \left(\frac{K_{eff\_length,j} - 1}{K_{eff\_length,j}} - \frac{K_{eff600\_j} - 1}{K_{eff600\_j}} \right) \Big/ (\alpha_2 \cdot M_{Fuel}) \tag{4.26}$$

Where i represents the fuel channel (i=1, 2, 3 or 4), j the core burn-up (j=BOC, MOC or EOC), α_1 the fraction of reduction in the fuel density and α_2 the increase fraction in the fuel length. Both the α are equal to 0.05. The final value for this coefficient is the sum of these two contributions and it is expressed in $\left[\frac{pcm}{kg_{fuel}}\right]$. The two fuel masses at the denominator are evaluated as follow:

$$M_{Fuel\_i} = \sum_{k=1}^{5} \rho_{i,k} \cdot N_{Ui,k} \cdot A_{fuelpin} \cdot L_k \cdot 91 \cdot 19$$

$$M_{Fuel} = \sum_{i=1}^{4} M_{Fuel\_i}$$

where k is the axial level (k=1,2,3,4 or 5), $\rho_{i,k}$ the fuel density in the axial level k of the channel i, $N_{Ui,k}$ the percentage of Uranium nuclides in the fuel density, $A_{fuelpin}$ the fuel pin area per unit of pin and L_k the axial length of each axial level (22 cm). $91 \cdot 19$ represents the total number of fuel pins. The further subdivision of each channel in axial levels, it is needed since at MOC and EOC the fuel density and the percentage of uranium nuclides vary channel by channel and axial level by axial level. Instead at BOC, the fuel has the same composition and density, thus this subdivision is redundant.

4.2.2.1 BOC

The results for $K_{eff\_i,BOC}$ and $K_{eff\_length,BOC}$ of each channel are:

$$K_{eff\_1,BOC} = 0.99902 \tag{4.27}$$

$$K_{eff\_2,BOC} = 0.99124 \tag{4.28}$$

$$K_{eff\_3,BOC} = 0.99531 \tag{4.29}$$

$$K_{eff\_4,BOC} = 0.99683 \tag{4.30}$$

$$K_{eff\_length,BOC} = 1.00665 \tag{4.31}$$

Putting the previous values (4.27), (4.28), (4.29), (4.30) and (4.31) in the equations (4.25) and (4.26) with also the reference value (4.1), one obtains the data presented in the table 4.7.

$[pcm/kg_{fuel}]$	**Density**	**Length**	**Total**
$\boldsymbol{R_{F1}}$	-31.88	0.24	-31.64
$\boldsymbol{R_{F2}}$	-25.64	1.42	-24.2
$\boldsymbol{R_{F3}}$	-14.96	1.42	-13.54
$\boldsymbol{R_{F4}}$	-11.01	1.42	-9.59
$\boldsymbol{R_{F}}$	-17.53	4.51	-16.61

Table 4.7: Fuel axial expansion coefficient at BOC.

4.2.2.2 MOC

The results for $K_{eff\_i,MOC}$ and $K_{eff\_length,MOC}$ of each channel are:

$$K_{eff\_1,MOC} = 0.99305 \tag{4.32}$$

$$K_{eff\_2,MOC} = 0.98582 \tag{4.33}$$

$$K_{eff\_3,MOC} = 0.98914 \tag{4.34}$$

$$K_{eff\_4,MOC} = 0.99059 \tag{4.35}$$

$$K_{eff\_length,MOC} = 1.00094 \tag{4.36}$$

Putting the previous values (4.32), (4.33), (4.34), (4.35) and (4.36) in the equations (4.25) and (4.26) with also the reference value (4.1), one obtains the data presented in the table 4.8.

$[pcm/kg_{fuel}]$	**Density**	**Length**	**Total**
$\boldsymbol{R_{F1}}$	-29.46	0.40	-29.06
$\boldsymbol{R_{F2}}$	-24.68	2.40	-22.28
$\boldsymbol{R_{F3}}$	-15.40	2.40	-13.0
$\boldsymbol{R_{F4}}$	-11.47	2.40	-9.07
$\boldsymbol{R_{F}}$	-17.83	7.54	-15.56

Table 4.8: Fuel axial expansion coefficient at MOC.

4.2.2.3 EOC

The results for $K_{eff\_i,EOC}$ and $K_{eff\_length,EOC}$ of each channel are:

$$K_{eff\_1,EOC} = 1.00432 \tag{4.37}$$

$$K_{eff\_2,EOC} = 0.99794 \tag{4.38}$$

$$K_{eff\_3,EOC} = 1.00066 \tag{4.39}$$

$$K_{eff\_4,EOC} = 1.00165 \tag{4.40}$$

$$K_{eff\_length,EOC} = 1.01153 \tag{4.41}$$

Putting the previous values (4.37), (4.38), (4.39), (4.40) and (4.41) in the equations (4.25) and (4.26) with also the reference value (4.1), one obtains the data presented in the table 4.9.

$[pcm/kg_{fuel}]$	Density	Length	Total
R_{F1}	-26.97	0.25	-26.75
R_{F2}	-21.94	1.50	-20.44
R_{F3}	-14.23	1.50	-12.73
R_{F4}	-11.56	1.50	-10.06
R_F	-16.4928	4.7013	-15.07

Table 4.9: Fuel axial expansion coefficient at EOC.

4.2.2.4 Results Discussion

Analysing the tables 4.7, 4.8 and 4.9, it can be noted that the reduction of the fuel density has a negative feedback, while the gain in the fuel length produces a positive reactivity insertion. Anyway, the first effect is larger and their sum gives always a negative value, even if a little bit decreasing.

The values for both the terms of this coefficient were supposed to be slightly less negative as time goes on due to the formation of the activation and fission products in the fuel, instead oscillating results are found. The reason for that behaviour is the different condition in which they are assessed: BOC and EOC are in a supercritical configurations instead MOC is in a sub-critical one. In the latter case with respect to the other, the same fuel axial expansion produces a bigger positive reactivity insertion for the fuel length and a lower negative feedback for the fuel density because it creates a new fuel zone but with a reduced density in a system where the number of neutrons is decreasing. Since the fuel density component has a greater value, it provides a more negative feedback. However, the fluctuating behaviour, observed in the channel by channel analysis, is not evident comparing only the total coefficients for the whole core in the BOC, MOC and EOC configurations.

4.2.3 Cladding Axial Expansion Coefficient

The cladding axial expansion coefficient is assessed using the equation (4.42) and the values for $K_{eff\_i,j}$ are calculated setting zero the cladding density one by one in the 4 channels. Since the SAS4A/SASSYS-1 input file requires values per unit of cladding mass, they are normalized with the total core cladding mass (M_{Clad}). For this coefficient, contrary to the fuel axial expansion one, the effect of the gain in the axial length is negligible with respect to the one of density reduction.

$$R_{c\_i,j} = \left(\frac{K_{eff\_i,j} - 1}{K_{eff\_i,j}} - \frac{K_{eff600\_j} - 1}{K_{eff600\_j}} \right) \Big/ M_{Clad} \tag{4.42}$$

Where i represents the channel (i=1, 2, 3 or 4) and j the core burn-up (j=BOC, MOC or EOC). $R_{c\_i,j}$ is expressed in $[pcm/kg_{clad}]$.

4.2.3.1 BOC

The results for $K_{eff\_i,BOC}$ of each channel are:

$$K_{eff\_1,BOC} = 1.00178 \tag{4.43}$$

$$K_{eff\_2,BOC} = 1.00203 \tag{4.44}$$

$$K_{eff\_3,BOC} = 0.99834 \tag{4.45}$$

$$K_{eff\_4,BOC} = 0.99857 \tag{4.46}$$

$$K_{eff\_Tot,BOC} = 0.99743 \tag{4.47}$$

Putting the previous values (4.43), (4.44), (4.45), (4.46) and (4.47) in the equation (4.42) with also the reference value (4.1), one achieves the data shown in the table 4.10. The first value in the last line is calculated summing the ones of each channel, while the second is evaluated with all the cladding density setted to zero.

$[pcm/kg_{clad}]$	**Total**	**Per Assemblies (-)**
R_{C1}	0.21	0.21 (1)
R_{C2}	0.29	0.05 (6)
R_{C3}	-0.83	-0.14 (6)
R_{C4}	-0.76	-0.13 (6)
TOTAL	-1.09	-1.07

Table 4.10: Cladding axial expansion coefficient at BOC.

4.2.3.2 MOC

The results for $K_{eff\_i,MOC}$ of each channel are:

$$K_{eff\_1,MOC} = 0.99559 \tag{4.48}$$

$$K_{eff\_2,MOC} = 0.99676 \tag{4.49}$$

$$K_{eff\_3,MOC} = 0.99320 \tag{4.50}$$

$$K_{eff\_4,MOC} = 0.99305 \tag{4.51}$$

$$K_{eff\_Tot,MOC} = 0.99390 \tag{4.52}$$

Putting the previous values (4.48), (4.49), (4.50), (4.51) and (4.52) in the equation (4.42) with also the reference value (4.1), one achieves the data shown in the table 4.11. The first value in the last line is calculated summing the ones of each channel, while the second is evaluated with all the cladding density setted to zero.

$[\boldsymbol{pcm/kg_{clad}}]$	**Total**	**Per Assemblies (-)**
$\boldsymbol{R_{C1}}$	0.23	0.23 (1)
$\boldsymbol{R_{C2}}$	0.58	0.10 (6)
$\boldsymbol{R_{C3}}$	-0.51	-0.08 (6)
$\boldsymbol{R_{C4}}$	-0.55	-0.09 (6)
TOTAL	-0.25	-0.29

Table 4.11: Cladding axial expansion coefficient at MOC.

4.2.3.3 EOC

The results for $K_{eff\_i,EOC}$ of each channel are:

$$K_{eff\_1,EOC} = 1.00681 \tag{4.53}$$

$$K_{eff\_2,EOC} = 1.00891 \tag{4.54}$$

$$K_{eff\_3,EOC} = 1.00553 \tag{4.55}$$

$$K_{eff\_4,EOC} = 1.00505 \tag{4.56}$$

$$K_{eff\_Tot,EOC} = 1.00853 \tag{4.57}$$

Putting the previous values (4.53), (4.54), (4.55), (4.56) and (4.57) in the equation (4.42) with also the reference value (4.1), one achieves the data shown in the

table 4.12. The first value in the last line is calculated summing the ones of each channel, while the second is evaluated with all the cladding density setted to zero.

$[pcm/kg_{clad}]$	Total	Per Assemblies (-)
R_{C1}	0.25	0.25 (1)
R_{C2}	0.88	0.15 (6)
R_{C3}	-0.13	-0.02 (6)
R_{C4}	-0.27	-0.04 (6)
TOTAL	0.73	0.77

Table 4.12: Cladding axial expansion coefficient at EOC.

4.2.3.4 Results Discussion

Making a comparison between the data presented in the tables 4.10, 4.11 and 4.12, it can be observed that the channels 1 and 2 have a positive feedback, while the channels 3 and 4 ensure a negative reactivity insertion. In addition, the cladding axial expansion coefficient for the whole core, that has a negative feedback for the BOC and less negative for the MOC configurations, becomes slightly positive in the EOC one.

The explanation of a similar behaviour can be found analysing the different relative magnitude in the parameters variation, as a consequence of the same perturbation (a neutron spectrum hardening due to the reduction in the cladding density), between the increment in the ratio $\sum_{i=1}^{N} \frac{\sigma_{f,i}}{\sigma_{f,i}+\sigma_{c,i}}$ and in the leakages term. As it is possible to see in the table 4.13, in the central part of the core (channels 1 and 2) prevails the positive feedback related to the increment in the cross sections ratio with a lower decrease in the fast neutrons non leakage probability, while in the periphery (channels 3 and 4) happens the opposite and the leakages term outnumbers the positive reactivity insertion leading to a negative feedback. Moreover, in the third channel there are more leakages than in the fourth. It is a consequence of the different neutron energy in the two channel that is larger for the third.
In order to obtain the data in the table 4.13, these assumptions are done: ε=1.2, ν=2.51, the value for the cross sections ratio coming from the product $f \cdot \eta$ is calculated putting detectors [30] in the fuel with the purpose to evaluate the cross sections and the value of P_1 is assessed using the formula (3.6) in which is the only unknown. The K_{eff} for each channel is found reducing the cladding density of the 20%. The positive reactivity insertion in the channel 1 and the very low negative one in the others for factor P_1 are due to the approximation

[pcm]	$f \cdot \eta$	Change	P_1	Change
Reference	1.49159	-	0.55885	-
Channel 1	1.49184	25	0.55887	+2
Channel 2	1.49297	23	0.55849	-6
Channel 3	1.49252	15.5	0.55821	-10.7
Channel 4	1.49230	11.8	0.55827	-9.7

Table 4.13: Comparison between the variation in the product $f \cdot \eta$ and in the fast neutrons non leakage probability foe the cladding axial expansion coefficient at BOC.

of constant values for ε and ν. Since the gain in the energy leads to a greater values for these factors, it implies a lower value for P_1. Anyway these results have the purpose to show how the values change between them and they have to be seen in relative terms and not in an absolute framework.

At BOC the negative feedback related to the leakages is higher than the positive one linked to the product $f \cdot \eta$ and this coefficient for the whole core is negative, but with the burn-up increase this situation is reversed and at EOC it becomes slightly positive because of its more positive value in each channel. It is a result of the softening of the neutron spectrum that leads to a lower negative effort by the leakages but also of activation products generation that increment the total capture cross section. As a consequence, when the capture reaction rate becomes lower, due to the hardening in the neutron spectrum, there are more neutrons available and the positive feedback is larger. Thus, the ratio $\sum_{i=1}^{N} \frac{\sigma_{f,i}}{\sigma_{f,i}+\sigma_{c,i}}$ becomes higher for the greater reduction of $\sigma_{c,i}$ with respect to what happens for $\sigma_{f,i}$.

4.2.4 Coolant Void Worth

Before to start to describe how this coefficient is calculated and to present the results acquired, it is important to explain that for the coolant void worth it is necessary to use a non constant coolant temperature along the axial direction in the ring of 18 assemblies that are between the fuel region and the reflector one (figure 2.3). As a matter of fact, the comparative calculations done between the two temperature configurations have shown that it is the only coefficient in which there is an appreciable and not negligible change in its values. The reason for this behaviour is not totally clear but it is probably attributable to the SEALER design and to its high sensitivity at the leakages term due to the quite large surface to volume ratio.

The SAS4A/SASSYS-1 input file requires to insert values per unit of coolant

mass that causes the reactivity change. To determine the coolant void worth, the lead density is reduced by 20% from the nominal value in each channel and axial level, according to the updated Serpent core model. Proceeding on this way, one acquires 5 different constant values for each one of the 4 channels. With the purpose to obtain a more realistic dependence of the coolant void worth with respect to the axial direction, it is possible to make a regression of these data and to find a different value for each one of the 23 axial nodes that describe the related feedback in the SAS4A/SASSYS-1 model. The general formula to calculate the coolant void worth is:

$$\rho_{Ci,j,k} = \left(\frac{K_{eff\_i,j,k} - 1}{K_{eff\_i,j,k}} - \frac{K_{eff600\_j} - 1}{K_{eff600\_j}} \right) \Big/ (\alpha \cdot M_{Lead\_i,k}) \tag{4.58}$$

where i represents the fuel channel (i=1, 2, 3 or 4), j the core burn-up (j=BOC, MOC or EOC), k the axial level along the core axis (k=1,2,3,4 or 5) and $\rho_{Ci,j,k} = [\frac{pcm}{kg_{lead}}]$. $M_{Lead\_i,k}$ is assessed as follow:

$$M_{Lead\_i,k} = A_{flow} \cdot N_{pin} \cdot L \cdot \rho_{lead\_i,k}$$

where A_{flow} is the coolant flow area per unit of pin, N_{pin} the total number of pin, L the axial length of each axial segment and $\rho_{lead\_i,k}$ the density of the lead in the axial level k of the channel i.

4.2.4.1 BOC

The results for $K_{eff\_i,BOC,k}$ of each axial level and channel are outlined in the table 4.14. In the figure 4.2 the regression of these data in each channel is shown, while in the figure 4.3 the comparison between the regressed data of the each channel is presented.

[*pcm*]	**Channel 1**	**Channel 2**	**Channel 3**	**Channel 4**
Axial level 1	1.00023	0.99998	1.00005	1.00012
Axial level 2	1.00032	1.00021	0.99983	0.99985
Axial level 3	1.00038	1.00025	0.99963	0.99980
Axial level 4	1.00036	1.00015	0.99992	0.99993
Axial level 5	1.00030	1.00001	1.00010	1.00013

Table 4.14: K_{eff} values for the coolant void worth in each channel and axial level at BOC.

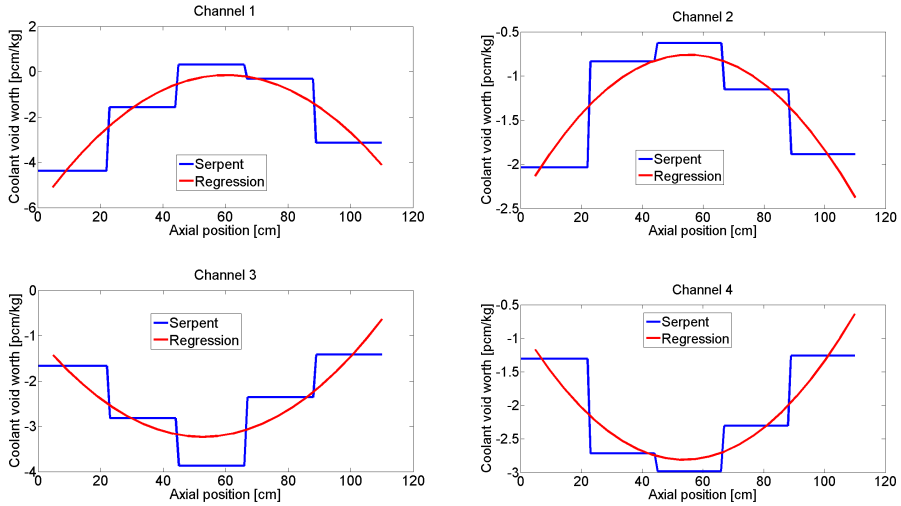

Figure 4.2: Regression of the coolant void worth values for the 4 channels at BOC.

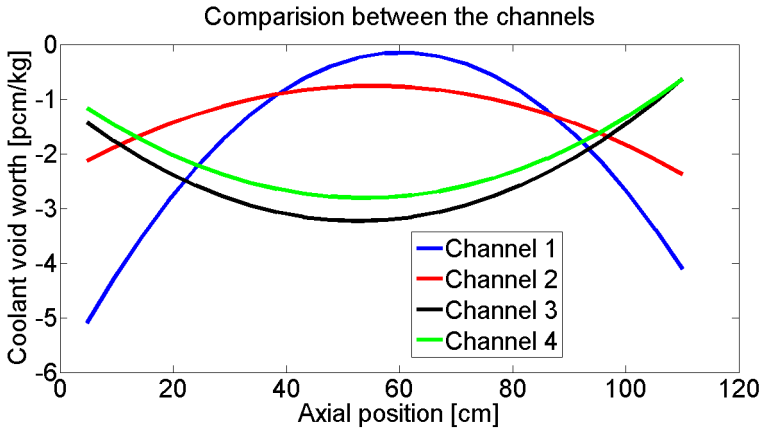

Figure 4.3: Trend comparison for the coolant void worth in the 4 channels along the axial direction at BOC.

4.2.4.2 MOC

The results for $K_{eff\_i,MOC,k}$ of each axial level and channel are outlined in the table 4.15. In the figure 4.4 the regression of these data in each channel is shown, while in the figure 4.5 the comparison between the regressed data of the each channel is presented.

[*pcm*]	Channel 1	Channel 2	Channel 3	Channel 4
Axial level 1	0.99431	0.99393	0.99407	0.99411
Axial level 2	0.99436	0.99436	0.99398	0.99399
Axial level 3	0.99445	0.99451	0.99395	0.99394
Axial level 4	0.99444	0.99429	0.99402	0.99397
Axial level 5	0.99430	0.99411	0.99411	0.99425

Table 4.15: K_{eff} values for the coolant void worth in each channel and axial level at MOC.

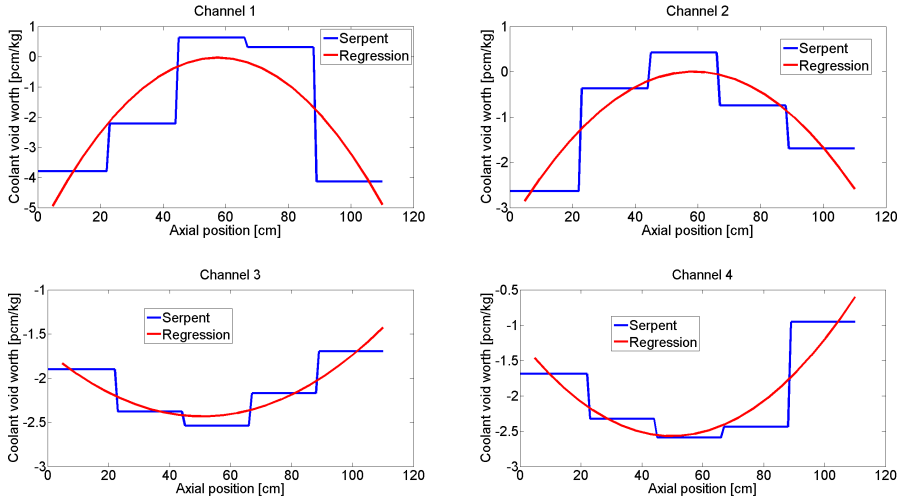

Figure 4.4: Regression of the coolant void worth values for the 4 channels at MOC.

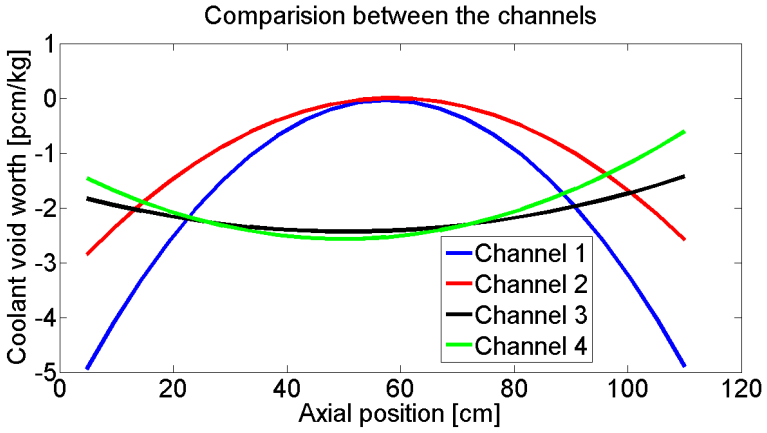

Figure 4.5: Trend comparison for the coolant void worth in the 4 channels along the axial direction at MOC.

4.2.4.3 EOC

The results for $K_{eff\_i,EOC,k}$ of each axial level and channel are outlined in the table 4.16. In the figure 4.6 the regression of these data in each channel is shown, while in the figure 4.7 the comparison between the regressed data of the each channel is presented.

$[pcm]$	Channel 1	Channel 2	Channel 3	Channel 4
Axial level 1	1.00573	1.00544	1.00552	1.00559
Axial level 2	1.00589	1.00577	1.00547	1.00554
Axial level 3	1.00588	1.00591	1.00551	1.00550
Axial level 4	1.00586	1.00589	1.00551	1.00557
Axial level 5	1.00574	1.00552	1.00553	1.00564

Table 4.16: K_{eff} values for the coolant void worth in each channel and axial level at EOC.

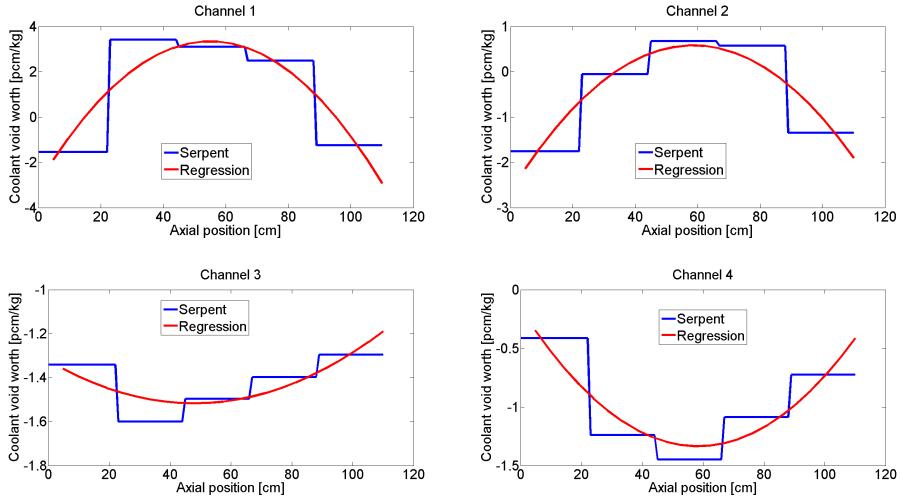

Figure 4.6: Regression of the coolant void worth values for the 4 channels at EOC.

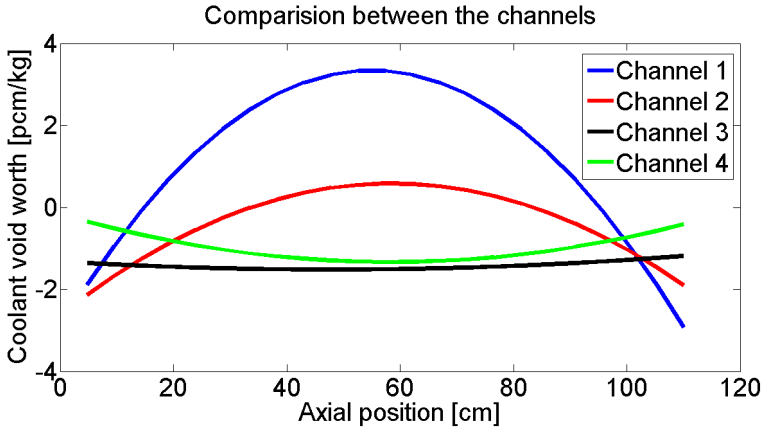

Figure 4.7: Trend comparison for the coolant void worth in the 4 channels along the axial direction EOC.

4.2.4.4 Results Discussion

In the figures 4.3, 4.5 and 4.7 the results for the coolant void worth with the new temperature configuration are shown. Putting the attention on the BOC configuration results (figure 4.3), it is possible to note that all the channels give negative feedback, with the central channels (1 and 2) that have a concave trend and with the peripheral channels (3 and 4) that have a convex one. This is due to the different dependence on the parameters, as a result of the same perturbation. The little hardening of the neutron spectrum, due to the decrease in the involuntary moderation of the coolant, leads to a gain in the leakages, with more effort in the core periphery (axial levels 1 and 5 and channels 3 and 4), and in the ratio $\sum_{i=1}^{N} \frac{\sigma_{f,i}}{\sigma_{f,i}+\sigma_{c,i}}$. The latter fact is a consequence of the gain in the σ_f^{238} and in the fall of the σ_c^{238} that have more effort than the reduction in both σ_f^{235} σ_c^{235}. In the central channels (1 and 2) the gain of this ratio is greater than that in the peripheral ones (3 and 4), while the increase in the leakages, that is higher in magnitude and has on opposite behaviour with respect to the cross sections ratio, explains the negative feedback and the combination of these two contributions clarifies the different concavity. The table 4.17 shows the results of a reduction of the lead density of 20% in each channel for the product $f \cdot \eta$ ($\approx \nu \sum_{i=1}^{N} \frac{\sigma_{f,i}}{\sigma_{f,i}+\sigma_{c,i}}$) and the fast neutrons non leakage probability (P_1). It can be seen that the increment in the product is proportional to neutron energy in the channels, while the leakages are more affected by the radial position, even if the value in the third channel is larger than the one in the fourth. This is due to the higher neutron energy and for the same reason together with the leakages at the top and bottom of the core, the channel 1 has the biggest negative variation for the factor P_1.

[pcm]	$f \cdot \eta$	Change	P_1	Change
Reference	1.49159	-	0.55885	-
Channel 1	1.49197	38	0.55857	-28
Channel 2	1.49340	30.2	0.55766	-19.8
Channel 3	1.49285	21	0.55720	-27.5
Channel 4	1.49252	15.5	0.55750	-22.5

Table 4.17: Comparison between the variation in the product $f \cdot \eta$ and in the fast neutrons non leakage probability foe the coolant void worth at BOC.

In order to obtain the data in the table 4.17 these assumptions are done: ε=1.2, ν=2.51, the value for the cross sections ratio coming from the product $f \cdot \eta$ is calculated putting detectors [30] in the fuel with the purpose to evaluate the cross sections and the value of P_1 is assessed using the formula 3.6 in which now is the only unknown.

Analysing the development of this coefficient over the reactor life (figure 4.8), it is observed that in the central part of the core (axial levels 2,3 and 4) there are a more positive values. This is a result of the activation products generation, like plutonium fertile isotopes, americium and neptunium that, with their capture cross sections, increase the capture reaction rate. Another contribution is given by the fission products that allow a greater moderation of the neutrons generating a softer spectrum. As a result, a raise in the neutron spectrum, following a reduction in coolant density, gives lower neutron captures and thus a more positive coolant void worth because it provides an higher gain in the product $f \cdot \eta$ as seen in the case of the cladding axial expansion.

Regarding the bottom and the top of the core (axial levels 1 and 5), also in these core regions, to find less negative values at MOC and EOC as a result of the softer neutron spectrum and thus to the less effort of the leakages was expected. Instead as shown in the figure 4.8, there is a fluctuating trend with a more negative value at MOC and a more positive one at EOC with respect to BOC. Once again this fact can be explained with the non criticality condition of the three configuration.

Despite the positive value for the coolant void worth in the central channel and in the center part of the second in the EOC scenario, the high leakages effect, due to small dimension of the core, provides a whole core value that is negative. The change in the concavity in the figure 4.8 between BOC, MOC and EOC is due to the decreasing effect of the leakages and to the increase in the growth of the cross sections ratio.

In the figure 4.9 also the data obtained with the old configuration, used for

all the other coefficients, are presented. This comparison is due with the purpose to understand the influence of the new temperature trend in the ring of control elements (burn-up and shutdown) in the assessment of this reactivity coefficient. It can be seen that with the new configuration there is a gain in the negative feedback for the whole core at BOC, while for the MOC and EOC there is a more positive value for the coolant void worth.

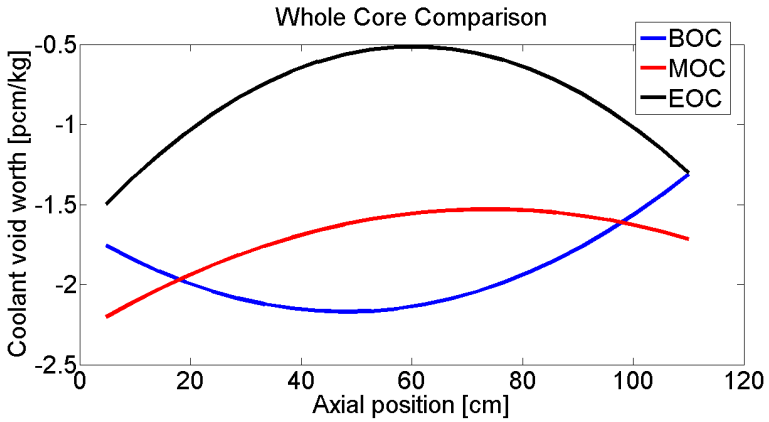

Figure 4.8: Comparison of the whole core coolant void worth in the three configurations of BOC, MOC and EOC.

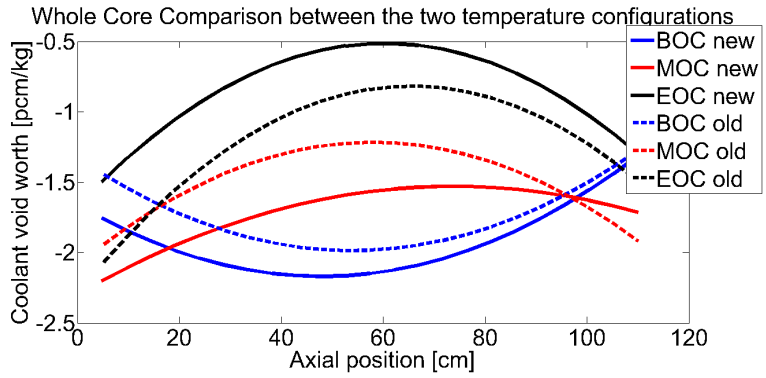

Figure 4.9: Coolant void worth comparison between the old and the new temperature configuration in the ring of burn-up and shutdown elements.

4.2.5 Radial Expansion Coefficient

For this coefficient, the approximation that all the core expands in the radial direction with the same amplitude is made, neglecting the core flower effect. As a matter of fact in the reality, the radial expansion increases along the axial direction because of the coolant temperature gain. This approximation can be

accepted because of the very low ΔT between the outlet and the inlet coolant temperature that characterizes the SEALER reactor ($\Delta \simeq 40$ ℃). The values for $K_{eff\_re\_j}$ are assessed increasing the nominal value of the pitch between the assemblies of 5%. In the SAS4A/SASSYS-1 input file, only one value valid for all the core calculated with the equation (4.59), is inserted:

$$C_{re\_j} = \beta \cdot \left(\frac{K_{eff\_re\_j} - 1}{K_{eff\_re\_j}} - \frac{K_{eff600\_j} - 1}{K_{eff600\_j}} \right) \Big/ \Delta T_{CI} \tag{4.59}$$

where j is the core burn-up (j=BOC, MOC or EOC), β the total effective delayed neutron fraction ($\beta = 0.00717$) and $\Delta T_{CI} = \varepsilon / \alpha_{SS316L}$, with $\varepsilon = 0.05$ as percentage gain in radial dimension and $\alpha_{SS316L} = 1.8 \cdot 10^{-5}$ as thermal expansion coefficient for stainless steel. C_{re_j} is expressed in [\$/K].

4.2.5.1 BOC

For this case, $K_{eff\_re,BOC} = 0.98667$ is found and including it in the equation (4.59) together with the reference value (4.1), one obtains:

$$C_{re,BOC} = -75.03 \ [\$/K]$$

4.2.5.2 MOC

For this case, $K_{eff\_re,MOC} = 0.97954$ is found and including it in the equation (4.59) together with the reference value (4.1), one obtains:

$$C_{re,MOC} = -80.79 \ [\$/K]$$

4.2.5.3 EOC

For this case, $K_{eff\_re,EOC} = 0.99207$ is found and including it in the equation (4.59) together with the reference value (4.1), one obtains:

$$C_{re,EOC} = -71.58 \ [\$/K]$$

4.2.5.4 Results Discussion

The feedback of the core radial expansion is negative with an oscillating evolution. The first thing is a result of the less reactivity zone in which the fuel assemblies are located after the radial expansion, while the second one is a consequence of the different conditions in which these three values are evaluated. Indeed at BOC and EOC the reactor is supercritical, while at MOC it is sub-critical (equation (4.1)). When a reactor is supercritical the neutron population is continuously increasing and a fixed core radial expansion produces a less negative feedback

with respect to the same one that happens in a sub-critical condition in which the neutron population is continuously decreasing. For a criticality condition this coefficients is expected to be flat over the entire reactor life.

4.3 Reactivity Coefficients Recap

The table presented below (table 4.18) summarizes the values, calculated with the rigorous definition and not according to the SAS4A/SASSYS-1 requests, of each reactivity coefficient in the three analysed configurations: BOC, MOC and EOC.

Parameters	BOC	MOC	EOC	Errors
$K_D[pcm]$	-259.1	-290.9	-366.5	± 8.0
$\alpha_{Fuel}[\frac{pcm}{K}]$	-0.3268	-0.2942	-0.2740	$\pm 1.8 \cdot 10^{-3}$
$\alpha_{Coolant}[\frac{pcm}{K}]$	-1.3086	-1.1638	-0.5853	$\pm 2.02 \cdot 10^{-2}$
$\alpha_{Cladding}[\frac{pcm}{K}]$	-0.1296	-0.0288	0.0886	$\pm 2.9 \cdot 10^{-3}$
$\alpha_{Radial}[\frac{pcm}{K}]$	-0.5188	-0.5512	-0.5001	$\pm 2.0 \cdot 10^{-3}$

Table 4.18: Summary of the reactivity coefficients development over the reactor lifetime.

The time evolution of the reactivity coefficients (more negative value for the Doppler and more positive values for all the other coefficients) is due to the activation products generation in the fuel that increase the capture cross section during normal operation and to the softening of the neutron spectrum as consequence of the withdrawal of the burn-up control elements (more reflection given by the reflector elements) and of the fission products formation in the fuel. Regarding the radial expansion coefficients and its fluctuating time evolution, this is due to the supercritical condition of the BOC and EOC scenarios and to the sub-critical one of the MOC. With a criticality condition, it should be constant over the reactor life. The errors shown in the last column are the same for the three analysed configuration of each reactivity coefficient.

Chapter 5

Transient Analysis

In this chapter will be outlined the results of the multi-channel transient simulations with the SAS4A/SASSYS-1 code under the three unprotected accidents of over power (UTOP), loss of flow (ULOF) and loss of heat sink (ULOHS). An unprotected accident consists in an initiator event such as a component failure or an external event that causes a deviation from the steady state condition and where both the reactor shutdown systems for some reasons are unable to operate. In a such dangerous situation, only a properly reactor design can provide inherent features (reactivity feedback given by the reactivity coefficients) able to prevent a damage to the core or to the reactor systems. The simulations are performed in three different configurations over the reactor life BOC, MOC and EOC.

From a nuclear safety point of view the two main important parameters to point out are the fuel and the cladding temperatures, the latter must be always less than safety limit setted for SEALER at 1200 K.

In the following chapter when it will speak about the axial expansion coefficient it means the sum of both the contributions given by fuel and cladding.

5.1 Unprotected Transient of Over Power (UTOP)

The over power transient happens when, starting from the steady state condition of equal power (generated and removed) from the reactor core, there is an increment in the generated one (fission power) keeping constant the removed one. It leads to an unbalanced condition in the core with an increase in the fuel, cladding and coolant temperatures controlled by the intrinsic core feedback. This kind of accident can be caused by an unintentional extraction of one or multiple burn-up control elements and for this reason it is more effective and potentially dangerous at BOC, when they are totally inserted in the core. This accident at BOC is simulated by a linear reactivity insertion of 0.5 $ in 1 second.

This reactivity worth is chosen under the hypothesis that only one burn-up control element can be suddenly withdrawn. Indeed, with the purpose to limit the dangerousness of such an event, the number of burn-up control elements (12) is selected in order to give at each element a worth equal to 0.5 $.

At MOC the linear reactivity insertion has a worth of 0.25 $ because of the burn-up control elements position inside the core. Since they should be half inserted, the accident following an unexpected withdrawal produces a reactivity insertion that is the half of the case at BOC. At EOC all the burn-up control elements are withdrawn and it is impossible to have an UTOP.

5.1.1 BOC

Since it is an unprotected accident, the reactor power behaviour is controlled by the reactivity feedback (net reactivity), that in their turn, depend on the reactivity coefficients calculated in the previous chapter and on the fuel and coolant temperatures, that in their turn, depend on the reactor power. It is clear that all these parameters are related to each others and in order to avoid confusion, it is needed to define the right relationship of cause and effect between them. The initiator event is a positive reactivity insertion whereby the net reactivity variation is the cause, the power change is the first effect followed by the fuel and the coolant temperatures one (second effect) and by the modification of the reactivity feedback values (third effect). At this point, the impact of the third effect on the primary cause (net reactivity) is evaluated and the assessment of the parameters with the properly order is restarted.

To understand the accident development, it is necessary to analyse and to compare the graphs of peak temperatures (figure 5.2), coolant temperatures (figure 5.3), normalized total power (figure 5.4) and reactivity (figure 5.6). Below also the figure of the peak heights (figure 5.1) and of the inverse period (figure 5.5) are shown.

After 100 seconds of steady state, there is the external reactivity insertion of 0.5 $ and the power undergoes a sharp increase. Also the fuel and coolant temperatures start to grow (figure 5.2 and figure 5.3), but with different trends and time lines. The first rises faster and with greater magnitude and it gives a strong negative prompt reactivity insertion, related to the negative feedback of the Doppler and of the axial expansion (respectively green and black lines in figure 5.6), that counterbalances and turns around the power sharp gain. During this phase, also the feedback that depend on the coolant temperature (delayed feedback), provide negative reactivity insertions (pink and yellow lines in figure 5.6), but their values are lower because the lead temperature needs more time to appreciate the change (the heat power generated in the fuel has to be transferred

to the coolant). The power drop, due to the net reactivity decrease, leads to even smaller increment (more flat derivative) of the temperatures up to which also these start to fall, always with the properly time lines. Since all the reactivity coefficients in the BOC configuration have a negative feedback, it brings to a little positive reactivity insertion with a raise in the net reactivity (figure 5.6). It is followed by a new small power increase (figure 5.4) that produces a second rise in the fuel and coolant temperatures that, in their turn, generate a more negative values for the reactivity feedback and at the end the net reactivity starts to decline again.

This continuous gain and drop of the net reactivity, with the related effects described above, is increasingly damped each time until a new reactor steady state condition is reached with the net reactivity equal to zero and a reactor power equal to 8 MW_{th}. This new steady state configuration, although it has the same thermal power of the initial one, provides greater fuel and coolant temperatures because it is necessary to counteract the external positive reactivity insertion with the reactivity feedback. As a result, also the cladding and the core structures operate at an higher temperature (≈200 K figure 5.2) with respect to operating limits specified in the chapter 2 (for the cladding 450℃). It could lead to some problems related to the enhancement of the corrosion and erosion phenomena especially for the cladding and the SGs materials.

Focusing the attention on the figure 5.6, it can be noted that the axial expansion and the Doppler feedback are the main responsible for the peak temperatures, while for the long term framework the core radial expansion becomes important as the axial one.

The data for the peak parameters in the table 5.1 show that there is a margin of 200 K for the PCT and of about 1100 K for the fuel before to start to melt in the hottest point, thus the SEALER design provides an excellent feedback. Regarding the time of the peak temperatures, it arrives before the one in the fuel with respect to the cladding.

Peak Parameters	**Fuel Center**	**Cladding**
Temperature [K]	2002.5	999.9
Height [node number]	14	23
Time [s]	162.6	215.4

Table 5.1: Fuel and cladding peak parameters under UTOP transient at BOC.

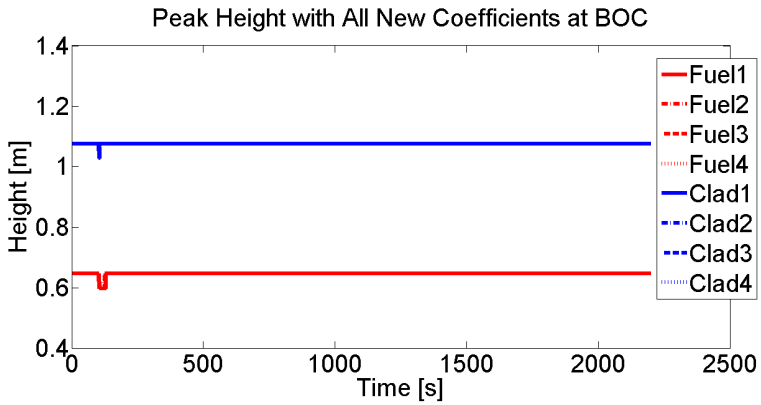

Figure 5.1: Peak heights time trend under UTOP transient at BOC.

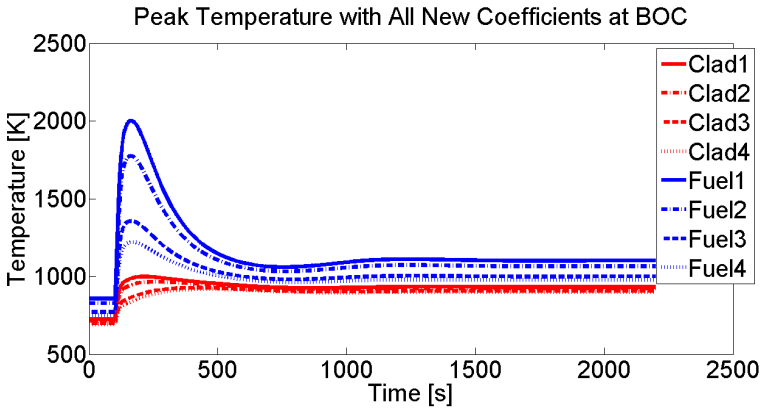

Figure 5.2: Peak temperatures time trend under UTOP transient at BOC.

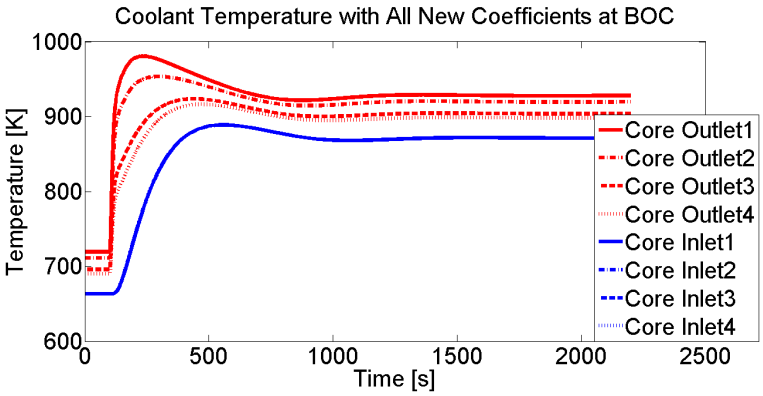

Figure 5.3: Coolant temperature time trend under UTOP transient at BOC.

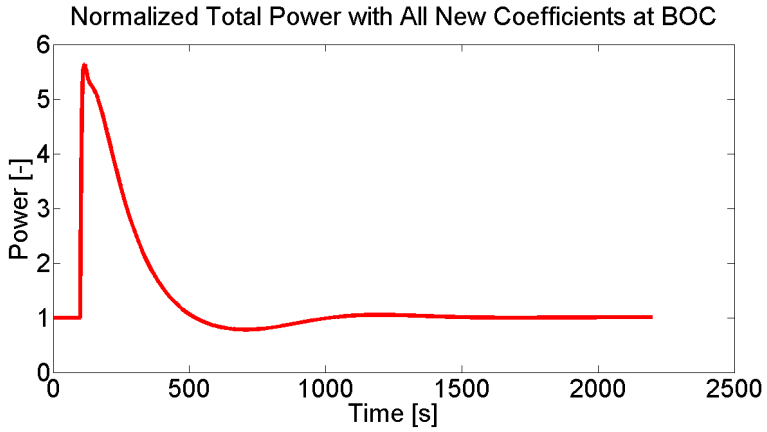

Figure 5.4: Total power time trend under UTOP transient at BOC.

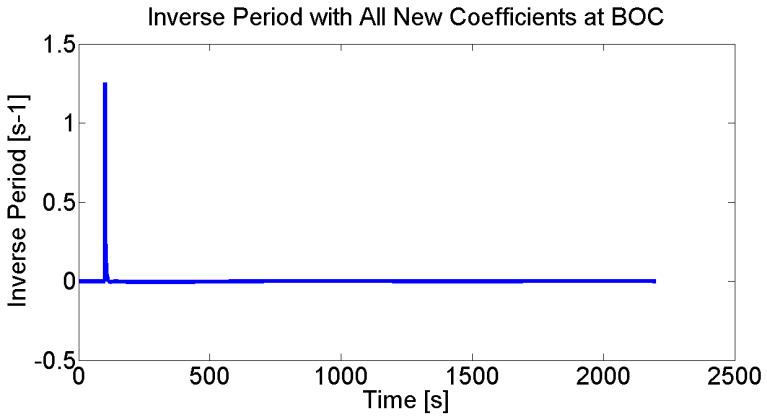

Figure 5.5: Inverse period time trend under UTOP transient at BOC.

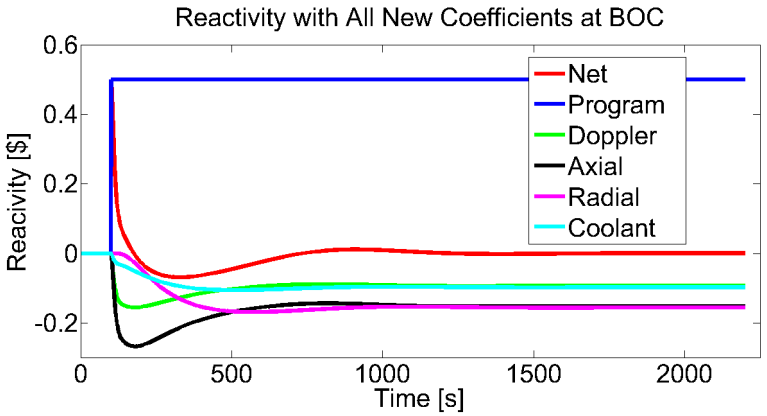

Figure 5.6: Reactivity contributions time trend under UTOP transient at BOC.

5.1.2 MOC

For what it concerns the UTOP scenario at MOC, the physics that explains that accident behaviour is the same. As presented in the main parameters graphs that follow the same trends of the ones presented above for the BOC configuration (figures 5.7, 5.8, 5.9, 5.10, 5.11, 5.12 and 5.13). The only things that change are the relative importance of the reactivity feedback and the peak parameters values. As a matter of fact, there is an external reactivity insertion that is the half of the previous one and since the reactivity coefficients are almost the same, all the temperatures (peak and long term) and the power peak are lower. It means that this type of accident is less dangerous as the reactor lifetime grows. It is confirmed by the data in the table 5.2, that if compared with ones for the BOC scenario give almost 150 K less for the PCT and about 700 K less for the fuel center temperature. In addition, the power peak during this transient scenario is a little bit more than the half of that during the UTOP transient at BOC: 23 MW_{th} versus 45 MW_{th}.

Comparing the two reactivity figures 5.6 and 5.13, it is possible to see that the peak temperatures values are controlled by the reactivity feedback related to the fuel temperature (black and green lines in the figure 5.13) and that the difference in the Doppler and axial expansion feedback coefficient is became lower thanks to their time evolution (more negative the Doppler and less negative the axial expansion). In a long term analysis the radial expansion is became more important than the axial one while the coolant decreased its negative feedback.

The same problem, regarding the corrosion and erosion enhancement due to the greater operating temperature for the cladding and the core structures, discovered for the BOC scenario, is valid for this transient even if with a less effort (≈100 K compared to ≈200 K of the BOC configuration).

Peak Parameters	**Fuel Center**	**Cladding**
Temperature [K]	1339.7	867.1
Height [node number]	14	23
Time [s]	196.8	265.8

Table 5.2: Fuel and cladding peak parameters under UTOP transient at MOC.

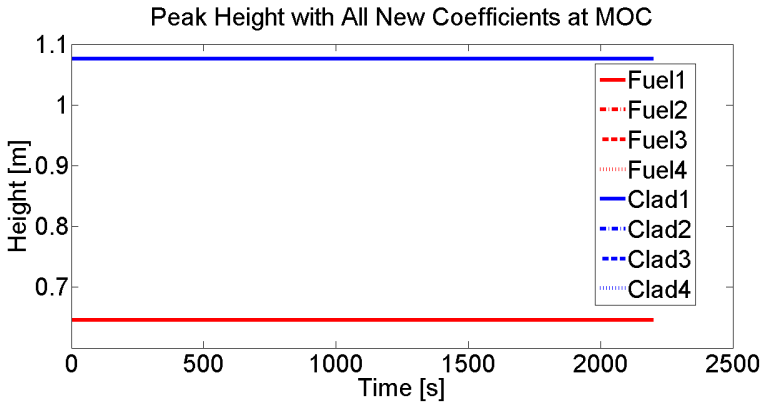

Figure 5.7: Peak heights time evolution under UTOP transient at MOC.

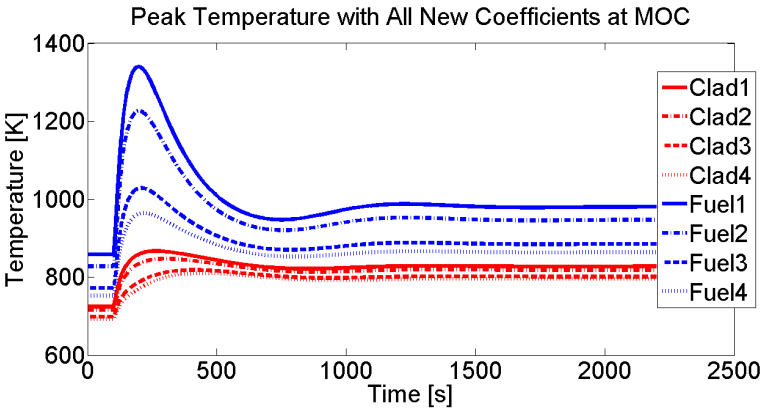

Figure 5.8: Peak temperatures time evolution under UTOP transient at MOC.

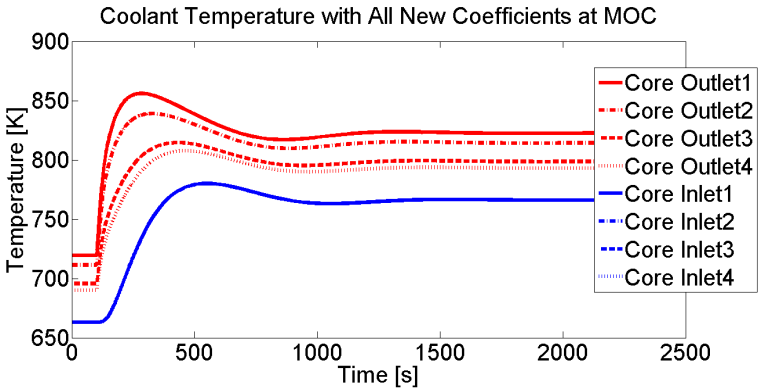

Figure 5.9: Coolant temperature time evolution under UTOP transient at MOC.

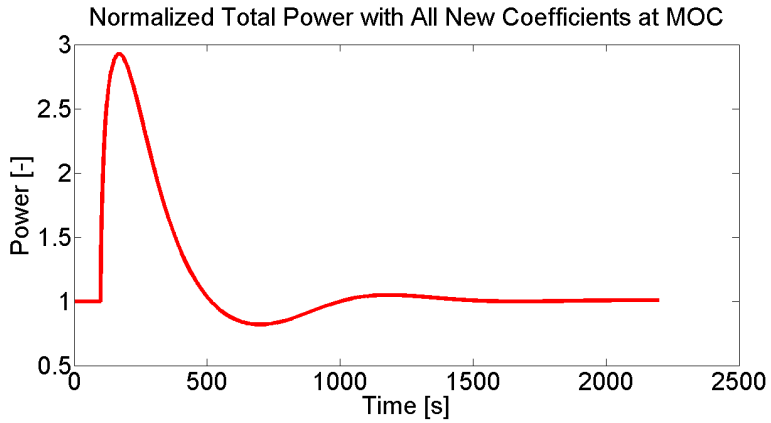

Figure 5.10: Total power time evolution under UTOP transient at MOC.

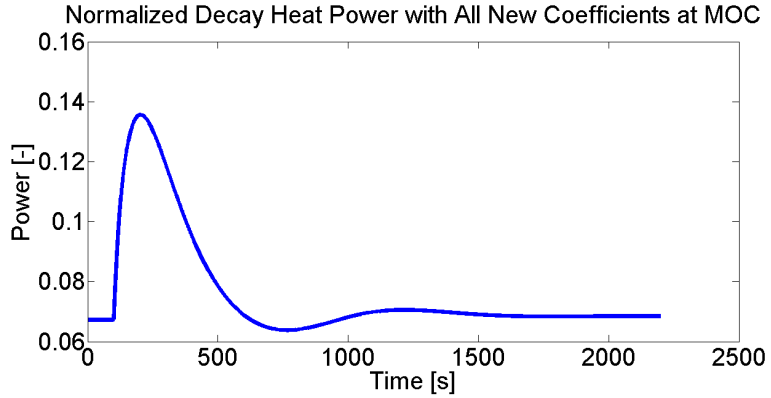

Figure 5.11: Decay heat power time evolution under UTOP transient at MOC.

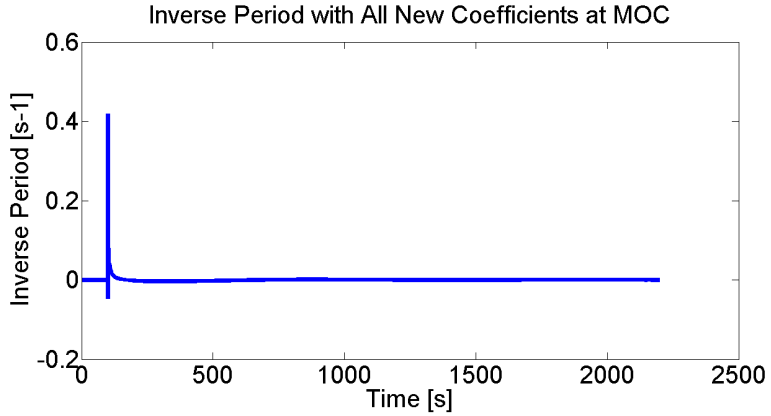

Figure 5.12: Inverse period time evolution under UTOP transient at MOC.

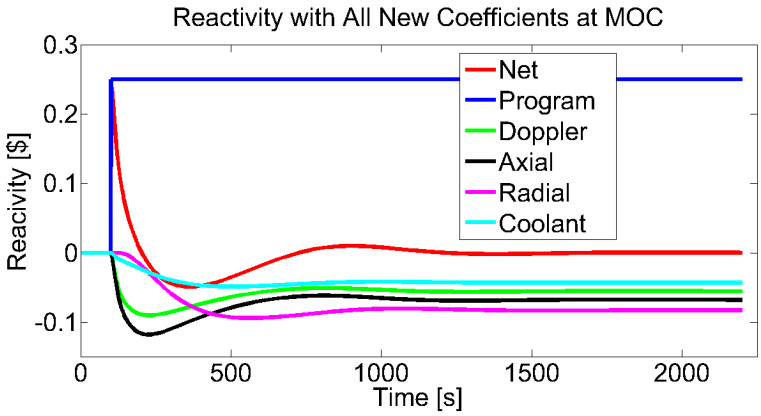

Figure 5.13: Reactivity contributions time evolution under UTOP transient at MOC.

5.2 Unprotected Loss Of Flow (ULOF)

The loss of flow accident is a consequence of an unbalanced condition between generated and removed power in the core induced by a reduction of the heat removal capabilities due to the loss of coolant flow. This kind of accident can be the result of a Station Black Out (SBO) or by any other cause that implies the loss of all the pumps simultaneously. It is simulated with a linear coast down of all the eight pumps in 10 seconds, with the purpose to reproduce the inertia effect of the impeller. Contrary to the UTOP, it could happen in all the three studied conditions over the reactor life and its evolution time is much longer. As a matter of fact, it requires 8 hours simulation to reach a stability condition with respect to less than 40 minutes required by the UTOP. During this accident development, it is really important to put besides the intrinsic negative reactivity feedback the establishment of a properly natural circulation, in order to ensure a minimum level of heat removal from the core.

5.2.1 BOC

Before to start to analyse the accident behaviour and the parameters trends, it is important to have clear in mind which are the phenomena that characterize the accident and which is their cause-effect relationship, as done before for the UTOP transient.

Here the initiator event is the loss of coolant flow (cause), followed by an increase in the fuel and coolant temperatures (first effect) that produces a negative reactivity insertion and thus a reduction in the net reactivity (second effect). It leads to a fall in the generated power with a consequent decrease in the fuel and coolant temperatures (third effect) that induces a positive reactivity

insertion and an increment in the power and in the temperatures. After awhile, the gain in the coolant temperature creates the right condition of difference in the coolant density between the core and the SG and the natural circulation enhances the mass flow rate, already ensured by this process. When it happens the heat removal is increased and the temperatures start to decrease again (fourth effect). It brings a gain in the net reactivity and in the generated power that produces the increment in the temperatures and the natural circulation is enhanced again. These cyclic processes go on until the reactor reaches the equilibrium condition where the coolant mass flow is ensured by the natural circulation.

The accident development is explained with the help of the figures 5.14, 5.15, 5.16, 5.17, 5.18, 5.19 and 5.20 that show respectively the peak heights, the peak temperatures, the coolant mass flow, the coolant temperatures, the normalized total power, the inverse period and the reactivity.

Analysing the coolant mass flow figure, it can be noted that after 100 seconds all the pumps are coasted down and there is a sharp drop that generates an increase in the fuel and coolant temperatures (figures 5.15 and 5.17). It produces a negative reactivity insertion and the power starts to decrease with a consequent effect on the temperatures that after awhile begin to decrease too. The mass flow trend is counterbalanced for a few minutes by a first gain in the natural circulation mechanism. The short time (more or less half a minute) is due to the sharp increase and decrease in the coolant temperature. The coolant mass flow, after this little increment, continues its falling trend until it reaches an almost constant value determined only by natural circulation process.

The evolution of the temperatures produces a change in the net reactivity that begins to surge even if the radial expansion contribution continues to have a declining behaviour. Indeed, it depends on the coolant inlet temperature and, as it is possible to see in the figure 5.17, the first maximum is reached in delay with respect to the outlet temperature and for this reason also its related feedback has a delayed behaviour that slows the growth of the net reactivity and thus the one of the reactor power and of all the temperatures.

The first positive peak in net reactivity after 4500 s has the effect to produce a peak also in the generated power and in the temperatures. Since the time of growth in coolant temperature is larger than in the first peak, the natural circulation is enhanced with more effort and, as it can be noted in the coolant mass flow figure, there is a little increase in the coolant mass flow. It leads to a gain in the removed power from the reactor core that creates a reduction in the fuel and coolant temperatures that, in their turn, generate a drop in the net reactivity and a reduction in the natural circulation mechanism.

At this point of the transient (7000 s), another cycle of gain and drop of

all the parameters and of the natural circulation process starts with the same behaviour of the previous one with the only exception that is damped. This series of oscillating cycles for the main parameters continues, even if each time more damped, until when the new reactor equilibrium condition is reached. The new steady state configuration provides a lower thermal power, around the 8% of the initial one (figure 5.18), that is equal to removed power ensured by the natural circulation of the coolant. In these final conditions the values of the cladding temperature are slightly higher (only few Kelvin $\approx$ 5-6 K) than those before the transient and it does not lead to a considerable gain in the corrosion and erosion phenomena of the materials, like seen before under the UTOP transient.

Making a comparison between the reactivity figures of the UTOP and of the ULOF transients both assessed at BOC (figures 5.6 and 5.20), it can be observed that, in this accident scenario, the coolant void worth has a greater impact on the peak temperatures than the Doppler. It is a consequence of the lower variation in the fuel temperature, during the ULOF accident, that reduces the negative feedback of its related coefficients. Anyway the axial expansion remains the most important feedback for the peak values. Although the delayed development of the radial expansion feedback, due its proportionality to the coolant inlet temperature, it is the main feedback in the long term, where the contribution to the net reactivity related to the fuel temperature become positive.

Moreover, analysing the peak parameters tables 5.1 and 5.3, it is noted that the peak temperatures for both fuel center and cladding are much lower under the ULOF transient. It is a foreseen thing, based on the different type of accident. During the UTOP scenario there is a peak in the fission power that increases strongly the temperatures, especially the fuel one, while in the ULOF accident the generated power is always decreasing. In addition, another interesting thing is the difference in the peak times. As a matter of fact, the UTOP is a more fast transient but the temperature peaks happen later with respect to the ULOF because of the power peak absence during the latter accident.

Peak Parameters	**Fuel Center**	**Cladding**
Temperature [K]	955.8	889.5
Height [node number]	19	23
Time [s]	150.5	147.5

Table 5.3: Fuel and cladding peak parameters under ULOF accident at BOC.

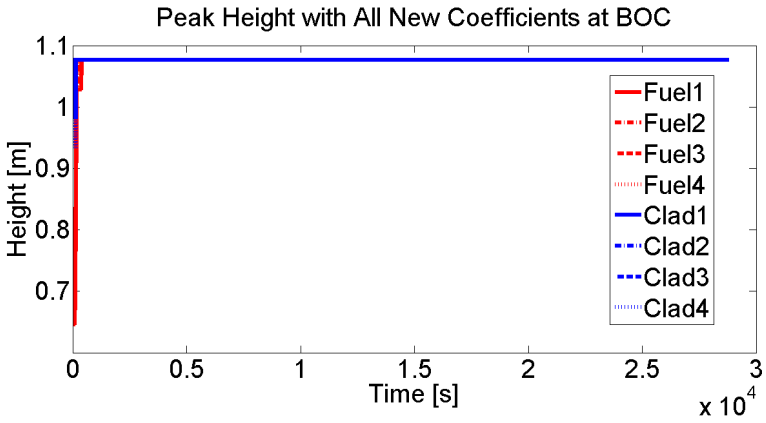

Figure 5.14: Peak heights time trend under ULOF accident at BOC.

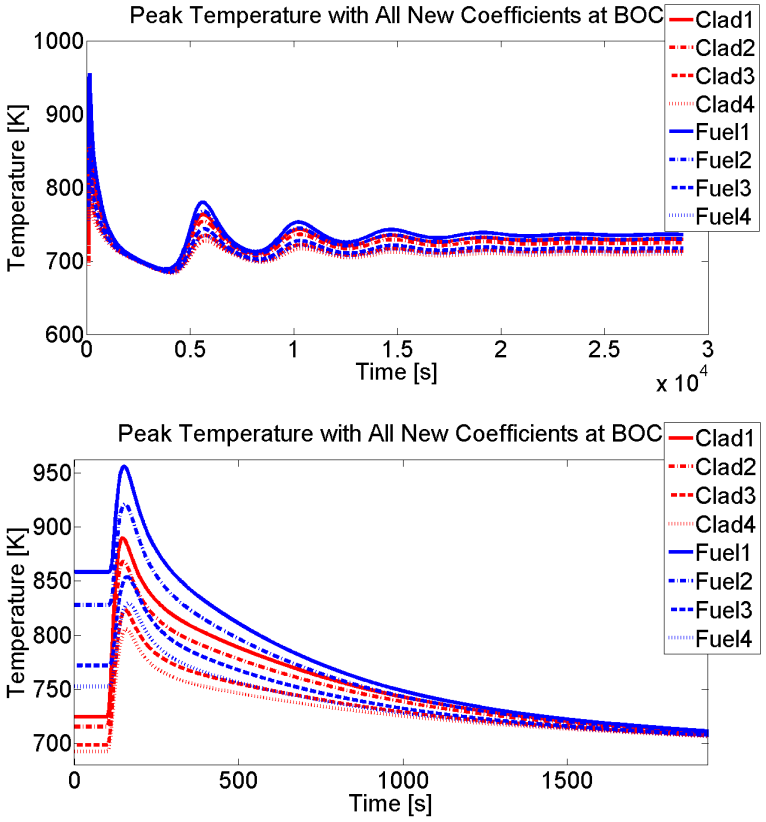

Figure 5.15: Peak temperatures time trend under ULOF accident at BOC (top), with a zoomed view on the first minutes (bottom).

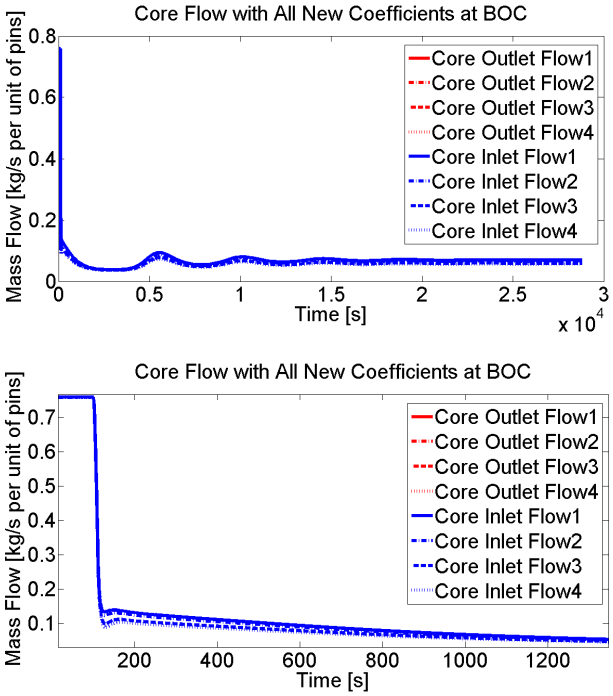

Figure 5.16: Core flow time trend under ULOF accident at BOC (top), with a zoomed view on the first minutes (bottom).

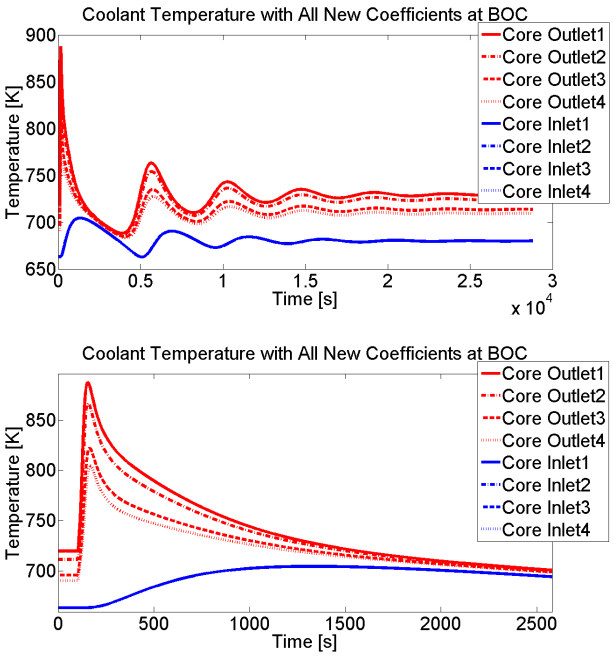

Figure 5.17: Coolant temperature time trend under ULOF accident at BOC (top), with a zoomed view on the first minutes (bottom).

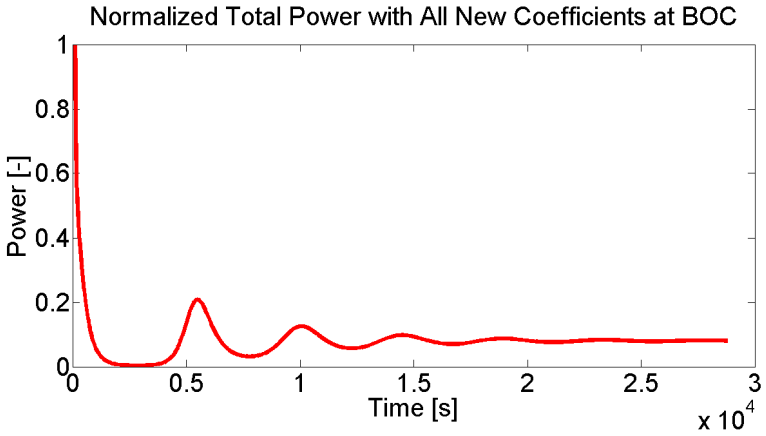

Figure 5.18: Total power time trend under ULOF accident at BOC.

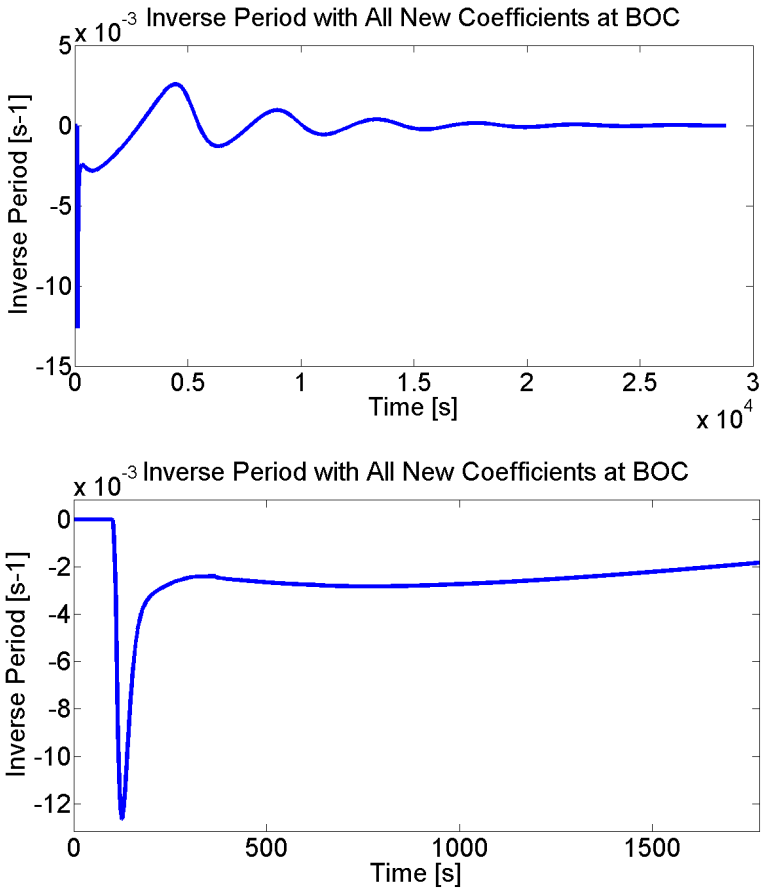

Figure 5.19: Inverse period time trend under ULOF accident at BOC (top), with a zoomed view on the first minutes (bottom).

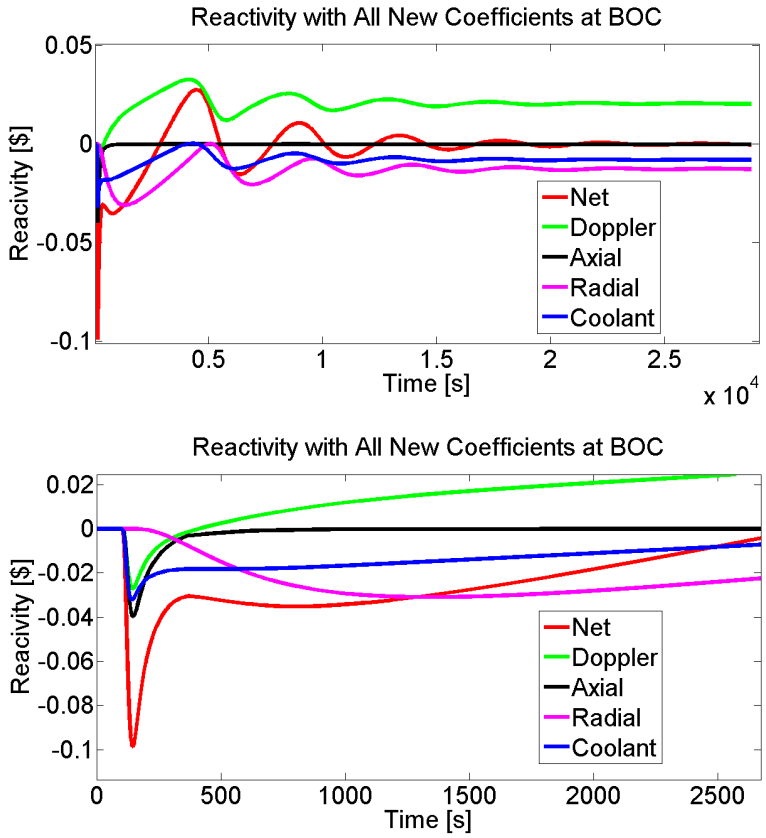

Figure 5.20: Reactivity contributions time trend under ULOF accident at BOC (top), with a zoomed view on the first minutes (bottom).

5.2.2 MOC

As it was said for the UTOP, the mechanisms that control the time evolution of the accident are the same whatever its moment of occurrence over the reactor lifetime, thus the considerations done for this transient at BOC are still valid for the MOC and EOC configurations. Examining the tables 5.3 and 5.4, it is possible to notice that the peak temperatures are slightly higher, while the time of the peaks are practically the same. The reasons for this little gain in the peak values are the marginally decrease in the reactivity coefficients negative values, the non time dependent initial event worth and the addition of the decay heat. In the figure 5.28, it can be seen the reduction of the coolant void worth negative feedback and the increase of the Doppler one that becomes more important, contrary to what is expressed during transient at BOC (figure 5.20). The axial expansion continues to be the most important feedback for the peak values and the same valid for the radial expansion in the long term framework.

Peak Parameters	Fuel Center	Cladding
Temperature [K]	960.7	892.4
Height [node number]	19	23
Time [s]	151.5	148

Table 5.4: Fuel and cladding peak parameters under ULOF accident at MOC.

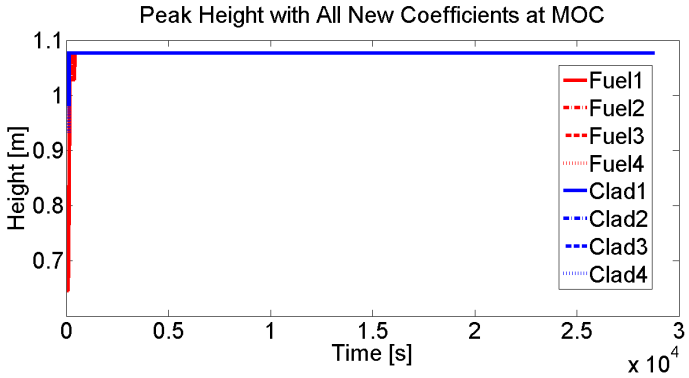

Figure 5.21: Peak heights time trend under ULOF accident at MOC.

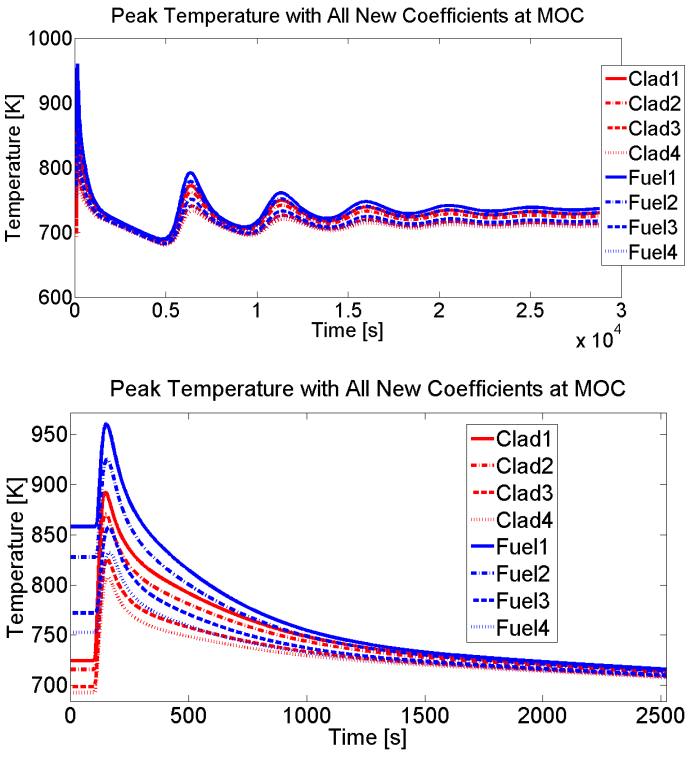

Figure 5.22: Peak temperatures time trend under ULOF accident at MOC (top), with a zoomed view on the first minutes (bottom).

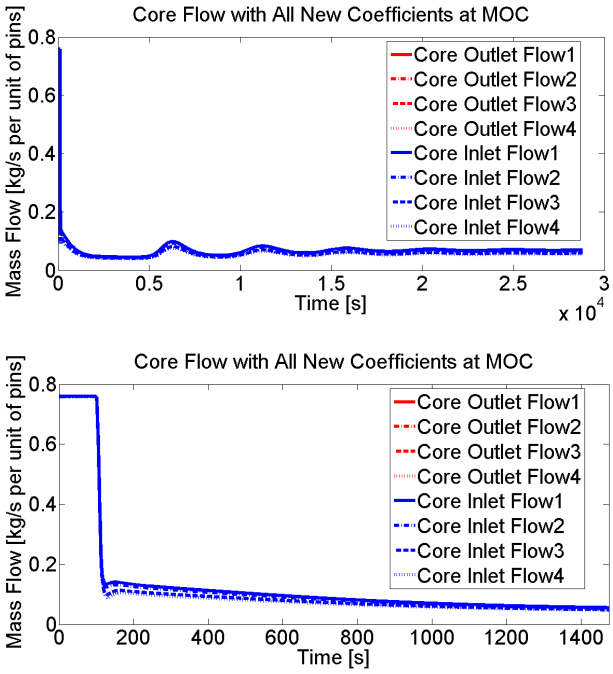

Figure 5.23: Core flow time trend under ULOF accident at MOC (top), with a zoomed view on the first minutes (bottom).

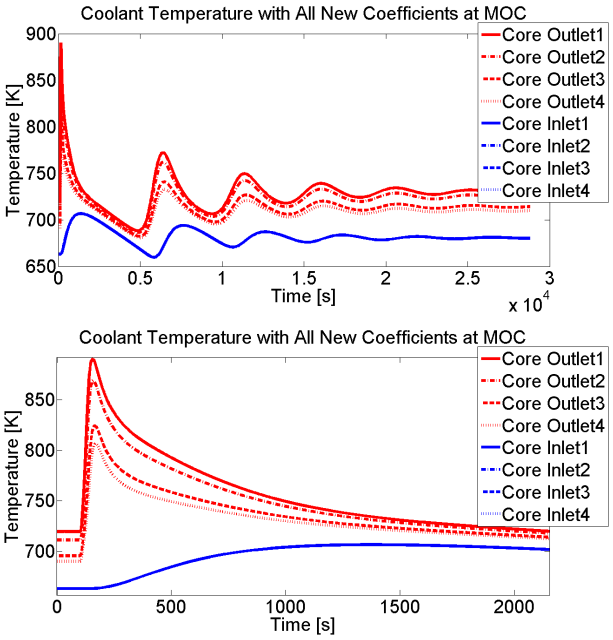

Figure 5.24: Coolant temperature time trend under ULOF accident at MOC (top), with a zoomed view on the first minutes (bottom).

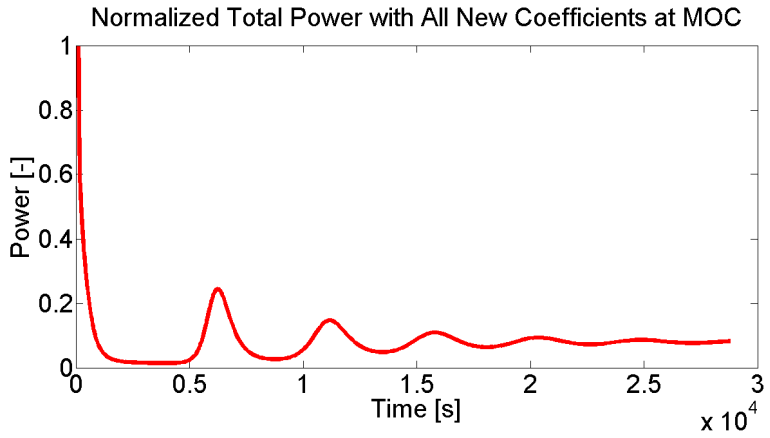

Figure 5.25: Total power time trend under ULOF accident at MOC.

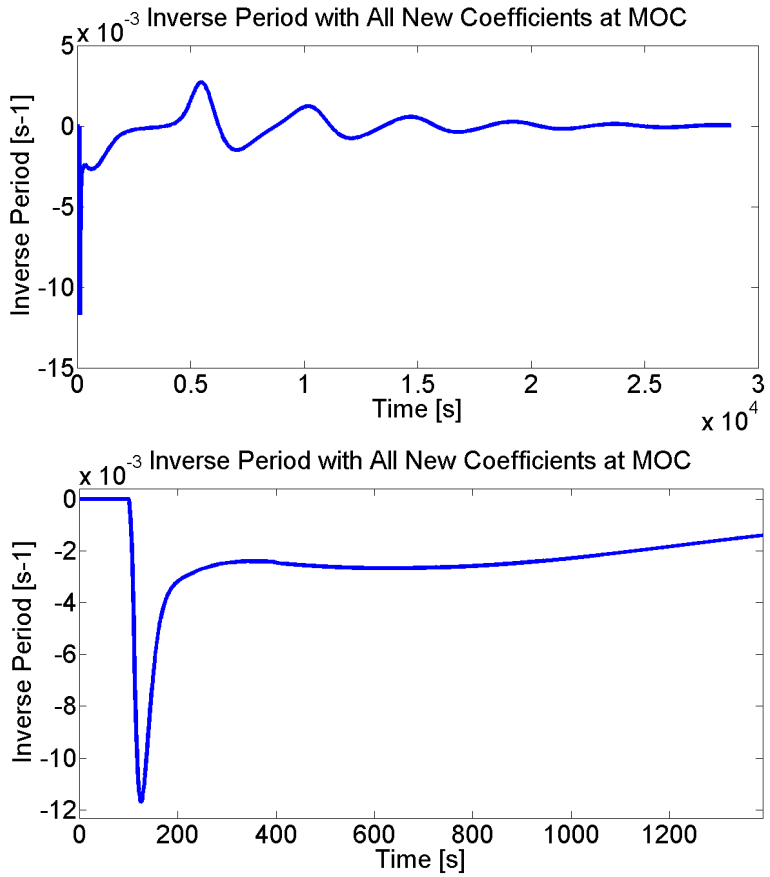

Figure 5.26: Inverse period time trend under ULOF accident at MOC (top), with a zoomed view on the first minutes (bottom).

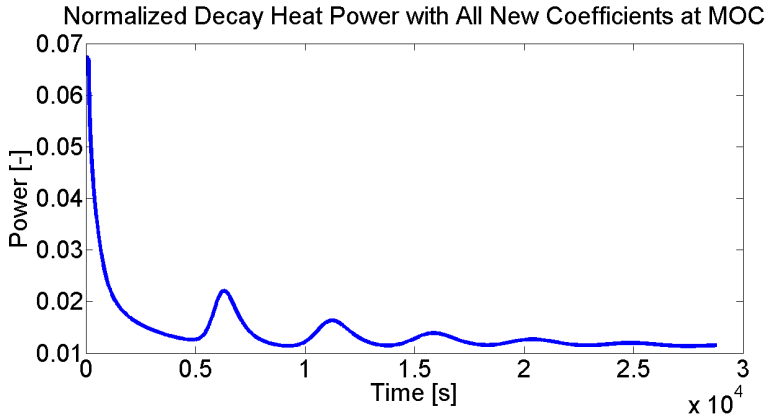

Figure 5.27: Decay heat power time trend under ULOF accident at MOC.

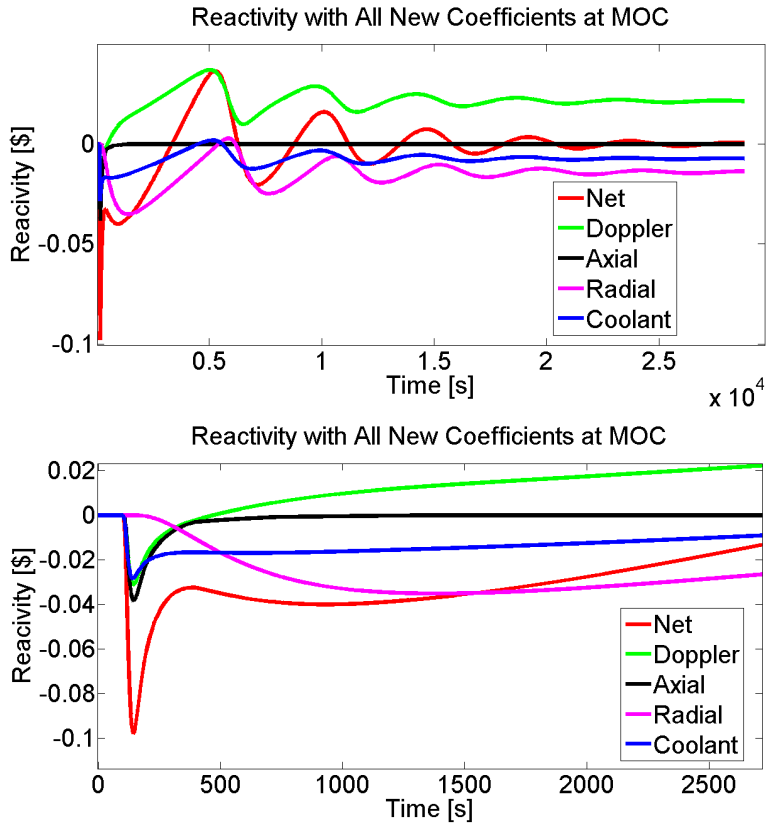

Figure 5.28: Reactivity contributions time trend under ULOF accident at MOC (top), with a zoomed view on the first minutes (bottom).

5.2.3 EOC

The accident development is shown in the figures 5.29, 5.30, 5.31, 5.32, 5.33, 5.34, 5.35 and 5.36. In the EOC scenario the ULOF accident gives a little bit higher peak temperatures for the cladding and the fuel (table 5.5). It is due to the evolution of the reactivity coefficients that decrease their values (except the Doppler) giving a less negative core feedback. As shown in the figure 5.36, the Doppler coefficient has a little bit more negative feedback of the axial expansion while the coolant void worth has a quite high reduction. All the other considerations done before for this accident and its behaviour in the BOC and MOC configurations are still valid.

Peak Parameters	**Fuel Center**	**Cladding**
Temperature [K]	966.1	895.7
Height [node number]	19	23
Time [s]	152	148

Table 5.5: Fuel and cladding peak parameters under ULOF accident at EOC.

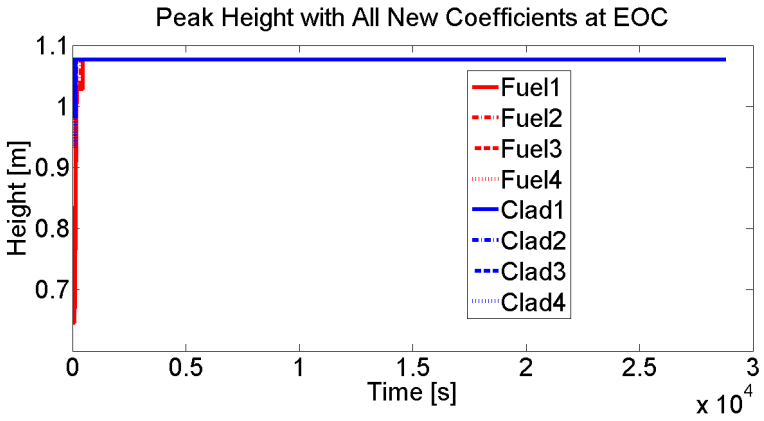

Figure 5.29: Peak heights time trend under ULOF accident at EOC.

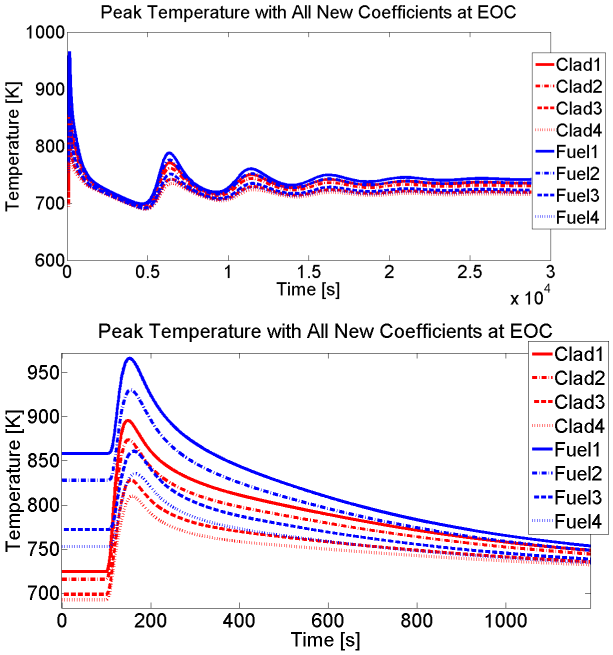

Figure 5.30: Peak temperatures time trend under ULOF accident at EOC (top), with a zoomed view on the first minutes (bottom).

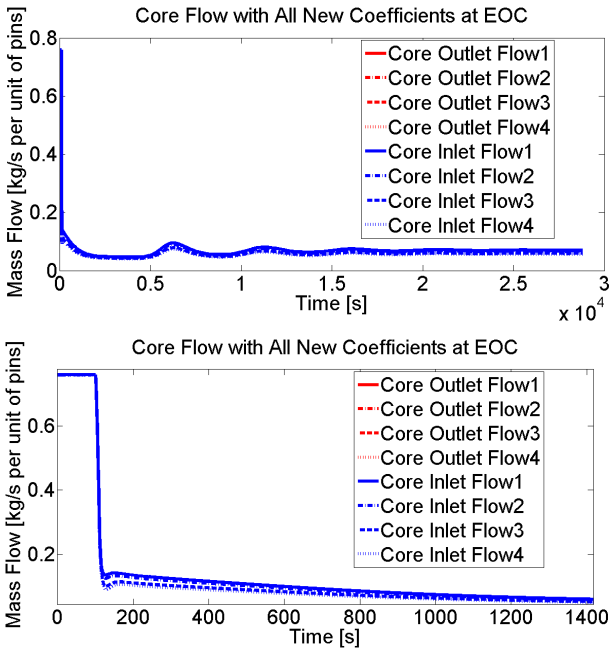

Figure 5.31: Core flow time trend under ULOF accident at EOC (top), with a zoomed view on the first minutes (bottom).

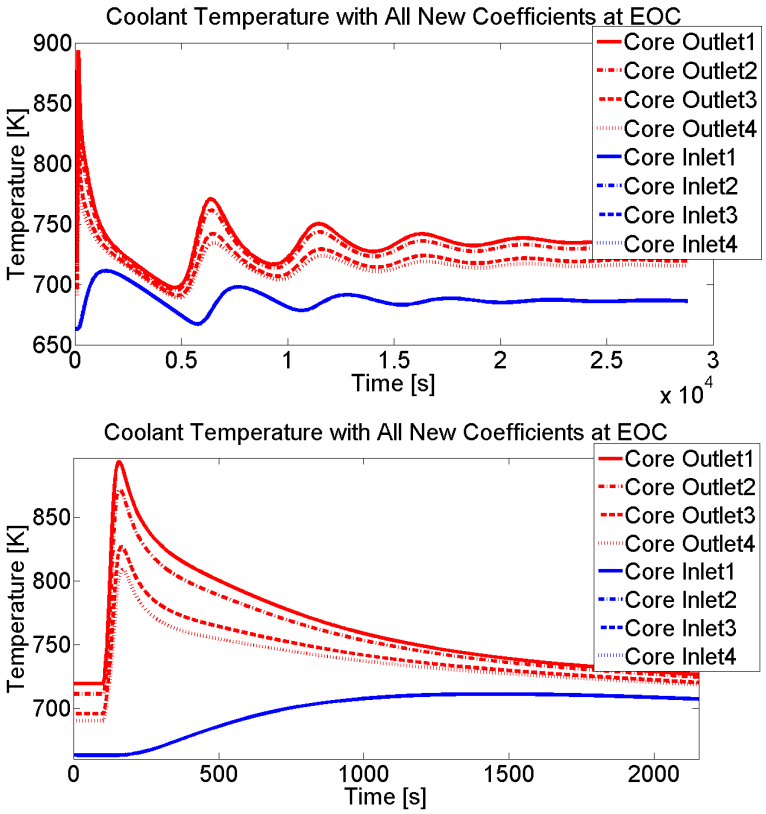

Figure 5.32: Coolant temperature time trend under ULOF accident at EOC (top), with a zoomed view on the first minutes (bottom).

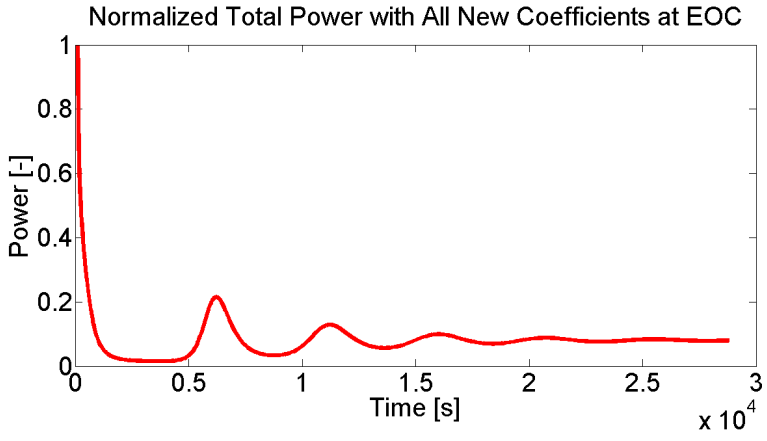

Figure 5.33: Total power time trend under ULOF accident at EOC.

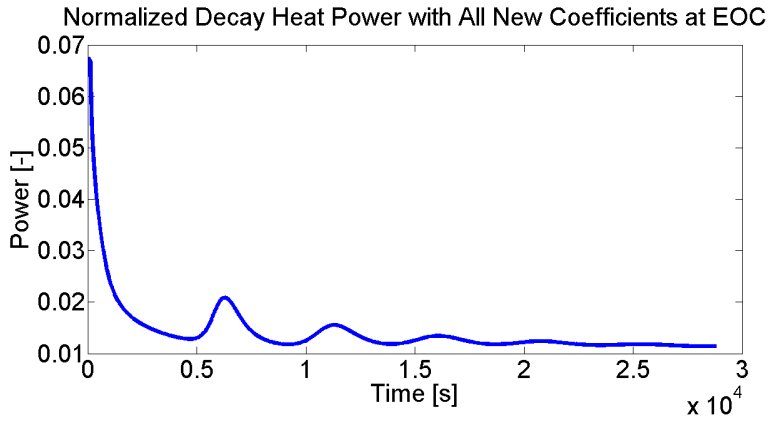

Figure 5.34: Decay heat power time trend under ULOF accident at EOC.

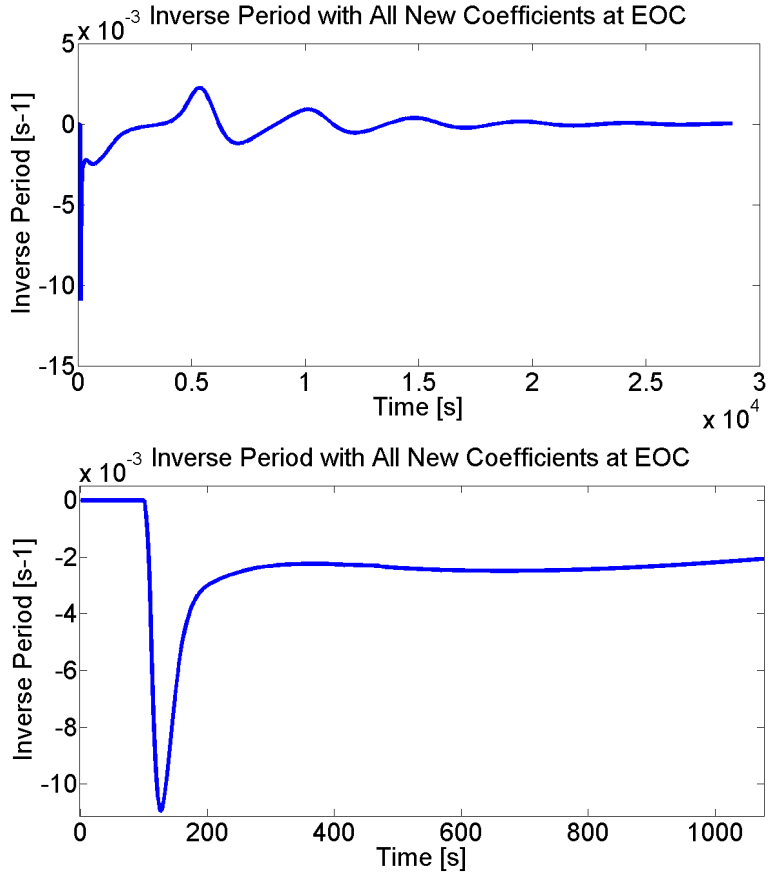

Figure 5.35: Inverse period time trend under ULOF accident at EOC (top), with a zoomed view on the first minutes (bottom).

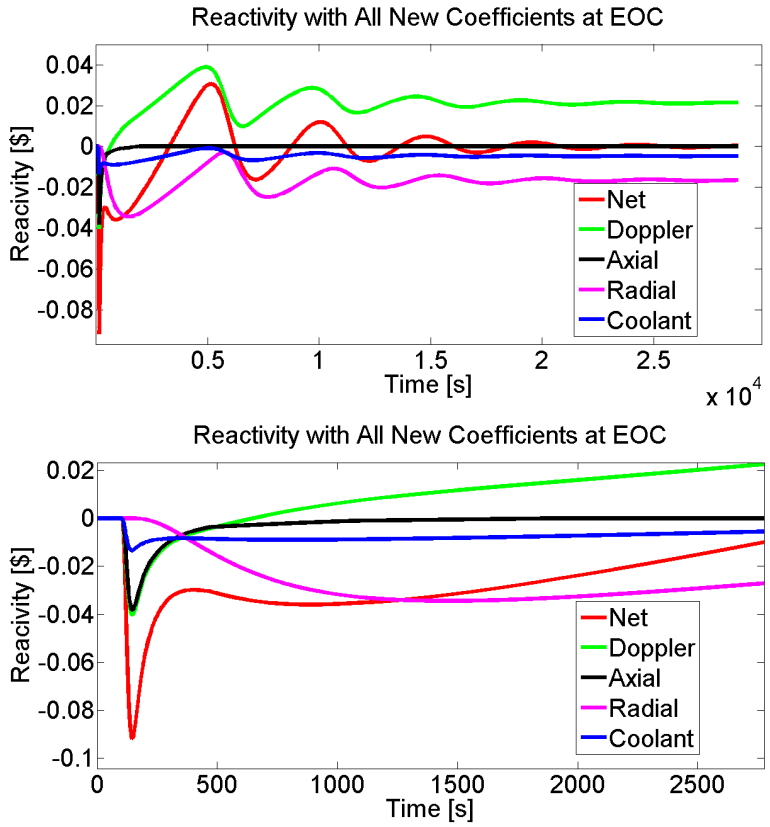

Figure 5.36: Reactivity contributions time trend under ULOF accident at EOC (top), with a zoomed view on the first minutes (bottom).

5.3 Unprotected Loss Of Heat Sink (ULOHS)

The loss of heat sink accident is a result of a total loss of removed power from the reactor core due to the completely loss of the heat removal capabilities following an unavailability of the SGs. When such an event happens the only way to remove the core power is the ultimate heat sink that is a radiative heat exchange between the vessel and the ground. This heat sink should be able to remove the decay heat under a protected transient and for this reason its reference value of removed power is taken as 5% of 8 MW_{th}. The ULOHS scenario requires about 12 hours of simulation to reach the new stability condition and it is much longer with respect to the other accidents analysed. In the EOC section of this accident, a transient simulation without the ultimate heat sink, in order to understand which is its effect on the accident scenario, is presented. Moreover, a parametric analysis of the parameters of main interest, setting the removed power also at 10% and 15% of the nominal one, is performed.

5.3.1 BOC

The cause-effect relationship between the main parameters is similar to the one explained for the ULOF accident. The completely loss of the heat removal capabilities of the SGs (cause) provides an increase in the fuel and coolant temperatures (first effect) that generate a drop in the net reactivity (second effect) due to the negative reactivity insertion. As a consequence, also the power starts to decrease (third effect) and it leads to a change in the increasing trend of the temperatures (fourth effect). At this point the evaluation of the parameters must be restarted following the order described.

The figures to refer in order to find out the accident behaviour are: coolant temperatures (figure 5.38), peak temperatures (figure 5.39), normalized power (figure 5.40) and reactivity (figure 5.42). In addition, also the figures of the peak heights (5.37) and of the inverse period (5.41) are presented. The initiator event is the loss of heat removal capabilities and it causes an increase in the fuel and coolant temperatures. It leads to an immediately negative reactivity insertion that reduces the power, that, in its turn, decreases the fuel and coolant temperatures. At this point during transient (1500 s), the reactor seems to have a self-shutdown behaviour due to the fact that the fuel, cladding and coolant temperatures become equal. The declining trend in the temperatures, that is a consequence of the ultimate heat sink, produces a gain in the net reactivity, due to the negative feedback of the reactivity coefficients, until it becomes positive generating an increase in the power. It provides a variation in the temperature trends that start to go up with the related feedback. This fluctuating behaviour of the parameters continues each time more damped, until the new steady state condition is reached. The reactor power of the new configuration is equal to the removed one and, thanks to the ultimate heat sink, the cladding temperatures (figure 5.39) are lower with respect to the nominal one in the 100 s of steady state. It leads to not have the problem of the enhancement in the corrosion and erosion phenomena seen before for the UTOP and to a lesser extent for the ULOF scenarios.

Peak Parameters	**Fuel Center**	**Cladding**
Temperature [K]	859.6	742.1
Height [node number]	14	23
Time [s]	135	328.5

Table 5.6: Fuel and cladding peak parameters under ULOHS transient at BOC.

Contrary to what happen in the other two accidents, the main responsible for the peak values are the feedback related to the coolant temperature (figure

5.42), since the gain in the fuel one (figure 5.39) is almost negligible (only 1-2 K) and immediately counterbalanced by the power reduction. The latter fact generates a negative feedback for the fuel temperature related feedback only in the first minutes of the transient (≈500-1000 s). In the long term framework, the feedback related to the fuel provide a positive feedback, while the coolant ones gives a negative reactivity insertion. The two contributions are equal in magnitude.

In table 5.6 are shown the peak parameters that, if compared with the other ones for the UTOP and ULOF scenarios at BOC (tables 5.1 and 5.3), give very small values for the temperatures. Regarding the peak times, the situation is the same of the one during the UTOP transient, with the peak temperature that is reached before in the fuel than in the cladding.

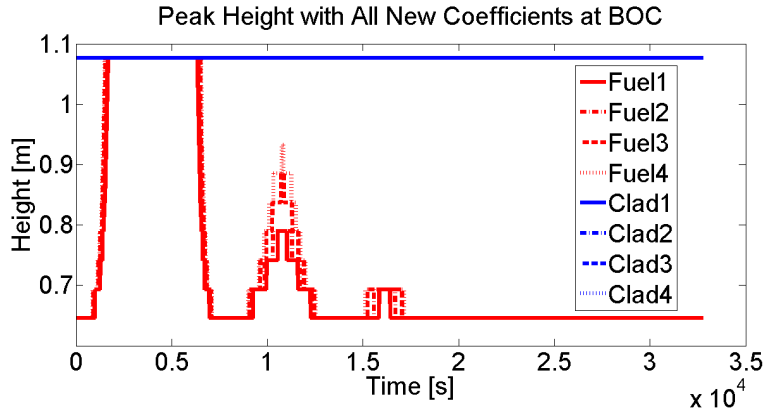

Figure 5.37: Peak heights time evolution under ULOHS scenario at BOC.

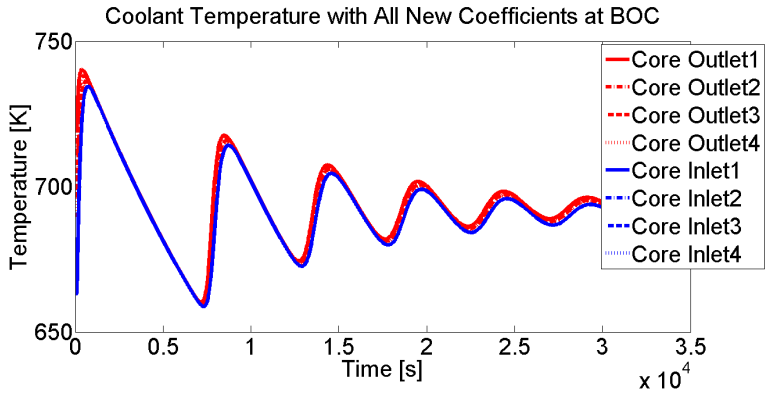

Figure 5.38: Coolant temperature time evolution under ULOHS scenario at BOC.

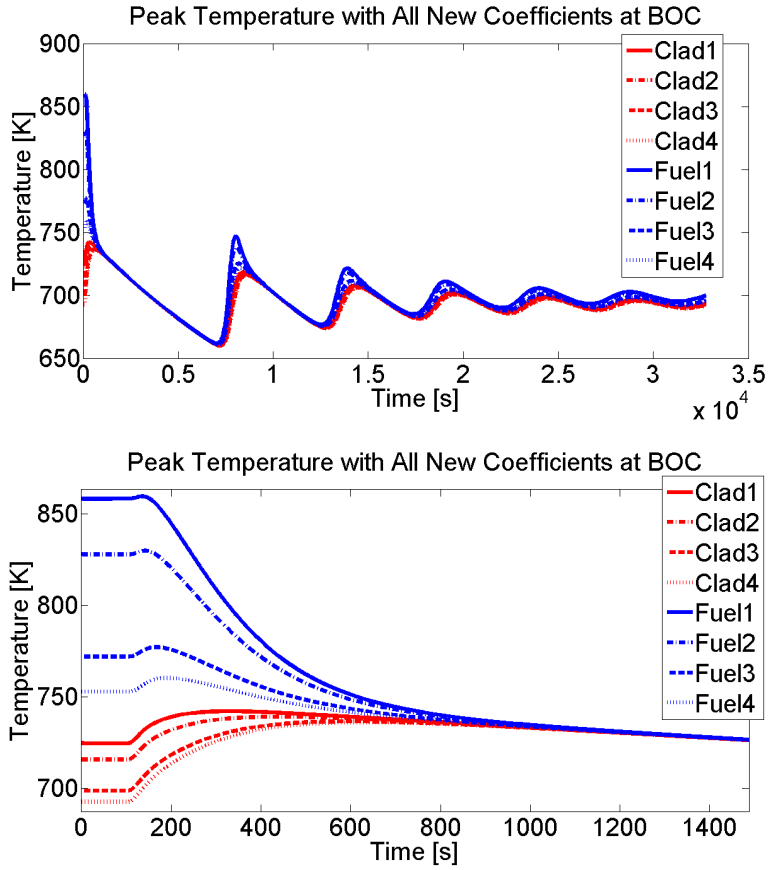

Figure 5.39: Peak temperatures time evolution under ULOHS scenario at BOC (top), with a zoomed view on the first minutes (bottom).

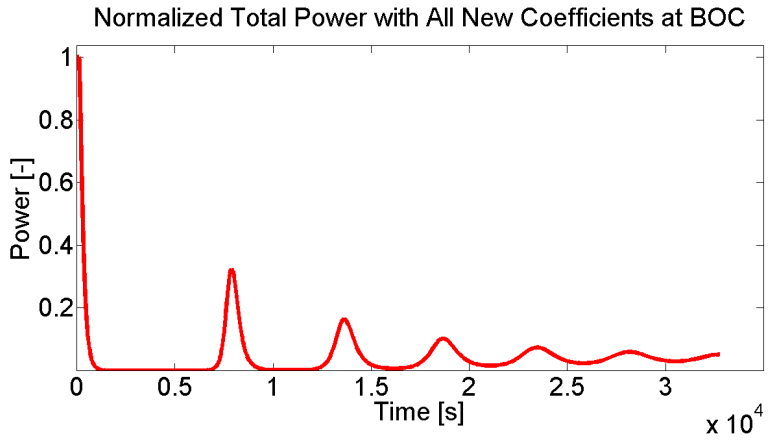

Figure 5.40: Total power time evolution under ULOHS scenario at BOC.

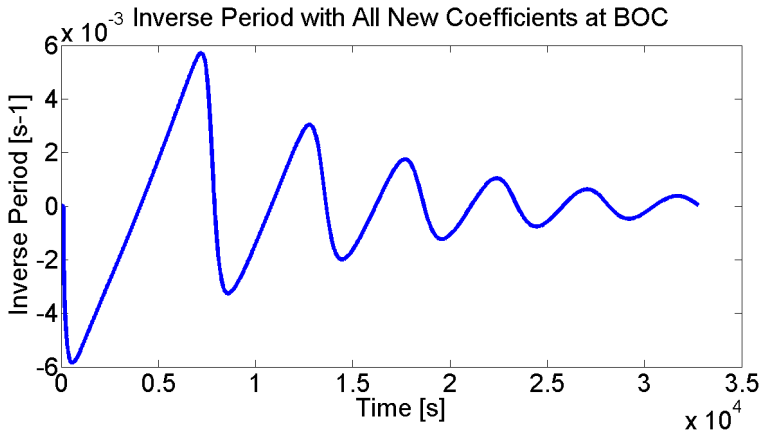

Figure 5.41: Inverse period time evolution under ULOHS scenario at BOC.

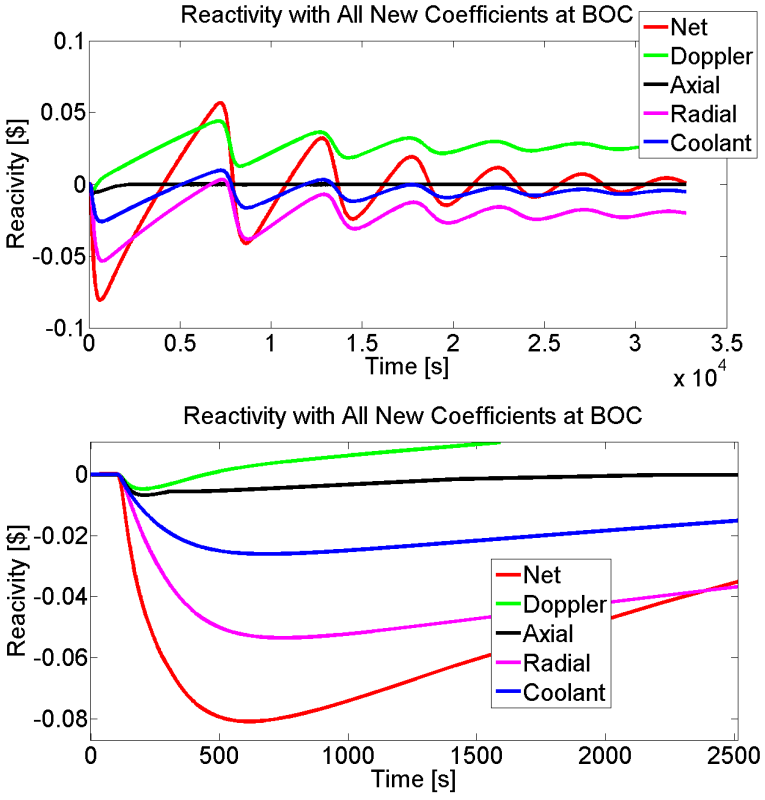

Figure 5.42: Reactivity contributions time evolution under ULOHS scenario at BOC (top), with a zoomed view on the first minutes (bottom).

5.3.2 MOC

The ULOHS accident, like the ULOF one, has an initiator event that does not change its worth over the reactor life and together with the reactivity coefficients time evolution and the decay heat power, these things provide very lightly higher peak temperatures (tables 5.6 and 5.7). In this configuration the presence of the decay heat provides that, in the first decrease of the temperatures (fuel, cladding and coolant), they do not reach an equal value like seen before in the BOC scenario (figure 5.39).

Regarding the reactivity figure (5.49), it shows the same behaviour of the net reactivity components during the BOC transient (figure 5.42): positive value for the fuel temperature related feedback, except for the first 500-1000 s, and a negative one for the feedback linked to the coolant temperature.

For the explanation of the accident behaviour the reader has to refer to the BOC section considering the figures presented below (5.43, 5.44, 5.45, 5.46, 5.47, 5.48 and 5.49).

Peak Parameters	**Fuel Center**	**Cladding**
Temperature [K]	859.8	742.8
Height [node number]	14	23
Time [s]	136.5	349.5

Table 5.7: Fuel and cladding peak parameters under ULOHS transient at MOC.

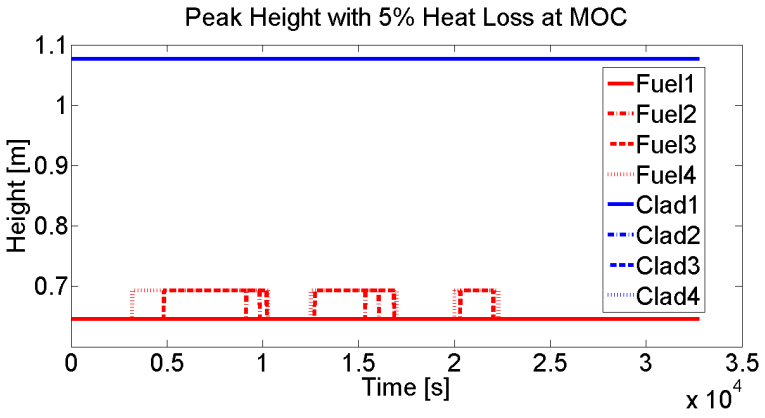

Figure 5.43: Peak heights time evolution under ULOHS scenario at MOC.

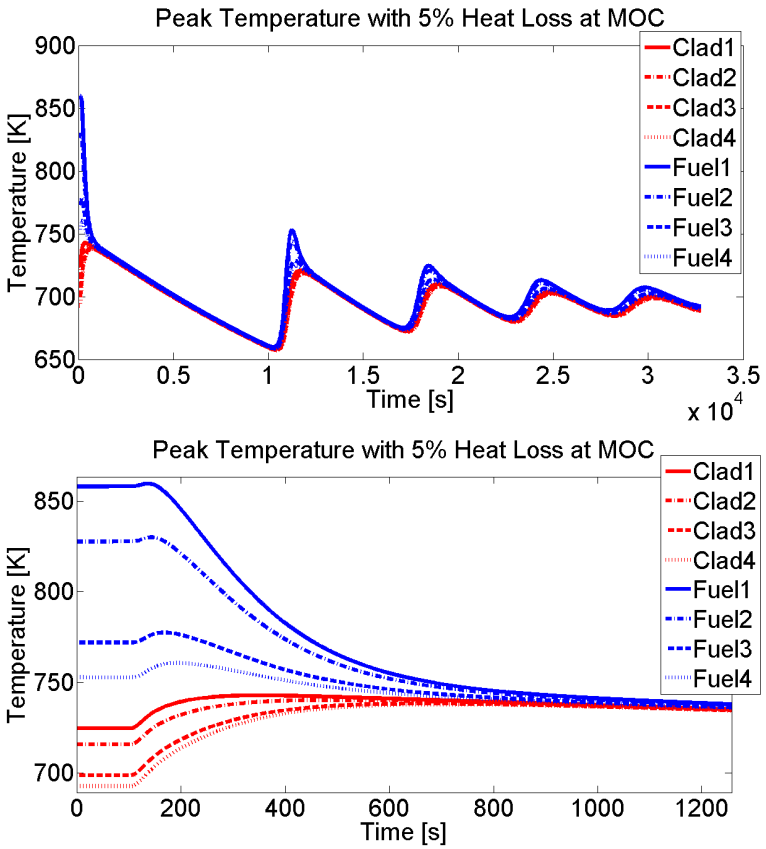

Figure 5.44: Peak temperatures time evolution under ULOHS scenario at MOC (top), with a zoomed view on the first minutes (bottom).

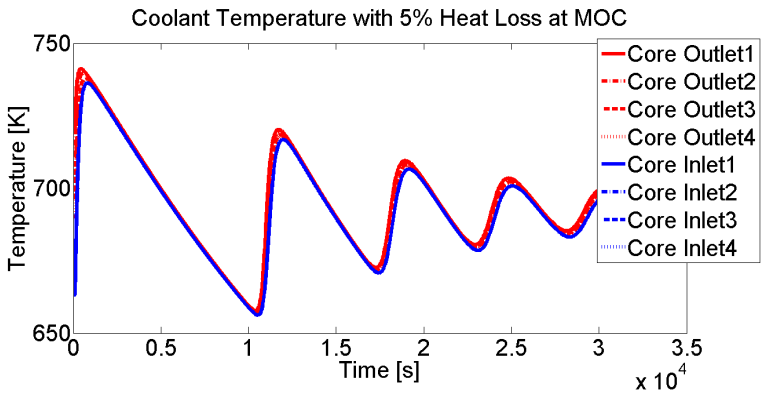

Figure 5.45: Coolant temperature time evolution under ULOHS scenario at MOC.

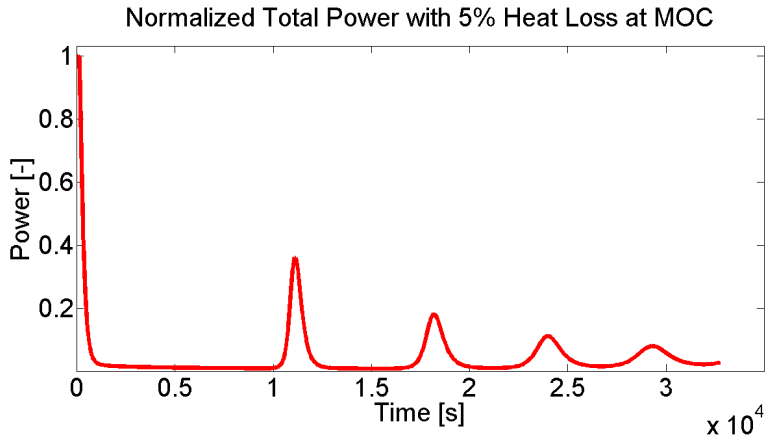

Figure 5.46: Total power time evolution under ULOHS scenario at MOC.

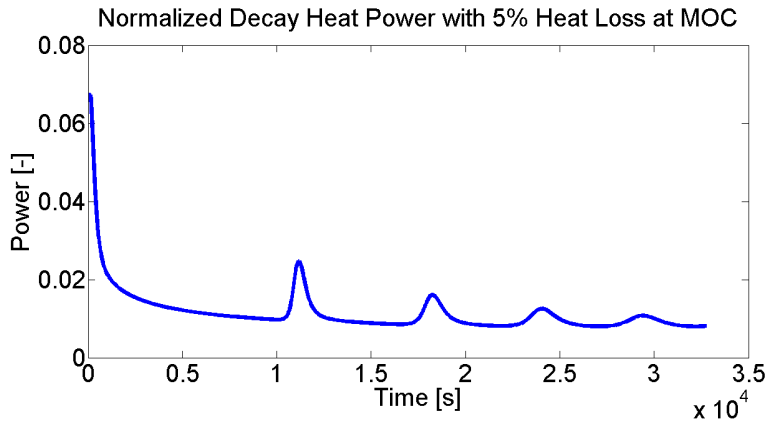

Figure 5.47: Decay heat power time evolution under ULOHS scenario at MOC.

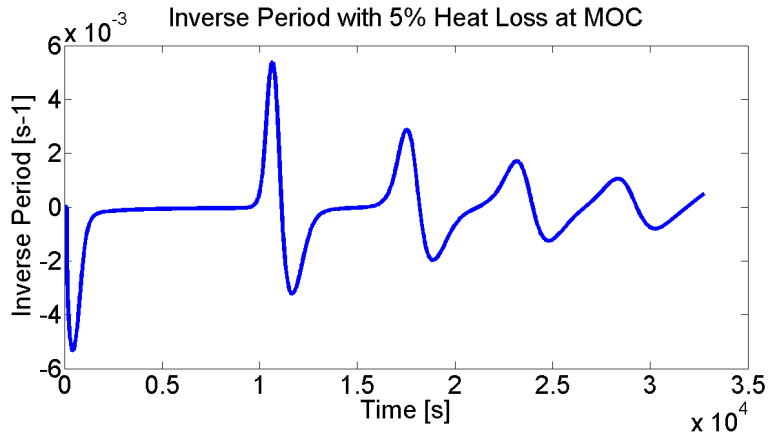

Figure 5.48: Inverse period time evolution under ULOHS scenario at MOC, with a zoomed view on the first minutes (top).

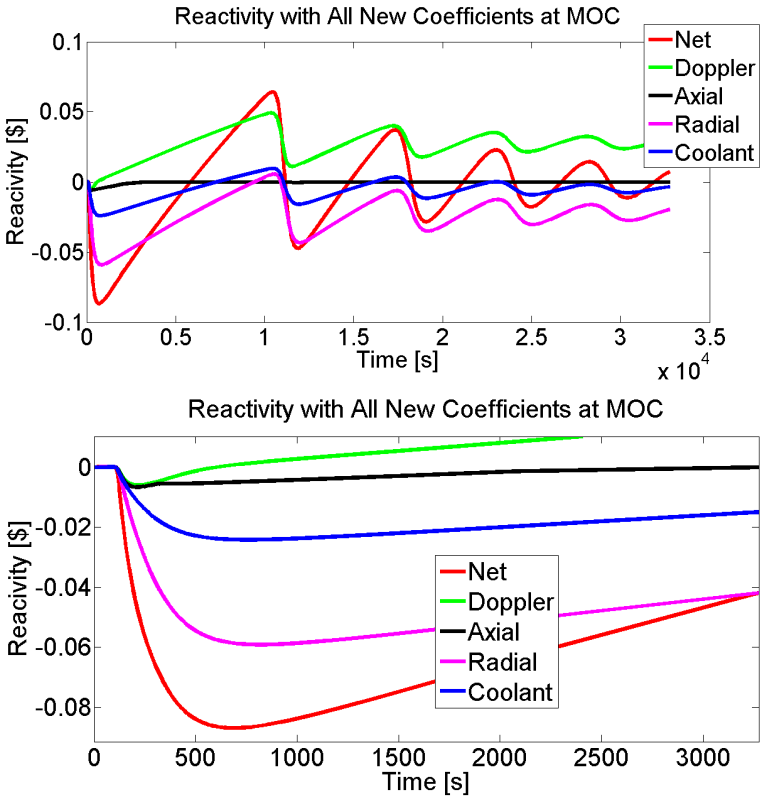

Figure 5.49: Reactivity contributions time evolution under ULOHS scenario at MOC (top), with a zoomed view on the first minutes (bottom).

5.3.3 EOC

In this section, in addition to the figures that show the accident behaviour for the EOC configuration (5.50, 5.51, 5.52, 5.53, 5.54, 5.55 and 5.56), there are two little subsections in which a transient simulation without the ultimate heat sink and a parametric analysis of removed power through the radiative heat exchange between the vessel and the ground are presented. They are located in this section because, as it can be noted confronting the tables 5.6, 5.7 and 5.8, in the EOC scenario this accident gives higher peak values with respect to the BOC and MOC ones. As already said, it is a result of the less negative reactivity insertion provided by the reactivity coefficients, of the decay heat presence and of the non time dependent worth of the initiator event. In particular, the greater increase in the peak temperatures compared to that between BOC and MOC is due primary to the decrease of the coolant void worth and to the related negative feedback (figures 5.42, 5.49 and 5.56). The physics that explains the accident development is the same of the BOC and MOC configurations.

Peak Parameters	Fuel Center	Cladding
Temperature [K]	860.4	746.3
Height [node number]	14	23
Time [s]	141	431.5

Table 5.8: Fuel and cladding peak parameters under ULOHS transient at EOC.

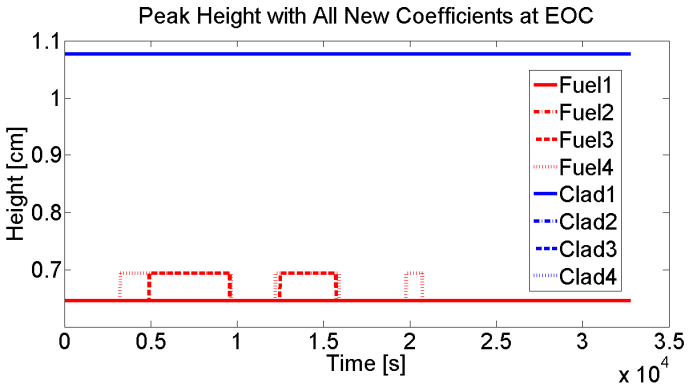

Figure 5.50: Peak heights time evolution under ULOHS scenario at EOC.

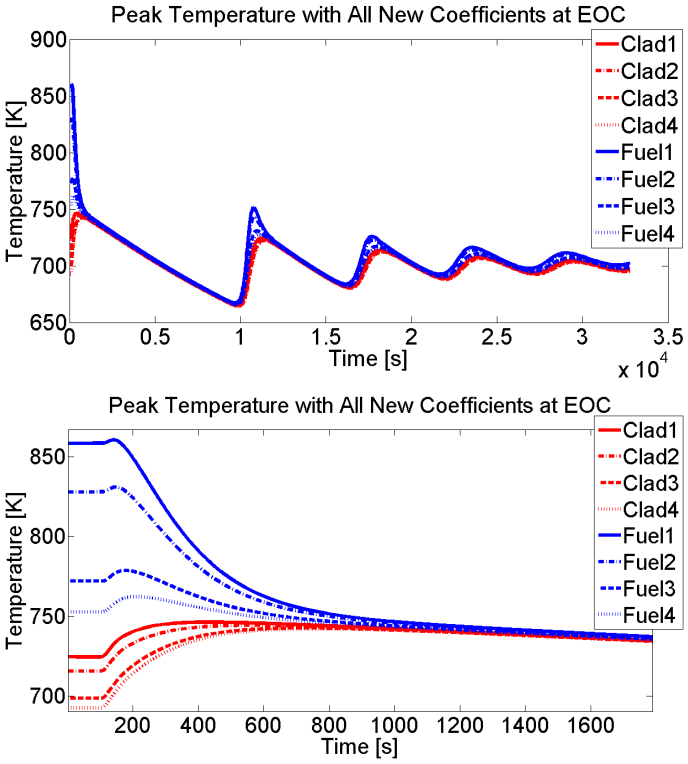

Figure 5.51: Peak temperatures time evolution under ULOHS scenario at EOC (top), with a zoomed view on the first minutes (bottom).

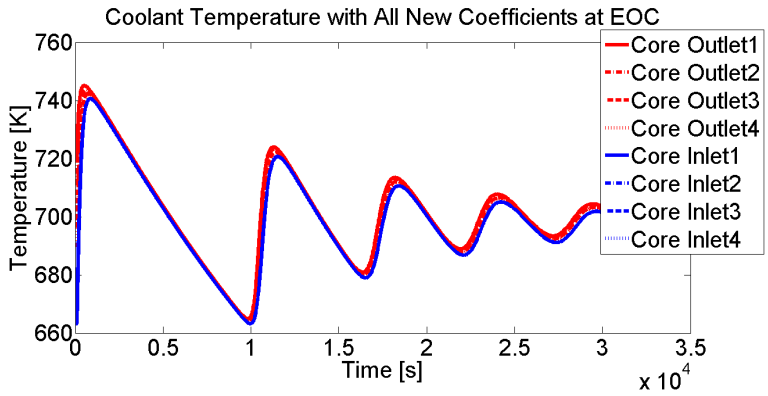

Figure 5.52: Coolant temperature time evolution under ULOHS scenario at EOC.

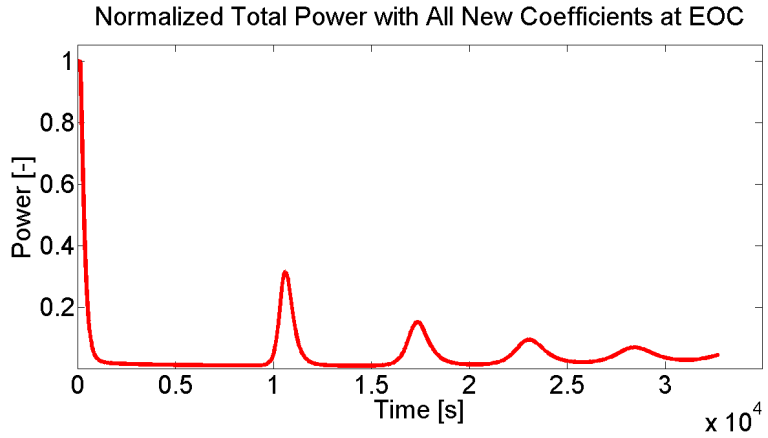

Figure 5.53: Total power time evolution under ULOHS scenario at EOC.

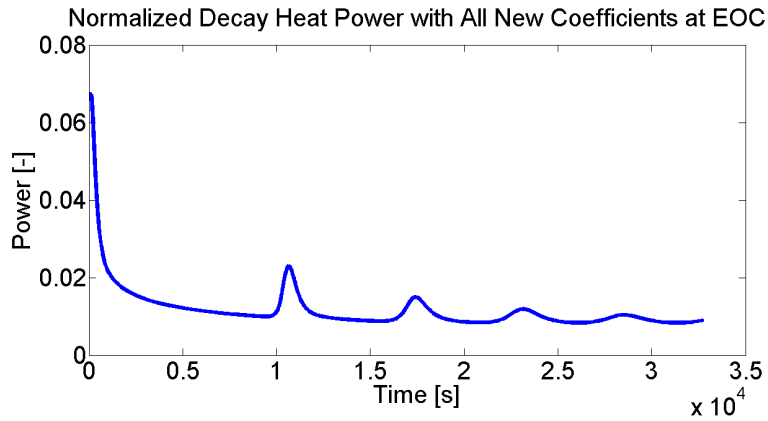

Figure 5.54: Decay heat power time evolution under ULOHS scenario at EOC.

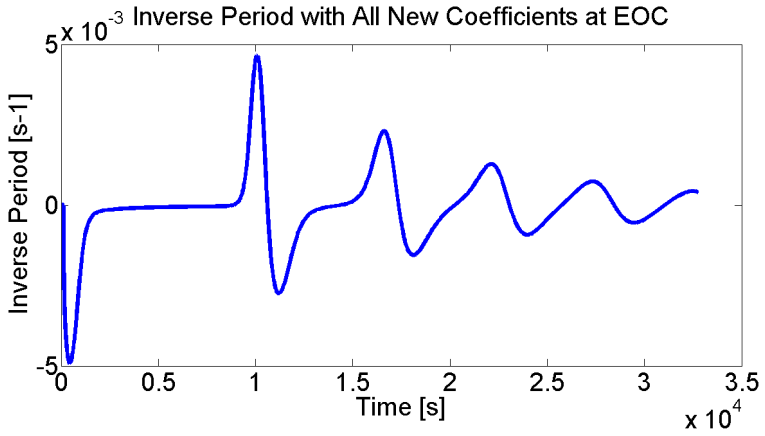

Figure 5.55: Inverse period time evolution under ULOHS scenario at EOC.

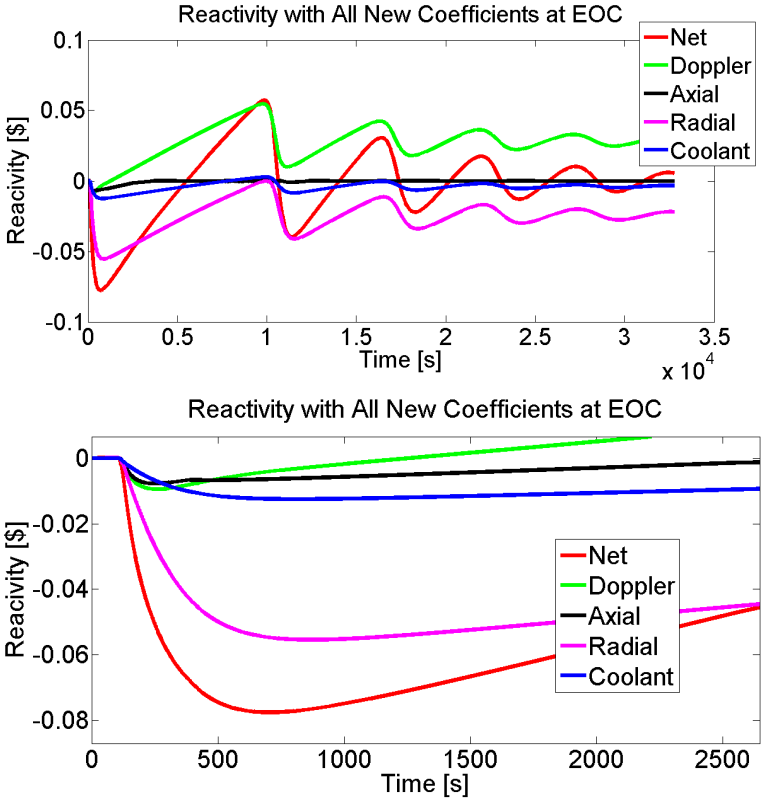

Figure 5.56: Reactivity contributions time evolution under ULOHS scenario at EOC (top), with a zoomed view on the first minutes (bottom).

5.3.3.1 Transient without the ultimate heat sink

The case of no radiative heat exchange and thus of no heat loss from the vessel is of quite simple explanation. After the initiator event (loss of heat sink) the temperatures start to grow (figures 5.58 and 5.59) and there is a negative reactivity insertion by all the four contributions to the net reactivity. It produces an immediately decrement of the reactor power (figure 5.60) and as a result the fuel temperature starts to fall until it reaches the same value of the cladding and coolant temperature (case of reactor shutdown, figure 5.58). At this point in the transient (≈1000 s) the reactor is self shutdown and the temperature continue to grow because of the absence of an heat sink. The value for this temperature is determined by the reactor linear power according to the conductivity integral and by the decay heat power that is the responsible for its continuous growth. As a consequence of the fuel temperature drop with respect to the initial value, its related feedback start to increase, becoming slightly positive. Anyway the strong negative feedback linked to the coolant temperature (radial expansion and coolant void worth) ensure the total negative reactivity and the reactor self shutdown (figure 5.63).

Peak Parameters	Fuel Center	Cladding
Temperature [K]	860.4	765.4
Height [node number]	14	23
Time [s]	139.4	3800

Table 5.9: Fuel and cladding peak parameters under ULOHS transient without the ultimate heat sink at EOC.

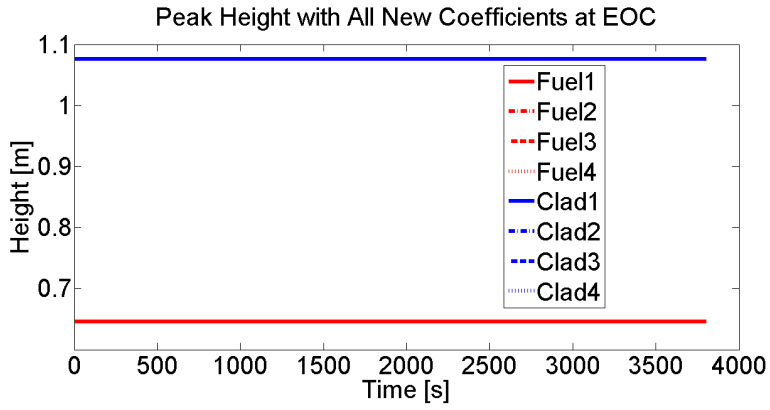

Figure 5.57: Peak heights time evolution under ULOHS scenario at EOC without ultimate heat sink.

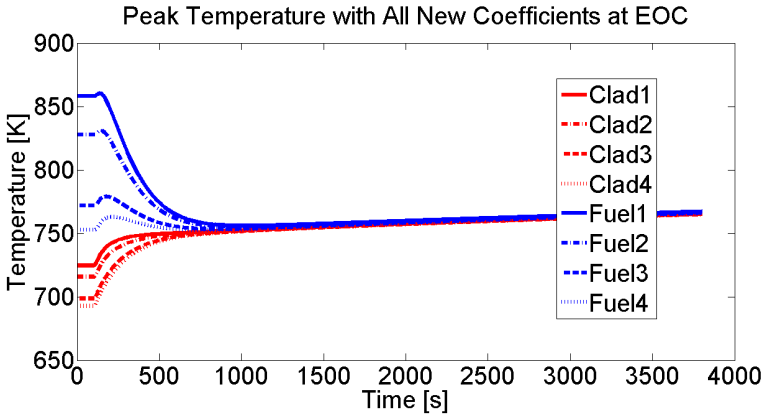

Figure 5.58: Peak temperatures time evolution under ULOHS scenario at EOC without ultimate heat sink.

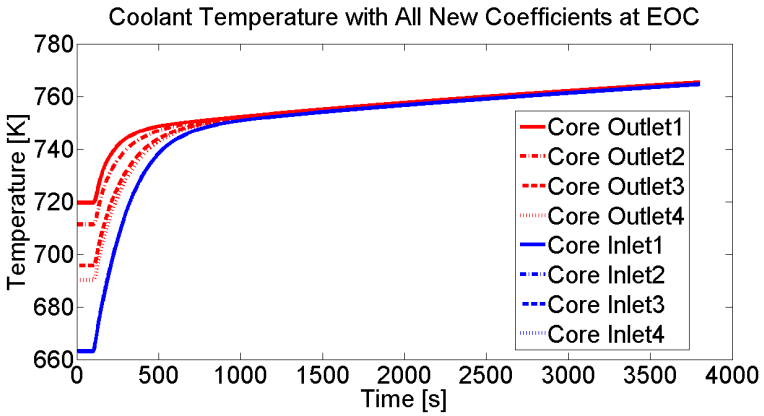

Figure 5.59: Coolant temperature time evolution under ULOHS scenario at EOC without ultimate heat sink.

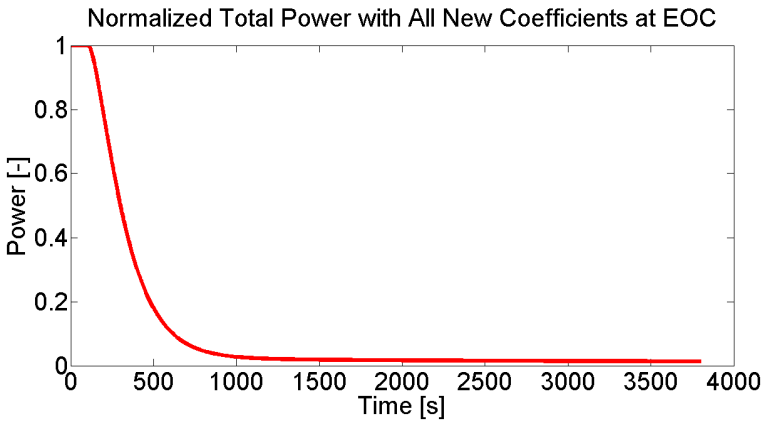

Figure 5.60: Total power time evolution under ULOHS scenario at EOC without ultimate heat sink.

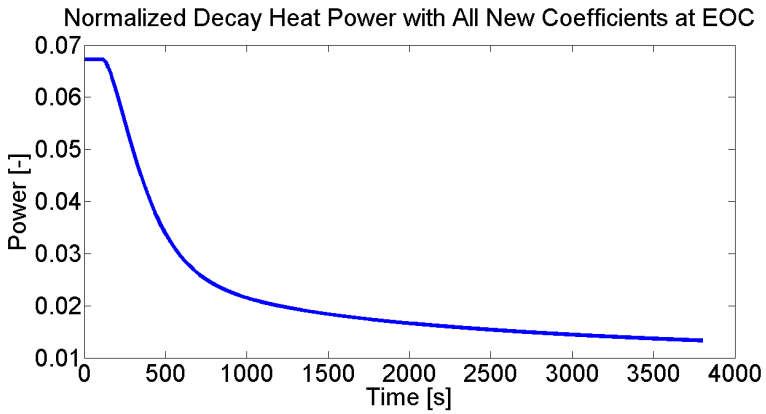

Figure 5.61: Decay heat power time evolution under ULOHS scenario at EOC without ultimate heat sink.

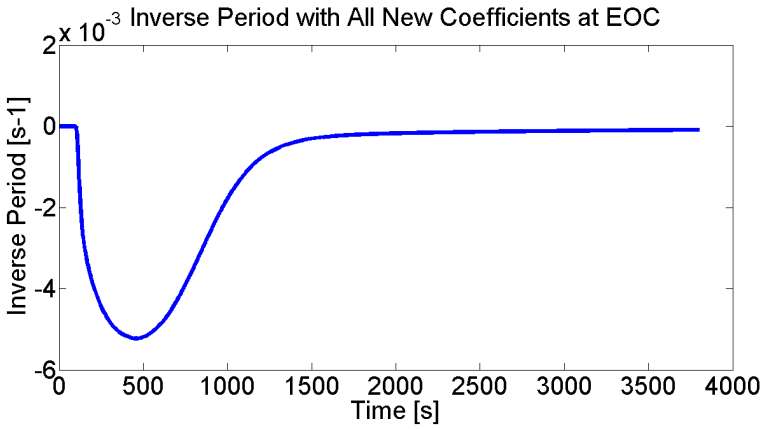

Figure 5.62: Inverse period time evolution under ULOHS scenario at EOC without ultimate heat sink.

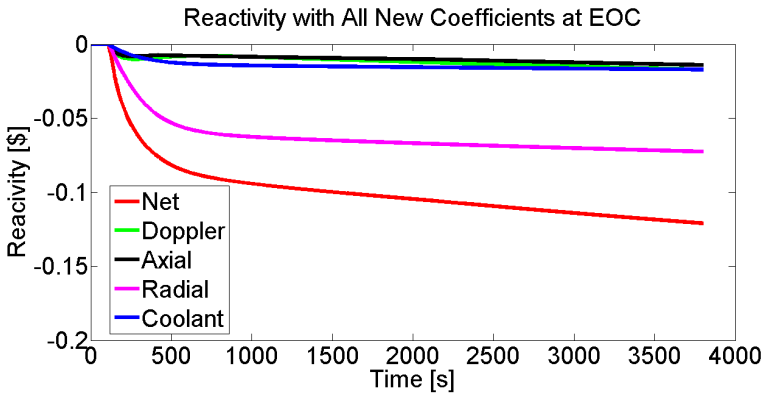

Figure 5.63: Reactivity contributions time evolution under ULOHS scenario at EOC without ultimate heat sink.

5.3.3.2 Parametric analysis of the removed power by the ultimate heat sink

In the figures 5.64, 5.65, 5.66, 5.67 and 5.68 the comparison between the case of 5%, 10% and 15% of removed power respectively for peak fuel temperature, peak cladding temperature, coolant temperature, normalized power and net reactivity is shown. It is possible to note that, increasing the removed power from the core, the transient is faster in reaching the steady state and that the peak fuel temperature is a little bit higher. The latter fact is due to the lower temperature that is achieved in the first peak in the inlet coolant that provides a lower negative feedback by the radial expansion that is the main responsible for the peak values. Contrary to the fuel, the PCT has an higher value with the case of 5% of removed power because of the greater coolant temperature that increases its value.

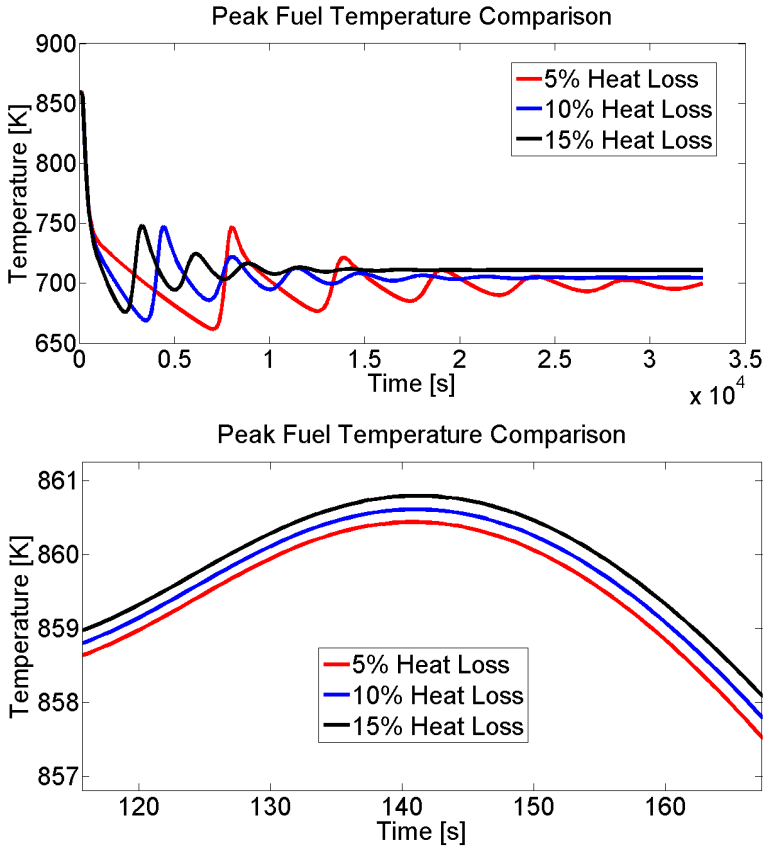

Figure 5.64: Peak fuel temperature dependence on different percentage of heat loss with the ultimate heat sink under the ULOHS accident at EOC (top), with a zoomed view on the different peaks (bottom).

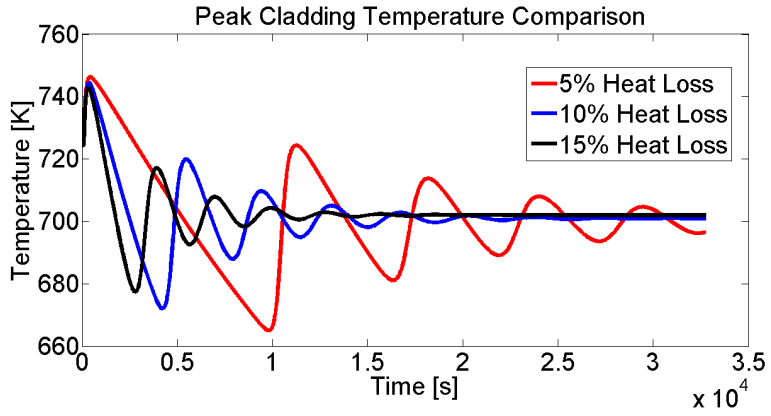

Figure 5.65: Peak cladding temperature dependence on different percentage of heat loss with the ultimate heat sink under the ULOHS accident at EOC.

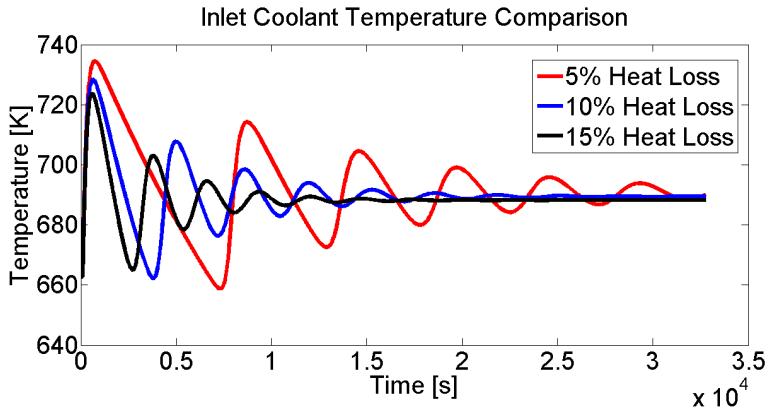

Figure 5.66: Inlet coolant temperature dependence on different percentage of heat loss with the ultimate heat sink under the ULOHS accident at EOC.

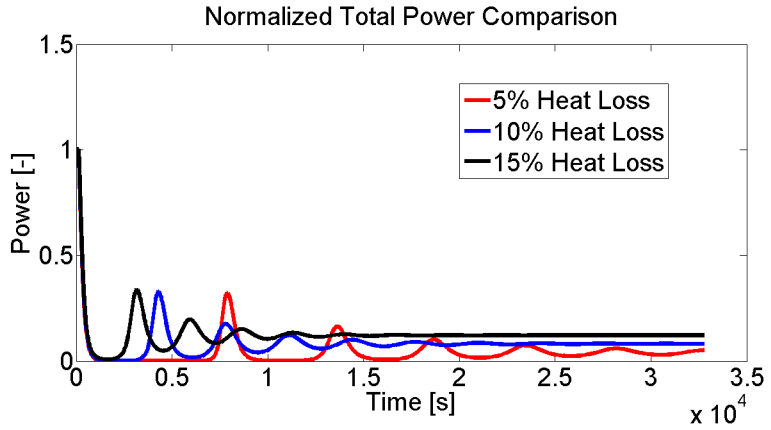

Figure 5.67: Total power dependence on different percentage of heat loss with the ultimate heat sink under the ULOHS accident at EOC.

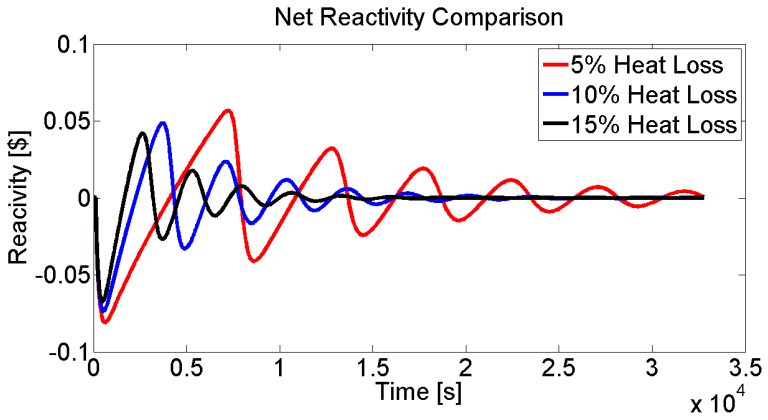

Figure 5.68: Net reactivity dependence on different percentage of heat loss with the ultimate heat sink under the ULOHS accident at EOC.

5.4 Sensitivity Calculations

During the transient analysis, it is seen that the SEALER design is such as to have an excellent feedback that provides quite low peak temperatures with respect to the temperature limits for all the accident scenarios. The sensitivity calculations outlined in this section have the purpose to understand which is the influence of each reactivity coefficient on the peak temperatures and which could be the amount of the reduction in the negative feedback before exceeding the limits for the fuel and cladding temperatures.

The data presented in this chapter are assessed for the UTOP transient scenario at BOC. Since it is the most dangerous accident to deal with, if the temperature limits for this accident are respected, it will be the same also for the others.

5.4.1 Results Discussion

In the figures presented below, how the peak fuel and cladding temperatures change their values according to the variation of one reactivity coefficient per time is shown. This hypothesis is obviously an approximation, since they are strictly related to the neutronics of SEALER and the alteration of only one parameter in the reactor design affects and modifies all of them. This assumption can be accepted because of the aim of this section described above.

In order to perform these calculations, an arbitrary value for the increase and the decrease of each one of the reactivity coefficient is chosen. The coolant void worth, together with the fuel and cladding axial expansion, suffered a reduction and a gain of the 30% in their values calculated at BOC, while the Doppler coefficient is setted to 200 pcm and 300 pcm. Regarding the radial expansion

coefficient, its values are fixed at +15% and at -25% of the initial one.

It can be noted that the reactivity coefficients linked to the fuel temperature vary the peaks of about hundreds of Kelvin for the fuel center (figures 5.69 and 5.71) and of about tens of Kelvin for the cladding (figures 5.70 and 5.72). Regarding the reactivity coefficients related to the coolant temperature, they modify the peak values of about only of tents of Kelvin (figure 5.73) and of some Kelvin (figures 5.74, 5.75 and 5.76). These results reflect perfectly the situation presented in the figure 5.6, in which the main responsible for the peak temperatures in order of importance are: axial expansion, Doppler, coolant void worth and radial expansion. The cladding axial has a very limited and negligible influence on the peak temperatures (figures 5.77 and 5.78) and as a consequence it is not a real concern that its value becomes positive in the EOC configuration.

In addition, a calculation in which all the coefficients are setted with their reduced value is performed. The result is a peak fuel center temperature of 2445.9 K and PCT=1094.6 K. Thus, also in this configuration with a lower total negative feedback the temperature limits are respected with a good margins ($\approx$ 700 K for the fuel and $\approx$ 100 K for the cladding), which are almost halved with respect to the reference case (PCT=999.9 K with margin of 200 K and peak fuel temperature of 2002.5 K with a margin of 1100 K).

As a consequence of these results, it could be considered the hypothesis to reduce a little bit the negative feedback of the reactivity coefficients in order to match a better mechanical or thermal hydraulic or neutronic design. In such analysis should be taken into account also the costs.

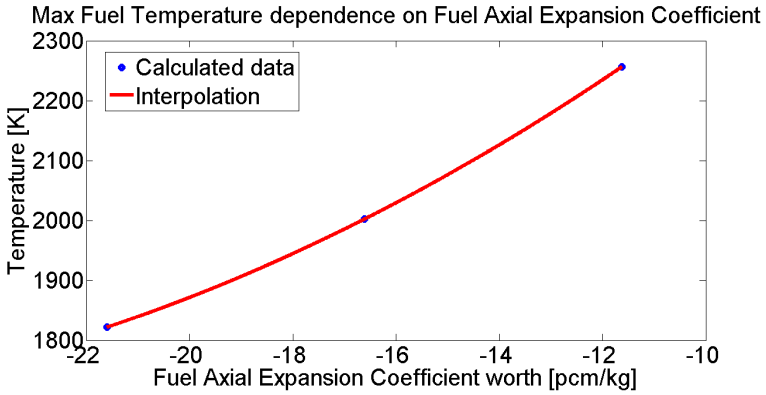

Figure 5.69: Peak fuel temperature dependence on fuel axial expansion coefficient.

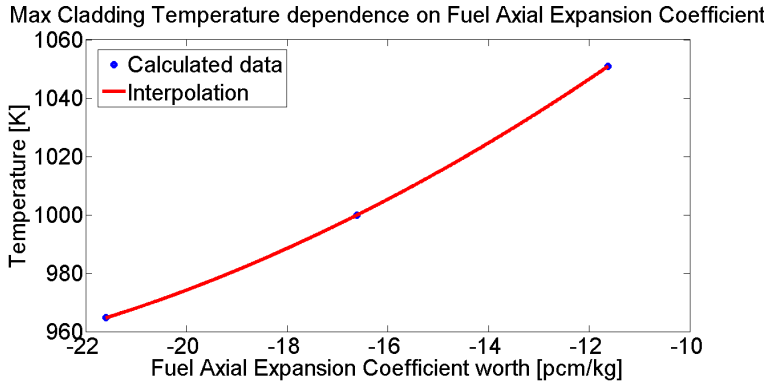

Figure 5.70: Peak cladding temperature dependence on fuel axial expansion coefficient.

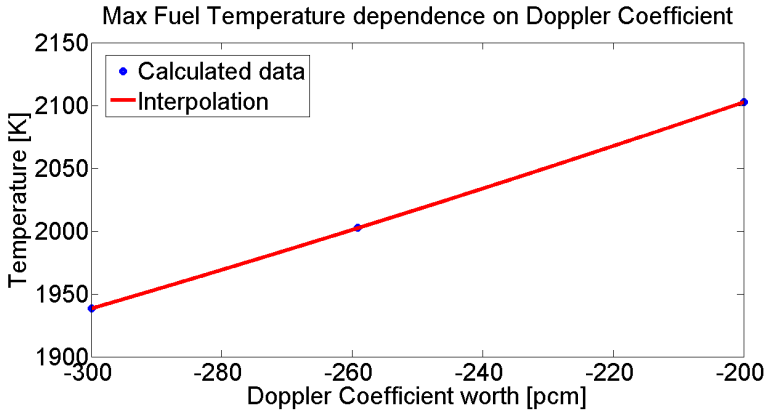

Figure 5.71: Peak fuel temperature dependence on Doppler coefficient.

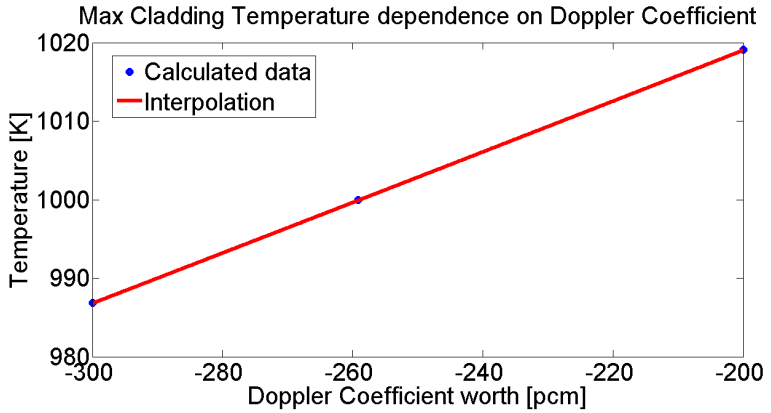

Figure 5.72: Peak cladding temperature dependence on Doppler coefficient.

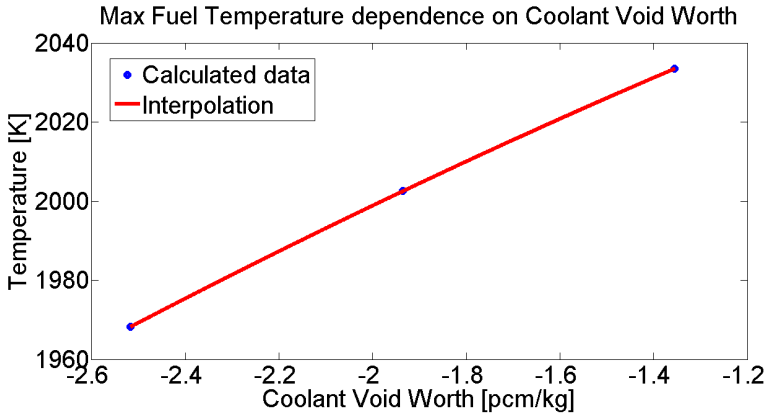

Figure 5.73: Peak fuel temperature dependence on coolant void worth.

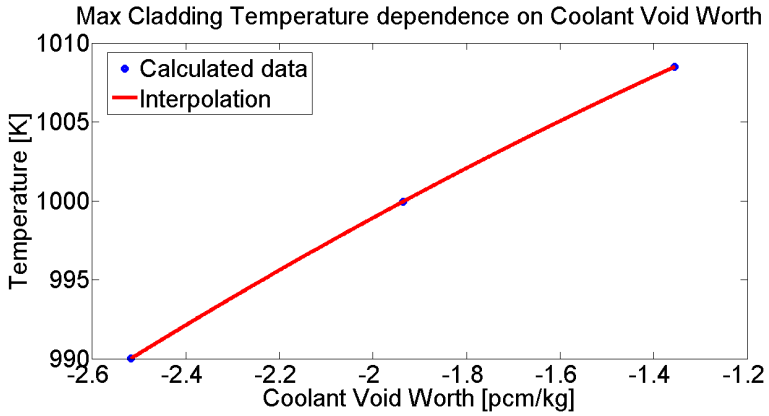

Figure 5.74: Peak cladding temperature dependence on coolant void worth.

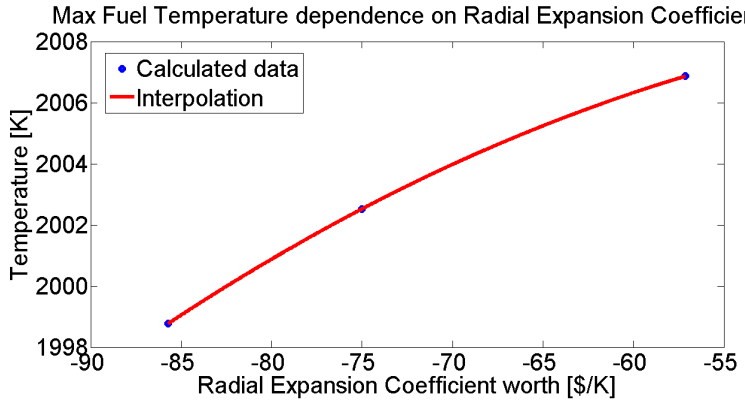

Figure 5.75: Peak fuel temperature dependence on radial expansion coefficient.

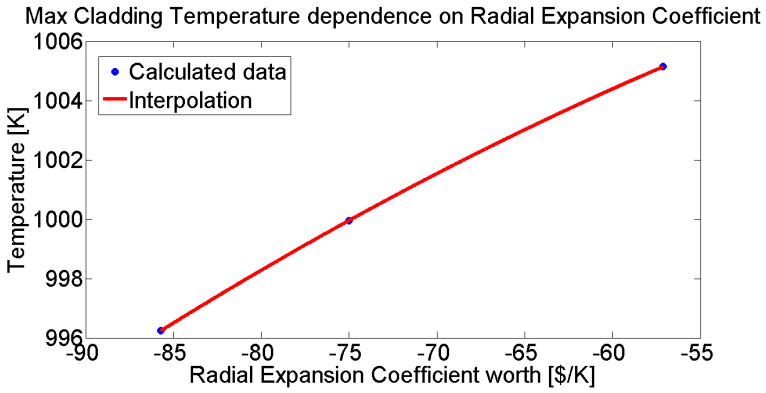

Figure 5.76: Peak cladding temperature dependence on radial expansion coefficient.

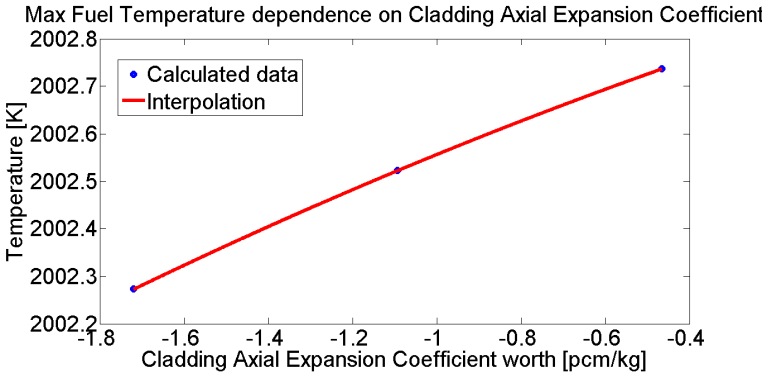

Figure 5.77: Peak fuel temperature dependence on cladding axial expansion coefficient.

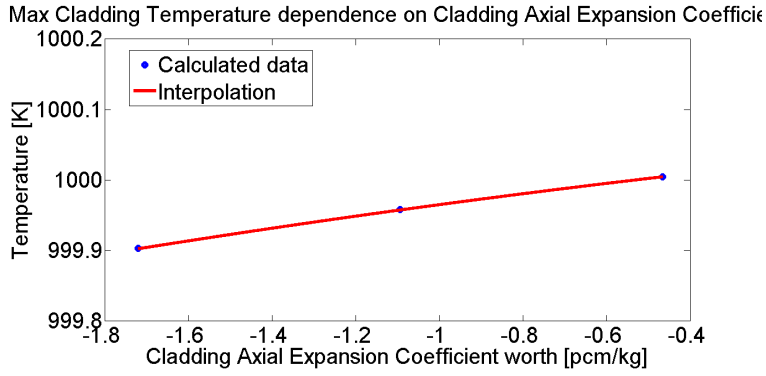

Figure 5.78: Peak cladding temperature dependence on cladding axial expansion coefficient.

Chapter 6

Conclusions

In this last chapter a summary of the main results achieved during the work is reported. Since the aim of the work was the study of the transient behaviour of the SEALER reactor under the three hypothetical accidents, most of the attention was dedicated to this subject, but with a focus also on the evolution of the reactivity coefficients evaluated using their rigorous definition.

In the last section some advices, as possible future improvements of the analysis, are suggested.

6.1 Transient Results

In the chapter five the SEALER transient behaviours under the three main accidents that could happen over the reactor life are presented. By a comparative analysis between them, it is possible to note that, as expected, the most potential dangerous accident is UTOP at BOC. This is a combination of two features, respectively: the type of accident and the worth of the initiator event. Since the UTOP is a Reactivity Initiated Accident (RIA), the unbalanced condition of greater generated power is determined by the value of inserted reactivity and thus it could be whatever value. For SEALER its maximum value is determined by the design of the burn-up control elements that provides a worth of 0.5 \$ per each one of them when they are completely inserted in the core (BOC). The results found for this accident at BOC show a power peak of about 45 MW_{th}, a PCT=999.9 K, that fully matches the safety limit of 1200 K setted for SEALER, and a peak fuel temperature of 2002.5 K, that is more or less 1100 K lower than the melting temperature for the uranium dioxide. At MOC all the peak values are lower due to the lower reactivity insertion (0.25 \$) and they are: power peak=23 MW_{th}, PCT=867.1 K and peak fuel temperature=1339.7 K. In both these transients, a new steady state condition is reached. It means

that SEALER has a such safety features for which, even in the case of no human intervention, it can self-sustained its behaviour. The problem is that the new operating temperatures for the fuel, the cladding, the coolant and all the other core structures are higher than their nominal values. It implies that the reactor can continue to work in these temperature conditions but for a limited period of time, in order to avoid some drawbacks like cladding or SGs tubes failure before the end of the reactor life (30 years) due to enhancement of the corrosion and the erosion phenomena.

In the other two accident scenarios, the first consequence of the initiator event is the partial and the total loss of removed power from the core. The negative feedback of the reactivity coefficients provides that the reactor power is always lower than the initial value of 8 MW_{th} over the entire transient in all the three analysed configurations and that the peak temperatures are lower than the reference ones for the case of UTOP at BOC.

For the ULOF, the natural circulation process, together with the action of the SGs, provides a long term heat sink with the purpose to remove the decay heat from the core. Moreover, it brings to an another criticality condition with a lower power, the value of which is determined by the driving force connected to the difference in the relative elevation of the SGs thermal center with respect to the core one. Regarding the ULOHS, the case of no heat loss through the vessel brings to a self-shutdown of the reactor, but it does not represent the real situation because the ultimate heat sink, supplied by the radiative heat loss between the vessel and the ground, is not taken into account. Also in this case, a new steady state is reached with a reactor power equal to the percentage of heat loss through the vessel. The parametric analysis of the removed power by the ultimate heat sink shows that an its increase leads to a little bit higher peak fuel temperature together with a lower peak temperatures for the cladding and the coolant and to a shorter development of the transient.

As shown before, in all the transients a new criticality is achieved without the human intervention. Anyway, the temperature values at the end of the transients could be a concern, since they can exceed the operating temperature limits that ensure a safe worth for corrosion and erosion phenomena especially in the cladding (UTOP and ULOF accidents).

In the table 6.1 are shown the data for the peak temperatures in the most dangerous conditions for the three reference accidents. It can be noted that for the ULOF and ULOHS scenarios the worst situation happen at EOC. This is a consequence of the reactivity coefficients variation over the reactor lifetime, of the fact that the accident initiator event does not change its worth like in the UTOP case and of the decay heat power presence in the MOC and EOC configurations.

Peak Temperature [K]	Fuel Center	Cladding
UTOP at BOC	2002.5	999.9
ULOF at EOC	966.1	895.7
ULOHS at EOC	860.4	765.4

Table 6.1: Summary of the greater peak temperatures over the reactor lifetime for the three accident scenarios.

For what it concerns the reactivity coefficients, the Doppler coefficient is the only one that becomes more negative with a burn-up increase, while all the others have a less negative trend, with exception of the radial expansion coefficient that has a oscillating time evolution. The latter consideration can be explained with the different conditions of the core: supercritical in the BOC and EOC configurations and sub-critical in the MOC one. It leads to a fluctuating results also in the channel by channel evaluation of the axial expansion (fuel and cladding) and of the coolant void worth. Anyway this variation from the criticality condition produces quite small and acceptable errors. The reason for which all the reactivity coefficients have a similar behaviour is the softening of the neutron spectrum due to the fission products generation in the fuel and to the withdrawal of the burn-up control elements that allows a more efficient moderation given by the reflector. In addition, it has to be taken into account also the activation products that are generated in the fuel and their contribution in the increase of the capture cross section.

6.2 Future developments

The SEALER behaviour under the analysed transients are quiet satisfying, but in order to reach best estimate calculations, especially for the peak temperatures, it is necessary to reduce the number of assumptions and approximations done during both reactivity coefficients evaluations and transient simulations. For the latter case, it could be done a better assessment of the coast down time for the pumps in the ULOF scenario, or a change in the pumps position from the coldest to the hottest part in the primary circuit as done in the last reactor design version, or parametrize the peak temperatures with respect to the withdrawal time for the burn-up control element under the UTOP transient, or again calculate the peak factors also for the MOC and the EOC configurations.

Besides to improve these accidents, it could be interesting to investigate the event of coolant freezing. It can happen as a result of a protected accident, in which the removed power from the SGs is higher than the decay heat one.

For what it concerns the reactivity coefficients, a possible improvement consists in the reduction of the supercriticality and sub-criticality worth in which they are assessed, improving as much as possible the discretization of the axial length to obtain a better positioning of the burn-up control elements. In addition, it must be taken into account the different fuel axial expansion based on the channels peak factors or the flower effect in the case of the radial expansion coefficient, or again calculate the fuel composition in the MOC and EOC configurations also for the fourth channel and do not assume that is equal to the third one.

Considering the quite high safety margins obtained for the peak temperatures and the results of the sensitivity calculations with a less negative feedback, another interesting improvement, that could be done, is an optimization of the reactivity coefficients with the purpose to better match the design features in the thermal hydraulic, mechanical or neutronic fields. In such analysis should be taken into account also the costs.

Appendix A

Numerical Discretization Methods

The present appendix wants to deal with the general properties of the numerical discretization methods and, in the last part, to focus on the method used in the SAS4A/SASSYS-1, in order to have a better comprehension on how this code solves the partial differential equations.

A.0.1 General properties

Starting from the partial differential equations already presented in the chapter 3 (set of equations (3.2)), it is clear that to use a discretization method it is necessary to solve the mass, momentum and energy partial differential equations that describe the physics of the real problem.

$$\begin{cases} \dfrac{\partial \rho}{\partial t} + \dfrac{1}{A}\dfrac{\partial (GA)}{\partial z} = 0 \\ \dfrac{\partial G}{\partial t} + \dfrac{1}{A}\Big(\dfrac{G^2 A}{\rho}\Big) = -\dfrac{\partial p}{\partial z} - \rho g sin(\theta) - \tau_w \dfrac{P_f}{A} \\ \dfrac{\partial \rho e}{\partial t} + \dfrac{1}{A}\dfrac{\partial [GA(e+pv)]}{\partial z} = q^{''}\dfrac{P_h}{A} + q^{'''} \end{cases}$$

To discretise these equations means to replace the mathematical scheme in the continua of space and time with a new one in which the space and the time are subdivided into discrete subset, where the solution is assessed in a point-wise form. Below in the figure A.1, the principal steps for the partial differential equations problem solution are shown. The choice of the discretization process and method are very important phases of it. In addition, it is possible to see which are the three classic numerical scheme used by a code:

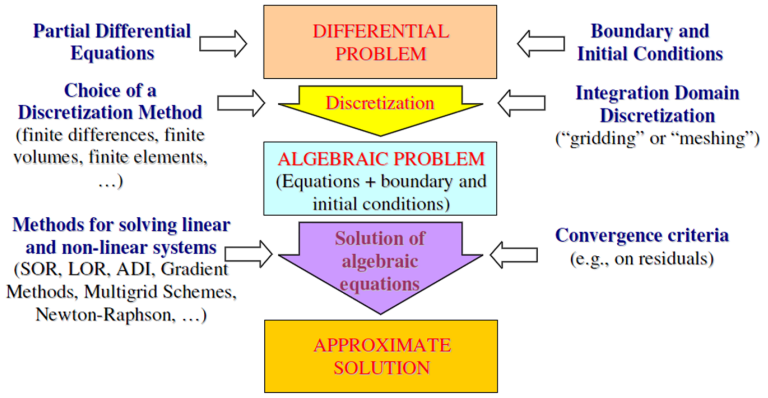

Figure A.1: General discretization scheme.

- finite differences: the partial derivatives in the equations are substituted with finite differences of the independent variable with finite increments in space and time;
- finite volumes: the domain is discretised in control volumes and the problem governing equations are integrated over these volumes.
- finite elements: the domain is subdivided in elements and the governing equation are substituted by local approximating functions depending on the unknown variables.

Before to speak about the method used by SAS4A/SASSYS-1, it is important to give a general perspective on the main mathematical and non features that must be possessed by a discretization method. Starting from a general form for a partial differential problem:

$$\frac{\partial \Psi}{\partial t} = A\Psi$$

where Ψ is a vector function of a general variable and A a linear differential operator. By a discretization in both space and time, it can be found:

$$B_1 \Psi^{n+1} = B_0 \Psi^n$$

where B_1 and B_0 are finite difference operators depending on some variables including that used for the discretization ($\Delta t, \Delta x, \Delta y$ and Δz). With the assumption that exists the inverse operator of B_1, the previous equation becomes:

$$\Psi^{n+1} = B_1^{-1} B_0 \Psi^n = C\Psi^n$$

where $C = B_1^{-1} B_0 = C(\Delta t, \Delta x, \Delta y, \Delta z, ...)$. In addition, it is possible to assume

that there is a link between the space and time increments such as all of them will vanish when $\Delta t \to 0$. For this approximation the operator C can be considered function only of time in the discretization framework (C(Δt, ...)).

A discretization process has the purpose to approximate the differential partial equations of a problem with their respective algebraic ones and, for this reason, it introduces the so called *discretization error*, defined as follow:

$$\delta^n = \Psi_e^n - \Psi^n$$

where Ψ_e^n represent the exact solution at the time step n and Ψ^n the solution found with the discretization process. Moreover, it is composed by two terms: the truncation error and the propagation one, obtained using the previous definition and adding and subtracting the quantity $C(\Delta t)\Psi_e^{n-1}$:

$$\delta^n = \Psi_e^n - C(\Delta t)\Psi^{n-1} = \Psi_e^n - C(\Delta t)\Psi^{n-1} + C(\Delta t)\Psi_e^{n-1} - C(\Delta t)\Psi_e^{n-1}$$

$$\delta^n = \Psi_e^n - C(\Delta t)\Psi_e^{n-1} + C(\Delta t)\delta^{n-1}$$

The difference between the first two terms represents the inaccuracy in the approximation of the partial differential equations with the new set of discretised equations and it refers to the truncation error, while the last term refers to propagation of the error starting from initial data evaluated step by step.

For what just said, it is clear that is crucial to know if the solution given by the discretised scheme is consistent with the one of the initial differential problem. In order to ensure that this happens, there is a theorem that must be satisfied. It is the *Lax Equivalent Theorem*:

Given a properly posed linear initial value problem and a finite difference approximation to it that satisfies the consistency condition, stability is the necessary and sufficient condition for convergence.

Consistency and stability are therefore the properties to be possessed by a numerical scheme to achieve convergence. Defining the concept of consistency, stability and convergence:

- Convergence: a numerical method is said to be "convergent" if the solution of the discretised equation tends to the exact solution of the differential equation as the grid spacing tends to zero. This means that the total error introduced by the numerical scheme tends to zero.
- Consistency: a numerical scheme is said to be "consistent" with the

differential problem if the difference equations representing it tend to those of the differential problem as the grid spacing tends to zero. This means that the truncation errors tends to zero.

- Stability: a numerical scheme is said "stable" if it does not amplify the errors appearing during the numerical solution process.

Using the Taylor series expansion, it is possible to assess the order of truncation error in Δt and Δx and to understand how faster this error goes to zero when the spatial mesh tends to zero. Moreover, with the purpose to ensure the stability of the problem, avoiding the growth of the discretization errors, there are different techniques that can be considered, one of these is the *von Neumann stability criterion*. It consists into give a perturbation at the time step n in the value of the variable calculated at previous one *n-1* and to see how it is propagated in space and time. It is assumed that the error between the perturbed and the non perturbed value can be expressed as a complex exponential:

$$\delta(x,t) = \Psi_p(x,t) - \Psi_{np}(x,t) = \delta_i^n e^{\alpha(t-t^n)} e^{i\beta(x-x_i)}$$

where δ is the error, Ψ_p and Ψ_{np} respectively the perturbed and non perturbed variable values and α and β a complex and a real number. Since both the variables have to satisfy the same equation, it can be wrote:

$$\Psi_{np}(x,t+\Delta t) = C(\Delta t, \Delta x)\Psi_{np}(x,t)$$

$$\Psi_p(x,t+\Delta t) = C(\Delta t, \Delta x)\Psi_p(x,t)$$

and making the subtraction side by side of the previous equation, it is found:

$$\delta(x,t+\Delta t) = C(\Delta t, \Delta x)\delta(x,t)$$

Defining the quantity $G(\Delta t, \Delta x)$ as an amplification factor of the error between two consecutive time steps:

$$G(\Delta t, \Delta x) = \frac{\delta(x,t+\Delta t)}{\delta(x,t)}$$

it is possible to arrive at the *von Neumann stability criterion*:

$$|G(\Delta t, \Delta x)| = |e^{\alpha \Delta t}| \leq 1 \tag{A.1}$$

$$|G(\Delta t, \Delta x)| \leq 1 + K\Delta t \tag{A.2}$$

This criterion expresses that if a physical system is perturbed and this perturbation propagates in space and time, it is not amplified by the mathematical method if the condition of negative real part for α is achieved ($\mathrm{Re}(\alpha)<0$). Thus, the satisfaction of this criterion implies a damping in the errors given by the mathematical scheme and that if the solution diverges this is due to the behaviour of the physical phenomenon analysed. The difference between the equations (A.1) and (A.2) is that the first refers to problems in which the real solution does not increase with the time, while the second takes into account this possibility.

A.0.2 Finite Difference Method

As explained above, the finite difference is the discretization method implemented in SAS4A/SASSYS-1 and it consists in the substitution of the partial derivatives in the equations (3.2) with finite differences of the independent variable with finite increments in space and time.

$$\frac{\partial \rho}{\partial t} + \frac{1}{A}\frac{\partial (GA)}{\partial z} = 0 \Rightarrow \frac{\rho_i^{n+1} - \rho_i^n}{\Delta t} + \frac{1}{A}\frac{G_{i+1}^n A - 2G_i^n A + G_{i-1}^n A}{\Delta z} = 0$$

In a general framework of this method, there are three type of choices for the approximation of the spatial partial derivatives, evaluated in the point x_i, as it is possible to see in figure A.2:

- backward difference
$$\left(\frac{\partial \phi}{\partial x}\right)_{x_i} \approx \frac{\phi_i - \phi_{i-1}}{x_i - x_{i-1}}$$
- forward difference
$$\left(\frac{\partial \phi}{\partial x}\right)_{x_i} \approx \frac{\phi_{i+1} - \phi_i}{x_{i+1} - x_i}$$
- centered difference
$$\left(\frac{\partial \phi}{\partial x}\right)_{x_i} \approx \frac{\phi_{i+1} - \phi_{i-1}}{x_{i+1} - x_{i-1}}$$

Generally, the choice of the centered difference approach is done. Since its accuracy in the finite difference approximation is proportional to Δx^2, while for the other two possibilities there is only a linear proportionality with respect to Δx. It means that the truncation error goes to zero faster when the spatial mesh tends to zero. For what it concerns the time discretization, it is possible to do the same considerations just done for the spatial derivatives.

For a more general approach with both spatial and time discretization, it is more useful to take slightly different assumptions to deal with them:

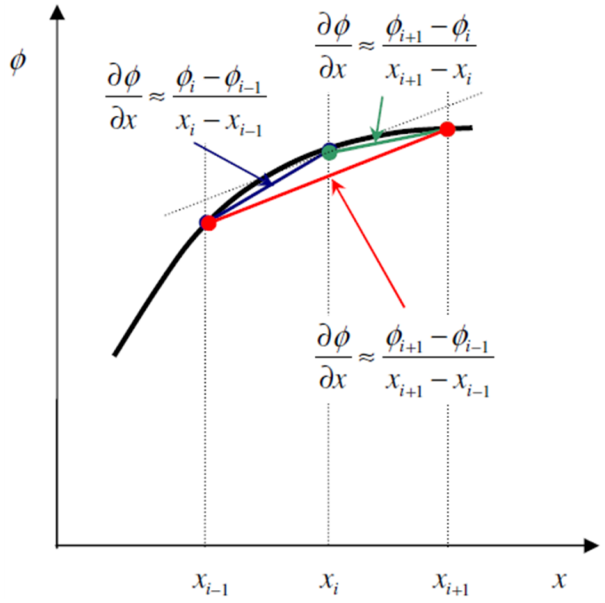

Figure A.2: Different choices of spatial discretization for the finite difference method.

- explicit method

$$\frac{\phi_i^{n+1} - \phi_i^n}{\Delta t} = \frac{\phi_{i+1}^n - \phi_i^n}{\Delta z}$$

  with this method the value of the variable ϕ at the time step *n+1* is evaluated simply making use of known values of the variable at previous time step n. The drawbacks for this rather simple formulation is the conditional stability, according to the *von Neumann criterion* (equation A.1).

- implicit method

$$\frac{\phi_i^{n+1} - \phi_i^n}{\Delta t} = \frac{\phi_{i+1}^{n+1} - \phi_i^{n+1}}{\Delta z}$$

  the advantage of this method is the unconditional stability and its deficiency is that it has a greater truncation error. Moreover, in order to know the value of the variable ϕ at time step *n+1*, the solution of coupled equations is required. as a matter fact, this formulation solves simultaneously the equations in each spatial cell between two time steps n and *n+1*.

- semi-implicit method or Crank-Nicolson method

$$\frac{\phi_i^{n+1} - \phi_i^n}{\Delta t} = 0.5\left[\frac{\phi_{i+1}^n - \phi_i^n}{\Delta z}\right] + 0.5\left[\frac{\phi_{i+1}^{n+1} - \phi_i^{n+1}}{\Delta z}\right]$$

this method is based on an average of the previous two and it is more accurate than them, since it is similar to the centered difference explained above.

Making use of three methods described above, it is possible to derive a general formula in which the definition of the coefficients θ_1 and θ_2 determines the degree of implicitness of the scheme ($\theta_1 = 1$ and $\theta_2 = 0$ explicit method, $\theta_1 = 0$ and $\theta_2 = 1$ implicit method and $\theta_1 = 0.5$ and $\theta_2 = 0.5$ semi-implicit method):

$$\frac{\phi_i^{n+1} - \phi_i^n}{\Delta t} = \theta_1 \left[\frac{\phi_{i+1}^n - \phi_i^n}{\Delta z} \right] + \theta_2 \left[\frac{\phi_{i+1}^{n+1} - \phi_i^{n+1}}{\Delta z} \right] \tag{A.3}$$

with the condition that $\theta_1 + \theta_2 = 1$.

The choice of the method to use is related to the characteristic time of the phenomenon that has to be described. For a detailed time analysis, that requires very small time step in order to follow the development of the phenomena studied, it is preferable to use the explicit method because the stability condition is nearly always satisfied with very low values for the time step. While for phenomena that do not require detailed informations on short time windows, it is better to use the implicit method because the greater size of the time step could create some stability problems for the explicit discretization. For complex system, characterized by phenomena with different time scale, two type of alternative choices can be done: fully implicit approach or partially implicit method splitting the phenomena (explicit for the faster and implicit for the slower).

After the discretization of the problem and the passage to the algebraic equations, it is necessary to use a numerical method to solve them and to find the approximate solution (figure A.1). In SAS4A/SASSYS-1 the *Thomas' algorithm*, that is a very simple scheme derived from the Gaussian elimination one in the case of tridiagonal matrix, is implemented. It consists of two steps: the first, with increasing index, is to eliminate the unknowns in the equations and the second, with decreasing index, is to solve the upper triangular system obtained as a result of the first step. The upper triangular matrix can be found getting the first equation as a function of one unknown in the second one and then substituting it in that one. Continuing this process until the last equation is reached, an equation that has only one unknown is found and now it is possible to come back to the first one having only one unknown in each equation.

Bibliography

[1] *The Generation IV International Forum.* `http://www.gen-4.org/gif/jcms/c_9260/Public`.

[2] A .Alemberti, J. Carlsson, E. Malambu, A. Orden, D. Struwe, P. Agostin and S. Monti. "European lead fast reactor-ELSY". In: *Nuclear Engineering and Design,* 241, (2011), pp. 3470–3480.

[3] ELSY Work Program, EURATOM. "European Lead-Cooled System (ELSY) Project". In: (2006). Techical Report.

[4] *LEADER-Lead-cooled European Advanced DEmonstration Reactor.* `http://www.leader-fp7.eu`.

[5] G. Grasso, C. Petrovich, D. Mattioli, C. Artioli, P. Sciora, D. Gugiu, G. Bandini, E. Bubelis and K. Mikityuk. "The core design of ALFRED, a demonstrator for the European lead-cooled reactors". In: *Nuclear Engineering and Design,* 278, (2014), pp. 278–301.

[6] L. Damiani, M. Montecucco and A. Pini Prato. "Conceptual design of a bayonet-tube steam generator for the ALFRED lead-cooled reactor". In: *Nuclear Engineering and Design,* 265, (2013), pp. 154–163.

[7] H. A. Abderrahim et al. "MYRRHA, a Multipurpose Hybrid Research Reactor for High-End Applications". In: *Nuclear Physics News,* 20, (2010), pp. 1–24.

[8] H. A. Abderrahim, P. Baeten, D. De Bruyn and R. Fernandez. "MYRRHA - A multi-purpose fast spectrum research reactor". In: *Energy Conversion and Management,* 63, (2012), pp. 4–10.

[9] S. Bortot, E. Suvdantsetseg and J. Wallenius. "BELLA: a multi-point dynamics code for simulation of fast reactor". In: *submitted to Annals of Nuclear Energy,* (2014).

[10] E. Suvdantsetseg, J. Wallenius and S. Bortot. "Optimization of the reactivity control drum system of ELECTRA". In: *Nuclear Engineering and Design,,* 252, (2012), pp. 209–214.

[11] J. Wallenius, E. Suvdantsetseg and A. Fokau. "ELECTRA: European Lead Cooled Training Reactor". In: *Nuclear Technology,* 177, (2012), pp. 303–313.

[12] S.Qvist. "Optimization method for the design of hexagonal fuel assemblies". Proc. PHYSOR 2014, Kyoto, Japan. 2014.

[13] M. Del Giacco, A. Weisenburger and G. Mueller. "Fretting corrosion in liquid lead of structural steels for lead-cooled nuclear systems: Preliminary study of the influence of temperature and time". In: *Journal of Nuclear Materials,* 423, (2012), p. 79.

[14] A. Weisenburger, G. Müller et al. "T91 cladding tubes with and without modified FeCrAlY coatings exposed in LBE at different flow, stress and temperature conditions". In: *Journal of Nuclear Materials,* 376, (2008), p. 274.

[15] A. Weisenburger et al. "Creep, creep-rupture tests of Al-surface-alloyed T91 steel in liquid lead bismuth at 500 and 550°C". In: *Journal of Nuclear Materials,* 431, (2012), p. 77.

[16] G. Müller, G. Schumacher and F. Zimmermann. "Investigation on oxygen controlled liquid lead corrosion of surface treated steels". In: *Journal of Nuclear Materials,* 278, (2000), p. 85.

[17] G. Müller et al. "Behaviour of steels in flowing liquid PbBi eutectic alloy at 420-600°C after 4000-7200 h". In: *Journal of Nuclear Materials,* 335, (2004), p. 163.

[18] A. Gessi et al. "Corrosion tests in HLM". Proc. GETMAT final workshop, Berlin, September2013.

[19] A. Wilson. "Sandvik Tubes for Nuclear Applications". GenIV Fin Workshop, Lappeenranta, Finland. September 30–October 1, 2011.

[20] E. Adamov, V. Orlov, A. Filin, V. Leonov, A. Sila-Novitski, V. Smimov and V. Tsikunov. "The Next Generation of Fast Reactor". In: *Nuclear Engineering and Design,* 173 (1997), p. 143.

[21] J.Lim et al. "Design of alumina forming FeCrAl steels for lead or lead-bismuth cooled fast reactors". In: *Journal of Nuclear Materials,* 441, (2013), p. 650.

[22] M. Ottolino et al. "Steam generator design report and drawing". In: *ELSY delivery report DEL-10-016, Ansaldo Nucleare* (2010).

[23] L. Cinotti. "Pressurized-water-cooled nuclear reactor with compact steam generators". In: *European Patent Office, EP 2238599,* (2011).

[24] Nuclear Engineering Division, Argonne National Laboratory. *Standard Code Description*. http://www.ne.anl.gov/codes/sas4a.

[25] J.E. Cahalan, T. H. Fanning, F.E. Dunn, J.P. Herzog, A.M. White and R.A. Wigeland. *The SAS4A/SASSYS-1 Safety Analysis Code System*. 2012.

[26] VTT Technical Research Centre of Finland. *Serpent a Continuous-energy Monte Carlo Reactor Physics Burnup Calculation Code*. http://montecarlo.vtt.fi/.

[27] E. Suvdantsetseg, J. Wallenius. "Unprotected Loss of Heat Sink Analysis for the design of ELECTRA". In: *submitted to Annals of Nuclear Energy,* (2014). Techincal note.

[28] G. Bandini, P. Meloni and M.Polidori. "Thermal-hydraulics analyses of ELSY lead fast reactor with open square core option". In: *Nuclear Engineering and Design,* 241, (2011), pp. 1165–1171.

[29] *The MYRRHA sub-critical core configuration*. http://myrrha.sckcen.be/en/Engineering/Sub-critical_core.

[30] J.Leppänen. *Serpent User's Manual*. 2013.

[31] E. Suvdantsetseg. "Neutronics and Transient Analysis of a Small Fast Reactor Cooled with Natural Circulation of Lead". Doctoral Thesis in Phisics. Royal Institute of Technology, 2014.

[32] J. Wallenius. *Trasmutation of Nuclear Waste*. Leadcold books and games, 2011.